Evaluation of drug-like properties of innovative multitarget-directed ligands for treatment of Parkinson's disease

Ana Carolina Laranjo Sousa da Cunha

Master's Dissertation

Integrated Masters in Bioengineering – Molecular Biotechnology

Faculty of Engineering of the University of Porto

School of Medicine and Biomedical Sciences

Supervisor: Sofia Benfeito, PhD

Second supervisors: Daniel Chavarria, PhD and Professor Doctor Fernanda Borges, Associate Professor

June 30, 2021

I must endure the presence of a few caterpillars if I wish to become acquainted with the butterflies.

Antoine de Saint-Exupery, The Little Prince

AGRADECIMENTOS

Em primeiro lugar, um agradecimento especial à Professora Doutora Fernanda Borges, por me ter acolhido de braços abertos no seu grupo e ter permitido a minha participação neste projeto. Muito obrigada.

À minha orientadora, Sofia Benfeito, pela qual guardo um grande carinho e sem a qual esta dissertação seria possível. Muito obrigada pelo apoio incansável, pela motivação e, acima de tudo, pela partilha de conhecimento. Ao meu co-orientador, Daniel Chavarria, pela dedicação em acompanhar todo o meu trabalho. A todos no laboratório, por me receberem tão calorosamente e por sempre se disponibilizarem a ajudar. Um obrigada a todos a quem pedi as chaves emprestadas.

Tenho de agradecer aos meus amigos, que me acompanharam ao longo destes anos e me perdoaram todos os cafés a que faltei. Aos Gulosos por serem os melhores, mais estranhos amigos que poderia ter pedido. À Catarina e à Bruna, que sempre me apoiaram, mesmo sendo de artes. À Mariana, por ser a minha psicóloga não remunerada. À minha colega de casa, Miriam, que aturou as minhas tolarias quatro anos.

Um parágrafo especial para o Miguel. O Miguel é o meu companheiro de todas as horas. Não imagino estes cinco anos sem ele, nem um dia em que passemos menos de uma hora ao telefone. Obrigada por seres o melhor amigo que todos querem ter.

À minha família, que me inspira todos os dias a ser mais e melhor. Aos meus pais, Oscar e Fátima e ao meu irmão, João, as pessoas mais corajosas que conheço. E, claro, à Mila. Esta dissertação é para vocês.

Por fim, não posso deixar de agradecer ao Guilherme que, apesar de longe, sempre se fez sentir perto. Obrigada por nunca teres duvidado de mim e me dares força para aceitar novos desafios. Sem ti nada seria a mesma coisa.

ABSTRACT

Parkinson's Disease (PD), the second most common neurodegenerative disorder (ND) after Alzheimer's Disease, is associated with the selective loss of dopaminergic neurons in the brain's *substantia nigra*. The consequent decrease in the levels of the neurotransmitter dopamine triggers the motor and cognitive symptoms observed in PD. While the specific cause of dopamine loss in PD etiology is still unknown, cumulative evidence suggests that iron and copper accumulation in the brain, which leads to reactive oxygen species (ROS) production and neurotransmission disruption, play a key role in this disease. In addition, monoamine oxidases A and B (MAO-A and MAO-B, respectively) and catechol O-methyltransferase (COMT) decompose dopamine and contribute to the low levels of this neurotransmitter in PD patients.

Currently available drugs for the treatment of PD mainly aim at restoring brain dopamine levels and include the dopamine precursor levodopa, which is co-administered with COMT inhibitors to improve its brain bioavailability. When combined, these drugs boost cerebral dopamine levels and allow a symptomatic relief, but do not prevent neuronal death and thus have no net effect on disease progression. Moreover, COMT inhibitors in the market are associated with severe hepatotoxicity (tolcapone) and lack brain bioavailability (entacapone, opicapone). In this context, safe disease-modifying drugs to treat PD are urgently needed.

Recent clinical trials showed that deferiprone, an iron chelator used to treat thalassemia, improved symptoms and quality of life, suggesting a disease modifying effect in PD. By scavenging the excess iron in brain and redistributing it to other tissues in the CNS, deferiprone can provide a smart mode of iron chelation: it protects neurons from iron-induced cell death and yields a disease-modifying effect without causing systemic iron depletion. Moreover, unlike some COMT inhibitors, deferiprone can cross the blood-brain barrier (BBB) and presents effective antioxidant properties. This opens an exciting and unexplored window on CNS drugs.

With the aim of finding safe and effective pharmacotherapeutics for PD, deferiprone-based compounds were proposed as smart bifunctional drugs that can remove excess iron and copper and regulate the dopamine levels in the brain, and simultaneously act as antioxidant agents. Following the synthesis and structural elucidation of compounds **1,2, 5-8**, a thorough study of their physicochemical and pharmacological properties was carried out using RP-HPLC and spectroscopic techniques.

Overall, compounds derived from 2-methyl-4*H*-pyran-4-one (compounds **2**, **6** and **8**) positively stand out when compared to compounds derived from 3-hydroxy-4*H*-pyran-4-one (compounds **1**, **5** and **7**). In particular, compound **6** presents excellent drug-like, metal chelating and antioxidant properties. In addition, it displays adequate lipophilicity and is predicted to be BBB permeable. Additional studies concerning the BBB cross capacity using parallel artificial membrane permeability assay was planned to be performed, but due to time constraints, it couldn't be done.

Keywords: antioxidant activity, blood brain barrier, catechol-O-methyl transferase, chelating agents, deferiprone, monoamine oxidase, Neurodegenerative Disorders, Parkinson's Disease.

RESUMO

A Doença de Parkinson (DP) é a segunda doença neurodegenerativa (ND) mais comum depois da Doença de Alzheimer, estando associada à perda seletiva de neurónios dopaminérgicos na *substantia nigra* do cérebro. A diminuição dos níveis do neurotransmissor dopamina é responsável pelos sintomas motores e cognitivos observados na DP. Embora a etiologia na DP ainda seja desconhecida, evidências cumulativas sugerem que a acumulação de ferro e cobre no cérebro, que leva à produção de espécies reativas de oxigénio (ROS) e à perturbação da neurotransmissão, está associada ao desenvolvimento desta doença. Além disso, as Monoamina oxidases A e B (MAO-A e MAO-B, respetivamente) e a catecol O-metiltransferase (COMT) metabolizam a dopamina, contribuindo para os níveis baixos deste neurotransmissor em pacientes com a DP.

Os fármacos atualmente disponíveis para o tratamento da DP visam, acima de tudo, restaurar os níveis de dopamina cerebral. Estes incluem a levodopa, um precursor da dopamina, que é coadministrada com inibidores COMT para melhorar a sua biodisponibilidade no cérebro. A coadministração destes fármacos leva ao aumento dos níveis de dopamina no cérebro e permitem um alívio sintomático, mas não impedem a morte neuronal e, portanto, não têm qualquer efeito na progressão da doença. Além disso, os inibidores da COMT existentes no mercado estão associados a hepatotoxicidade grave (tolcapona) e falta de disponibilidade cerebral (entacapona e opicapona). Neste contexto, há uma grande necessidade de encontrar agentes modificadores da doença seguros para tratar a DP.

Ensaios clínicos recentes mostraram que a deferiprona, um quelante de ferro utilizado para tratar talassemia, melhora os sintomas e a qualidade de vida, sugerindo um efeito modificador da doença na DP. Ao quelatar o excesso de ferro no cérebro e redistribuí-lo por outros tecidos do sistema nervoso central (SNC), a deferiprona pode proporcionar um modo eficaz de quelação do ferro: protegendo os neurónios da morte celular induzida pelo ferro e produz um efeito modificador da doença sem causar a depleção sistémica do ferro. Além disso, ao contrário de alguns inibidores de COMT, a deferiprona pode atravessar a barreira hemato-encefálica (BHE) e apresenta boas propriedades antioxidantes. Isto abre uma janela promissora e inexplorada sobre os medicamentos dirigidos ao SNC.

Com o objetivo de encontrar um agente farmacológico seguro e eficaz para a DP, neste trabalho sintetizaram-se compostos baseados na deferiprona como fármacos bifuncionais inteligentes que podem remover o excesso de ferro e cobre, regulando os níveis

de dopamina no cérebro, e, simultaneamente, agir como agentes antioxidantes. Após a síntese dos compostos **1**, **2**, **5-8**, realizou-se um estudo exaustivo das suas propriedades físico-químicas e farmacológicas utilizando RP-HPLC e técnicas espectroscópicas.

De um modo geral, os compostos derivados da 2-metil-4*H*-piran-4-ona (compostos **2**, **6** e **8**) destacam-se positivamente em comparação com os compostos derivados de 3-hidroxi-4*H*-piran-4-ona (compostos **1**, **5** e **7**). Salienta-se que o composto **6** apresenta excelentes propriedades *drug-like*, de quelatação de ferro e cobre e antioxidantes. Adicionalmente, demonstra lipofilicidade adequada e previsões indicam que é capaz de atravessar a BBB. Foram planeados estudos adicionais relativos à capacidade de penetração da BBB, utilizando o ensaio de permeabilidade em membrana artificial paralela, mas devido a restrições de tempo, não foi possível realizá-lo.

Palavras-chave: agentes quelantes, atividade antioxidante, barreira hematoencefálica, catecol-O-metil transferase, deferiprona, doença de Parkinson, doenças neurodegenerativas, monoamina oxidase.

THESIS STRUCTURE

This thesis is organized in six chapters.

CHAPTER 1. *Introduction*. In this Chapter an introduction to the developed work can be found. A literature review concerning Parkinson's Disease, its etiology and the role and metabolism of dopamine in current therapies available for symptomatic treatment. The metal chelator deferiprone is introduced as well and its therapeutic potential. The Chapter also includes a brief introduction to drug design strategies commonly employed.

CHAPTER 2. *Materials and Methods*. Chapter containing a description of all the reagents, solvents and apparatus used in the synthesis of deferiprone-based compounds, as well as all the structural analysis and physicochemical tests carried out to assess drug-like properties.

CHAPTER 3. *Results and Discussion*. Includes a full structural and physicochemical analysis of the synthetized deferiprone-based compounds.

CHAPTER 4. *Conclusion and Future prospects*. Summary of the developed work together the highlights and future perspectives.

CHAPTER 5. *References*. List of all bibliographic references used in the previous chapters.

CHAPTER 6. *Appendix*. Additional data.

TABLE OF CONTENTS

LIST OF FIGURES

LIST OF TABLES

LIST OF ABBREVIATIONS

3-MT	3-methoxy-tyramine
3-OMD	3-O-methyl-levodopa
4-HQ	4-hydroxyquinoline
AD	Alzheimer's Disease
ADMET	Absorption, Distribution, Metabolism, Excretion and Toxicity
ALS	Amyotrophic Lateral Sclerosis
AT	Ataxia Telangiectasia
BBB	Blood Brain Barrier
BHE	Barreira hemato-encefálica
CAG	Three nucleotide repeat present in Huntington's Disease
CEMUP	Centro de Materiais da Universidade do Porto
CHI	Chromatographic Hydrophobicity Index
CMA	Chaperone-mediated Autophagy
CNS	Central Nervous System
COMT	Catechol-O-Methyltransferase
CSA	Camphor Sulphonic Acid
DCM	Dichloromethane
DDC	Dopa-decarboxylase
DEPT	Distortionless Enhancement by Polarization Transfer
DMSO	Dimethyl Sulfoxide
DNA	Desoxyribonucleic acid

DOPAC	3,4-dihydroxyphenylacetic acid
DOPAL	dihydroxyphenylacetaldehyde
DP	Doença de Parkinson
EC	Endothelial Cell
FAD	Flavin Adenine Dinucleotide
HBA	Hydrogen Bond Acceptors
HBD	Hydrogen Bond Donors
hMAO	Humam Monoamine Oxidase
HPLC	High Throughput Liquid Chromatography
HD	Huntington's Disease
HVA	Homovanilic acid
IAM	Immobilized Artificial Membrane
Km	Michaelis-Menten constant and corresponds to the concentration of substrate at half V_{max}
L-DOPA	3,4-dihydroxy-L-phenylalanine
MAO	Monoamine Oxidase
MB-COMT	Membrane Bound Catechol-O-Methyltransferase
MW	Molecular Weight
ND	Neurodegenerative Disorder
NMDA	N-methyl-D-aspartate
NMR	Nuclear Magnetic Resonance
NROTB	Non-Rotatable Bound Count
P-gp	P-glycoprotein
PD	Parkinson's Disease
ROS	Reactive Oxygen Species

RP-HPLC	Reverse Phase High Throughput Liquid Chromatography
S-COMT	Soluble Catechol-O-Methyltransferase
SAH	S-adenosyl-L-homocysteine
SAM	S-adenosyl-L-methionine
SNC	Sistema Nervoso Central
TH	Tyrosine hydroxilase
TLC	Thin Layer Chromatography
TMS	Tetramethylsilane
tPSA	Topological Polar Surface Area
UPS	Ubiquitin Proteosome System
Vmax	Velocity where all the enzyme is bound to the substrate i.e., the enzyme is saturated

CHAPTER I – Introduction

1.1 Neurodegenerative Diseases

The brain is the most complex organ in the human body. Together with the spinal cord, they constitute the Central Nervous System (CNS). The CNS's action can be separated into three major phases: receiving input from the periphery, make sense of those inputs and act upon them. Therefore, the CNS's functions are very diverse and range from movement to maintenance of homeostasis through body temperature, blood pressure, heart rate and higher intellect functions such as thoughts, memory and problem solving skills [12]. Neurons are the fundamental cells of the nervous system, and our brains have billions of them. They are capable of communicating with each other and other target cells by electrochemical signals. Besides neurons, glial cells (also known as glia or neuroglia) can also be found and these have a more supporting role: they maintain the extracellular environment, improve signal conduction and protect neurons [13].

Neurodegenerative diseases (NDs) are among the most common and debilitating diseases of our time. These are complex diseases that jeopardize the normal function of the CNS due to gradual and progressive loss of neuronal cells and synaptic connections. The CNS dysfunction can lead to the progressive loss of sensory, motor and cognitive functions. The most common NDs include Alzheimer's disease (AD), Parkinson's disease (PD), Amyotrophic Lateral Sclerosis (ALS), and Huntington's disease (HT).

Neurodegenerative diseases (NDs) are multifactorial, and the specific mechanisms that trigger NDs are highly diverse and unclear. However, it is well established that ageing and genetic history are the primary risk factors for neurodegeneration. Environmental factors such as exposure to specific metals, pollutants and pesticides may also play key roles [14]. Due to their complex nature, there is still no cure for NDs and therapeutic options for patients remain very limited, providing only symptomatic relief [12, 15].

1.2. Parkinson's Disease

1.2.1. Symptoms and Epidemiology

Parkinson's Disease (PD) was first described as *paralysis agitans* back in 1817 by the English surgeon James Parkinson. It is currently the second most common neurodegenerative disorder after AD [16] and the most common movement disorder [17]. Parkinson's Disease (PD) is characterized by a progressive loss of dopaminergic neurons, which leads to a

decrease in the levels of the neurotransmitter dopamine. Figure 1 shows how dopamine neurotransmission is compromised in the neurons of PD patients versus normal neurons.

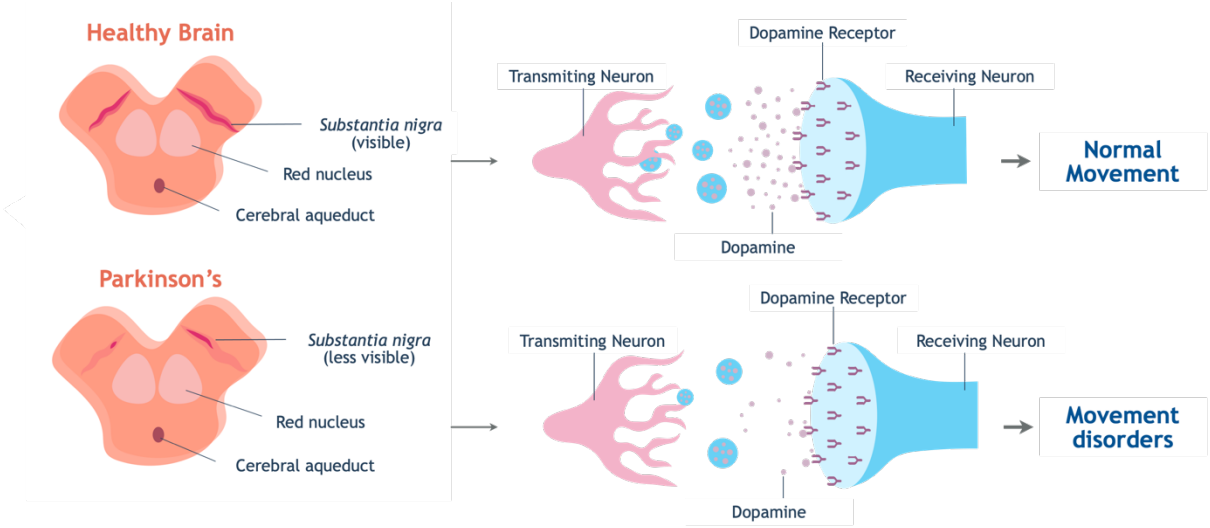

Figure 1: Substantia nigra *coloration and dopamine levels in normal neurons vs. neurons of PD patients. Adapted from [4].*

Dopamine is a neurotransmitter that plays a fundamental role in the CNS, regulating mood, motivation and movement. Its dysfunction is present in several nervous system diseases [18]. Its production takes place in the brain's *substantia nigra*, ventral tegmental area and hypothalamus [1]. Dopamine is a monoamine neurotransmitter, more specifically a catecholamine, just like norepinephrine and epinephrine (Figure 2). This class of neurotransmitters share biochemical characteristics: small size, charged nature and incapacity to cross the Blood Brain Barrier (BBB). They are synthesized from the amino acid tyrosine through a short metabolic route and regulated by enzymatic reactions. [18-20]

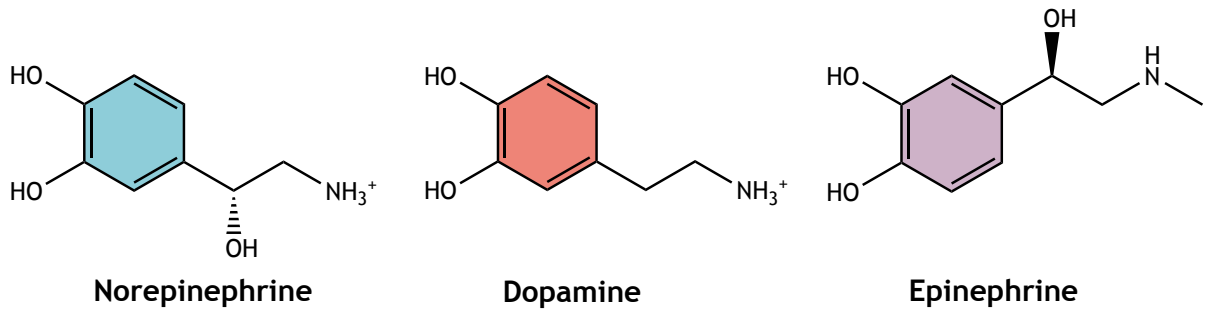

Figure 2: Chemical structures of norepinephrine, dopamine and epinephrine.

Dopamine is synthetized from tyrosine in the cytosol in two steps (Figure 3). The biosynthesis begin with the hydroxylation of tyrosine to 3,4-dihydroxy-L-phenylalanine (L-DOPA) by tyrosine hydroxylase (TH). Then, L-DOPA decarboxylation by dopa decarboxylase (DDC) yields dopamine. Tyrosine hydroxylation by TH is the rate limiting step of this process.

[1, 19, 21]. Following the activation of dopamine receptors, dopamine is metabolized by monoamine oxidases A and B (MAO-A and MAO-B, respectively) and catechol-O-methyl transferase (COMT).

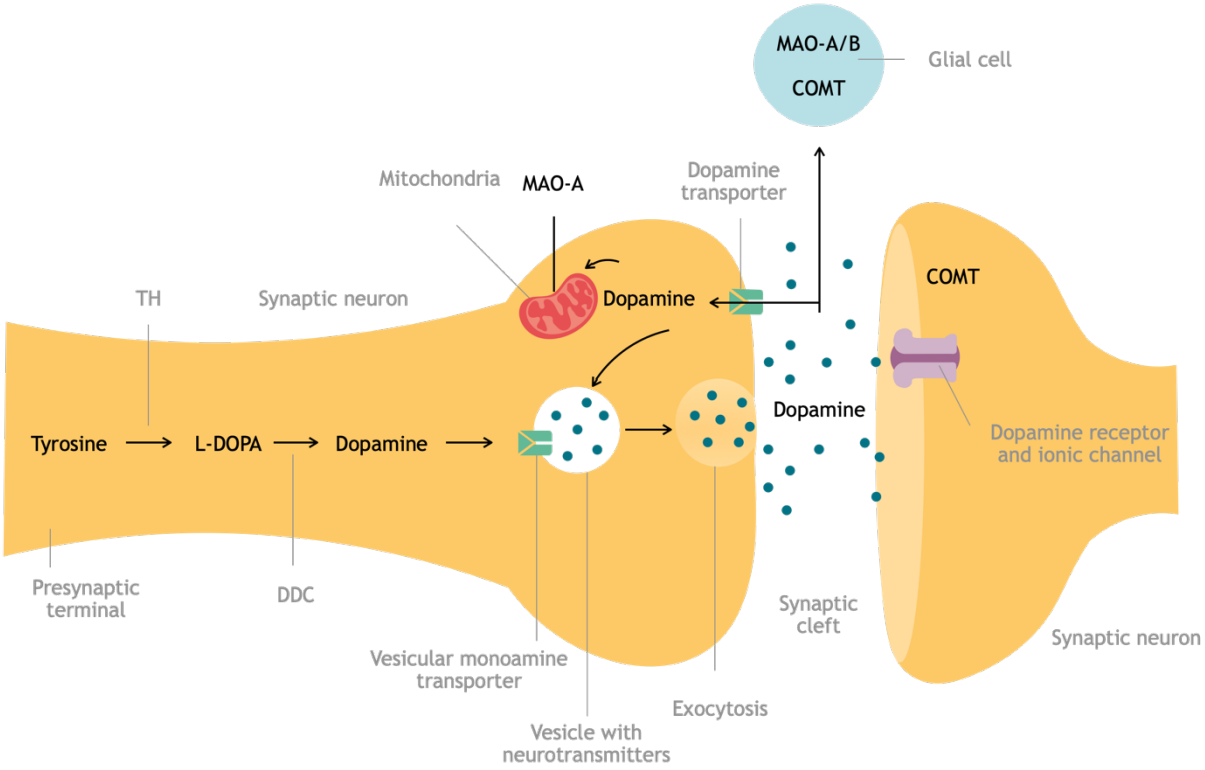

Figure 3: Dopamine synthesis and metabolism. Adpated from Olguín et al [1, 2].

Parkinson's Disease (PD) is mostly sporadic, resulting from a complex interplay between genetic susceptibility and environmental factors, and comprises about 95% of PD cases, [22]. However, it can also be caused by familiar genetic mutations representing 5% of PD cases [23]. Mutations in the gene for α-synuclein, SNCA/PARK1, cause an inherited form of PD. Genes like PINK1 and PRKN (gene that encodes for the protein parkin) are critical for mitochondrial quality control and mutated versions of these genes are also implicated with autosomal recessive PD and/or parkinsonism [24]. There is also evidence that mutations in the genes LRRK2 (regulates mitochondrial function and morphology), UCHL1 (encodes deubiquitinating enzyme and is required for axonal integrity) and DJ-1 (important for the inhibition of α-synuclein aggregates and protection from oxidative stress) are associated with familial forms of PD through dopaminergic neurodegeneration [25].

Clinical manifestations of PD include four cardinal motor symptoms commonly grouped under the acronym TRAP: Tremor at rest, Rigidity, Akinesia (or bradykinesia) and Postural instability (Figure 4). Tremors at rest are one of the most common PD symptoms, described as rhythmic involuntary movement of a body part and is usually unilateral. Rigidity

refers to the increased resistance and stiffness to movement of body parts. Bradykinesia is characterized by slow voluntary movements and is considered a hallmark of basal-ganglia disorders. Postural instability relates to balance impairments that compromise their ability to maintain an appropriate posture and in later stages of the disease patients experience higher rates of falls. [25, 26]

Parkinson's Disease (PD) symptomatology also comprehends non-motor symptoms (Figure 4), that may precede motor symptoms by years. These are diverse and range from olfactory dysfunction, cognitive problems (apathy, depression, anxiety and hallucinations), sleep disorders, psychiatric symptoms, bowel problems and dibbling of saliva. Aside from appearing during the disease progression, non-motor symptoms are also common side effects of drug therapies. For example, common side effects of dopaminergic drugs are nausea, psychosis and impulse control disorders (such as compulsive shopping, pathological gambling or binge eating) [11, 26-28].

Figure 4: Some of the most common motor (above) and non-motor (below) PD symptoms. Adapted from Váradi et al. [5]

The appearance of symptoms can be organized in three distinct stages: preclinical, prodromal and clinical (Figure 5). The preclinical stage corresponds to the starting point of degeneration in the *substantia nigra* and, at this point, there are no clinical manifestations. Neuronal loss progresses as patients reach the prodromal stage where non-motor symptoms start to be expressed. Over the past years, symptoms like rapid eye movement sleep behavior disorder, constipation, olfactory loss and depression have gained a new importance and have been increasingly associated with a higher risk of developing PD [5].

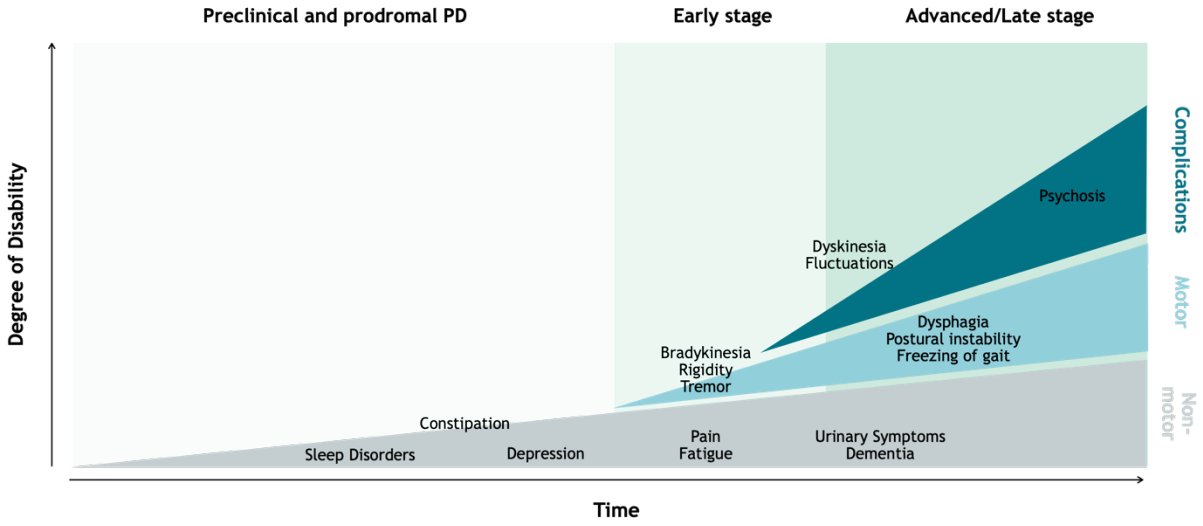

Figure 5: Symptoms over the time course of Parkinson's Disease progression. Adapted from Kalia et. al [11].

Patients only enter early-stage PD by the time 40%-60% of dopaminergic cells are lost and motor symptoms start manifesting. Tremors are usually the first motor symptoms to be noticed by patients [29]. Even though they can be managed with medication, early-stage tremors are known to impact negatively multiple aspects of daily life from personal relationships to self-esteem and, of course, their toll on tasks and overall daily life. Patients in more advanced stages of the disease are fully dependent and need 24-hour supervision, taking a toll on family relationships and overall quality of life [30].

The World Health Organisation recognized that PD affects individuals all around the world with an age-adjusted prevalence of 72-258.8 per 100.000 inhabitants per year [31]. The average age at PD onset is between 55 and 65 years old and the median duration of the disease from diagnosis to death is 15 years. Interestingly, it has been shown that men are more affected by this disorder than women and that the latter normally present milder symptoms and slower progression of motor problems [23].

Over the past generation, the global burden of the disease has more than doubled: in 1990 there were 2.5 million individuals with PD, in 2016 the number rose to 6 million and 2020 data show that PD now affects around 9.4 million people globally and numbers can rise up to more than 17 million in 2040 [32-34]. Parkinson's Disease (PD) poses an increasingly higher public health burden. In fact, NDs like PD are expected become the second most common cause of death by 2040, surpassing cancer [35].

As the disease progresses, so does the financial burden on both healthcare system and patients. Direct costs include patient care and drug prescriptions, while indirect costs tend to be higher, comprising productivity loss, reduced wages and carer burden [36]. Due

to the loss of equilibrium, PD are prone to fall-related fractures. A study carried out in Germany assessed that the mean revenue per patient and injury was 9295€ and the mean length of stay in the hospital was 13.5 days [37]. Parkinson's Disease (PD) is fueled by aging populations and, considering the increased life expectancy, better life quality and healthcare services, it is safe to conclude that the number of individuals affected by PD will continue to follow an upwards trend.

1.2.2. Hallmark Pathologies

In terms of pathophysiology, PD is primarily characterized by the loss of dopaminergic neurons (dopamine producing). The development of Lewy bodies in specific areas of the *substantia nigra* is also a major hallmark in PD. Lewy bodies are abnormal intracellular aggregates in neurons that contain deposits of the protein α-synuclein. When Lewy bodies are found in the brain stem and *substantia nigra* (movement control areas) there is loss of dopaminergic neurons [11, 25, 38]. These pathological features normally precede motor symptoms by many years and, by the time patients become symptomatic, a significant neuronal degeneration in the *substantia nigra* occurred [39].

Figure 6: Pathophysiological mechanisms that contribute to PD development and progression.

In addition to neuron death, NDs are also associated with the misfolding, aggregation and accumulation of proteins in specific areas of the brain. Such accumulation leads to cellular dysfunction, loss of connections and ultimately, brain damage [40]. In the particular case of PD, there is aggregation of α-synuclein, primarily. This protein is not only associated with sporadic forms of the disease, but also with genetic PD due to mutations in its encoding

gene (SNCA/PARK1). These aggregates take form in Lewy bodies and interfere with microtubule-based transport mechanisms, leading to synaptic dysfunction and overall disruption of the neuronal homeostasis [41].

There are several proteolytic systems responsible for the degradation and clearance of mislocated, misfolded, mutant and/or damaged proteins such as such as the ubiquitin proteasome system (UPS), chaperone-mediated autophagy (CMA) and autophagy-lysosomal pathway [42]. Soluble α-synuclein can be degraded through both UPS and CMA routes, but that does not apply for insoluble α-synuclein, which is the main component of Lewy bodies. Several lines of evidence have associated proteasomal dysfunction and reduction of several lysosomal components to α-synuclein accumulation in PD [25, 43].

Mitochondrial dysfunction and oxidative stress also contribute to neurodegeneration in PD. Healthy neurons have the ability to remove damaged mitochondria through the process of mitophagy. In familial forms of PD, mutations in genes like PINK1 and PRKN result in a reduced ability to perform quality control mechanisms such as mitophagy. Mutations in DJ-1 also affect mitochondria, as it is involved in oxidative stress responses [24, 44]. In addition to decreased energy supply, mitochondrial dysfunction is also intimately associated with oxidative stress. Damaged mitochondria produce higher levels of reactive oxygen species (ROS), which are highly toxic and are associated with increased oxidative damage of biomolecules (DNA, proteins, lipids) and disruption of signaling cascades [41].

Calcium (Ca^{2+}) homeostasis is fundamental for the normal functioning of neurons thus having implications in both synaptic activity and neuronal survival. There is growing evidence that the dysregulation of Ca^{2+} homeostasis is associated with the pathogenesis of PD. In fact, the Ca^{2+} pathway is associated with mitochondrial function, but also with oxidative stress, both of which play a major role in PD pathogenesis [45].

Another cellular hallmark of PD is the disturbance of iron metabolism. Even though iron levels increase with age, PD patients show even higher iron accumulation levels [46]. Free iron can catalyze Harber-Weiss and/or Fenton-like reactions (Figure 7). These are catalytic chemical reactions between hydrogen peroxide and iron ions (Fe(II) and/or Fe(III))

$$Fe^{3+} + O_2^{-\cdot} \longrightarrow Fe^{2+} + O_2$$

$$Fe^{2+} + H_2O_2 \longrightarrow Fe^{3+} + OH^- + OH^{\cdot}$$

Figure 7: Example of a Harber-Weiss (above) and a Fenton (below) reaction.

that result in highly toxic hydroxyl radicals such as •OH, which are the most damaging type of ROS [47]. Other metals such as copper and zinc have also been implicated in oxidative stress associated with NDs [48].

1.2.3. Etiology, Risk Factors and Diagnosis

The ultimate PD causes are unknown but risk factors include: ageing, family history and exposure to environmental chemicals and pesticides [39]. Ageing is the primary risk factor for PD, and the disease rarely affects people younger than 50 years old [49]. As we age there is a progressive loss of physiological integrity, which increases the vulnerability to several pathologies due to increased mitochondrial dysfunction, loss of proteostasis, cellular senescence and altered intercellular communication [50]. When it comes to family history, first degree family members of PD patients present a 2-3 fold higher risk of developing the disease as well [49]. There are also some well-known environmental risk factors such as exposure to different substances like toxins (paraquat and rotenone), methanol, heavy metals and carbon monoxide poisoning [5, 14].

There are no definitive biological or imaging markers to diagnose PD directly. Thus, diagnosis is based on physical exams and health history once motor symptoms arise. This means neurodegeneration can go for a decade until it is properly identified. The detection and recognition of early non-motor symptoms during prodromal PD would be the key timepoint to counteract the expression of other symptoms [5].

Once motor symptoms develop some helpful diagnostic features include neuromuscular dysfunction, rigidity and tremors [51]. Magnetic resonance imaging and other imaging studies can be used to exclude other conditions.

1.3. Parkinson's Disease Pharmacotherapy

1.3.1. Dopamine metabolism

When L-DOPA in synthetized peripherally through tyrosine hydroxylation, it can either be decarboxylated by a DDC to dopamine or O-methylated by COMT, which results in the production of 3-O-methyl-levodopa (3-OMD). Both L-DOPA and 3-OMD are able to cross the BBB. However, 3-OMD displays a much longer elimination half-life than L-DOPA (3-OMD: 12 hours; L-DOPA: 2 hours), which means it may compete with L-DOPA to cross the BBB through protein-mediated transport [52].

Once L-DOPA reaches the brain, it can be decarboxylated into dopamine by DDC. Then, dopamine is sequestered into synaptic vesicles which are stored in the presynaptic terminal until it is released into the synaptic cleft. Dopamine release is usually triggered by changes in the membrane potential and occurs through exocytosis. Once dopamine reaches the synaptic cleft, dopamine receptors can be found in both post and presynaptic neurons. Postsynaptic receptors recognize and interact with dopamine in order to cause depolarization of the postsynaptic cell and the initiation of a new action potential. Dopamine can then either be recycled into the synaptic vesicles of the pre-synaptic neuron or metabolized by neurons and glial cells [53].

Glial cells surrounding the synaptic cleft can take up and decompose dopamine with MAOs and/or COMT. Monoamine oxidases (MAOs) catalyze the oxidative deamination of dopamine into dihydroxyphenylacetaldehyde (DOPAL), with production hydrogen peroxide and ammonia. Dihydroxyphenylacetaldehyde (DOPAL) can be further metabolized by aldehyde dehydrogenase into 3,4-dihydroxyphenylacetic acid (DOPAC), whose high concentrations have been reported to be cytotoxic [54]. The O-methylation of DOPAC by COMT leads to the production of homovanilic acid (HVA). Alternatively, COMT can metabolize dopamine to 3-methoxy-tyramine (3-MT), which in turn can then be converted into HVA by MAOs [55]. Since, high levels of HVA in the cerebrospinal fluid have been correlated with PD, it is considered a potential biomarker for disease detection [56-58].

1.3.2 Pharmacotherapy

Currently available therapies for PD can address the disease symptomatology but are unable to stop the neurodegenerative process. Pharmacological therapies are the mainstay of treatment and dopaminergic therapies remain the gold standard for symptomatic management of PD [11]. The most prevailing therapeutic approach is related to the enhancement of dopamine concentration by administering L-DOPA, a precursor of dopamine, and targeting dopamine regulators, such as COMT, MAO-B, DDC and dopamine receptors (Figure 8).

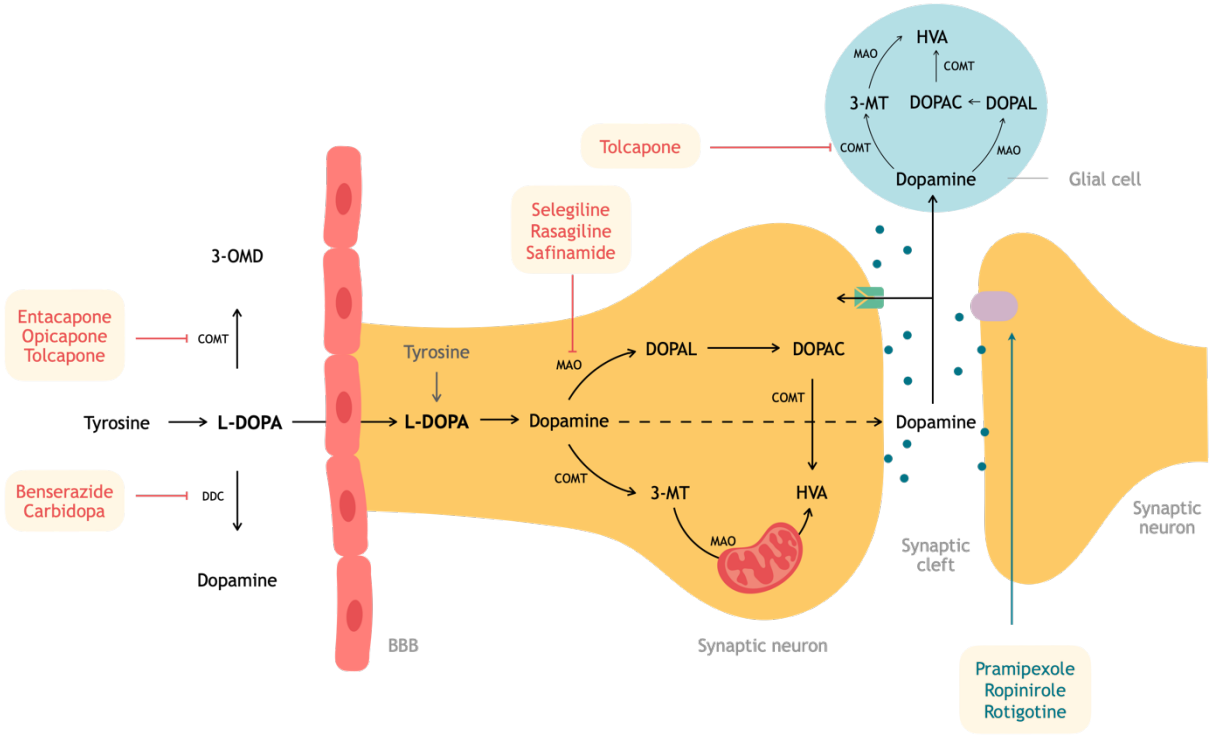

Figure 8: Mechanism of action of the different classes of dopaminergic drugs, adapted from Youdim [6].

Despite years of research, L-DOPA is still the most effective drug treatment since its establishment in 1970. However, L-DOPA has a low bioavailability and a short half-life (60-90 min) [59], and, consequently, multiple daily administration is required. Large doses are accompanied by adverse side-effects, such as anxiety and nausea. The co-administration of L-DOPA with inhibitors to the aforementioned targets, like DDC inhibitors (carbidopa, Sinemet®, or benserazide, Madopar®) (Table 1), reduce its peripheral metabolism and, consequently, the side effects [21]. However, it should be noted that prolonged co-administration with these inhibitors also has side-effects [60].

Table 1 Current dopaminergic drugs

Class	Drug	Structure	Increase of dopaminergic activity
Dopamine precursor	Levodopa	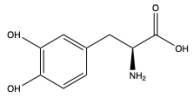	Increase the endogenous production of dopamine
DDC Inhibitors	Benserazide	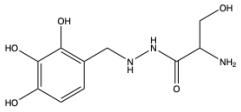	Reduce levodopa's peripheral metabolism
	Carbidopa	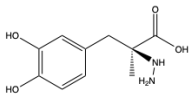	
COMT inhibitors	Entacapone	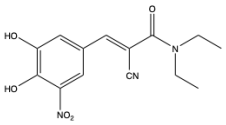	Prevent dopamine and L-DOPA metabolism in the CNS (tolcapone) and/or the peripheral tissues (entacapone and opicapone)
	Tolcapone	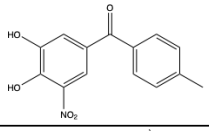	
	Opicapone	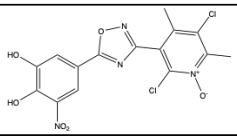	
MAO inhibitors	Selegeline	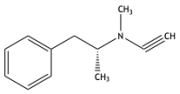	Prevent dopamine decomposition in the CNS
	Rasagiline	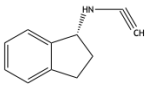	
	Safinamide	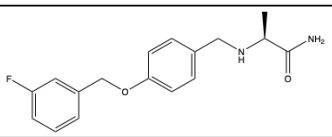	
Dopamine receptor agonists	Ropinirole	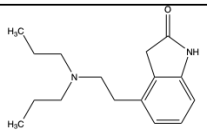	Mimic the effects of dopamine
	Pramipexole	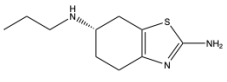	
	Rotigotine	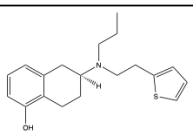	

Dopamine agonists were developed in an effort to avoid the side effects of L-DOPA in early-stage patients. Although they are associated with a lower risk of bradykinesia, these drugs have the added benefit of being independent of enzymatic activity [61]. Dopamine agonists work by mimicking the actions of dopamine on its receptors when levels are low. Hence, the brain is misled and acts as if it is receiving the amount of dopamine needed [62].

Nevertheless, new pharmacological targets have been studied and include neuroinflammation, mitochondrial dysfunction, oxidative stress and α-synuclein aggregation [11]. Additionally, cellular therapies are being developed in order to either rescue damaged neurons or to replace them [63]. In fact, a clinical trial involving induced pluripotent stem cell-derived dopaminergic neuron progenitors has been recently authorized. Pre-clinical data showed no tumorigenicity or toxicity of the cells and test animals showed behavioral improvements [64]. In addition to cellular approaches, viral vectors are also promising for regenerative treatment of PD. These vectors would be a vehicle for genes encoding for key enzymes in the dopamine biosynthesis, such as DDC and TH [65].

1.4. Parkinson's Disease and Catechol-O-methyl transferase

1.4.1. Catechol-O-methyl transferase

Catechol-O-methyl transferase (COMT) is a single-domain metabolic enzyme with two isoforms, one soluble cytosolic (S-COMT) and a membrane-bound (MB-COMT) form, both of which are encoded by the same gene. Despite not being tissue-specific, S-COMT and MB-COMT present different distribution in the organism. While S-COMT is highly expressed in peripheral organs such as the liver, MB-COMT is predominant in the brain [9]. The general function of COMT is the degradation of endogenous and exogenous catechols. COMT's active site doubles as catalytic site, binding both Mg^{2+} ion and the catechol substrate. The S-adenosyl-L-methionine (SAM) binding region is more buried in the structure. X-ray and kinetic studies showed that there is a sequential binding mechanism during the methylation reaction, starting with the binding of SAM, then the Mg^{2+} and finally the catechol substrate [66]. Being a Mg^{2+} dependent methyltransferase, COMT catalyzes the transfer of a methyl group from SAM to a hydroxyl group of a catechol substrate (such as catecholamines). The reaction products are the O-methylated catechol and S-adenosyl-L-homocysteine (SAH) (Figure 9) [67].

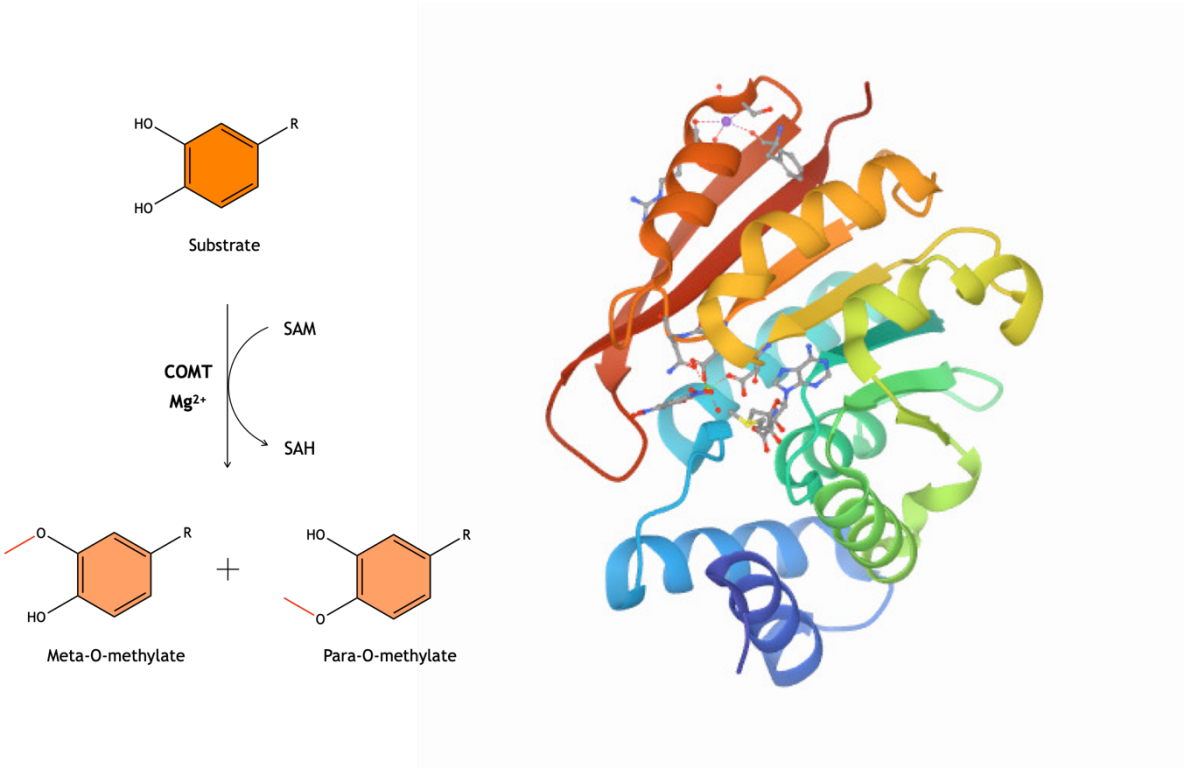

Figure 9: Schematic representation of O-methylation catalyzed by COMT (on the left) and three-dimensional structure of the enzyme (on the right). The S-adenosyl-L-methionine co-substrate (SAM), an inhibitor (3,5-dinitrocatechol) and the magnesium and potassium ions are depicted (PDB: 108V).

S-COMT and MB-COMT share biochemical properties, such as their affinity to SAM, magnesium dependency, calcium inhibition and optimal pH for enzyme activity [66]. The main difference between the two isoforms is the presence of an extra amino terminal peptide on MB-COMT that enables membrane anchoring. Thus, while S-COMT has a molecular weight of 24.3 kDa and 221 amino acid residues, MB-COMT presents a molecular weight of 24.7 kDa and 50 extra amino acids, making a total of 271 amino acids. Moreover, they have very distinct kinetics (Figure 10). While MB-COMT presents a higher substrate affinity (meaning a lower K_M[1]), S-COMT has a higher metabolic capacity (i.e., higher V_{max}[2]). Thus, while MB-COMT is involved in the termination of catecholaminergic neurotransmission at low physiological levels, S-COMT is capable of acting when a higher metabolic activity is required, such as sudden increase of endogenous and exogenous catecholamine levels [9].

[1] K_M: Michaelis-Menten constant and corresponds to the concentration of substrate at half V_{max}

[2] V_{max}: velocity where all the enzyme is bound to the substrate i.e., the enzyme is saturated

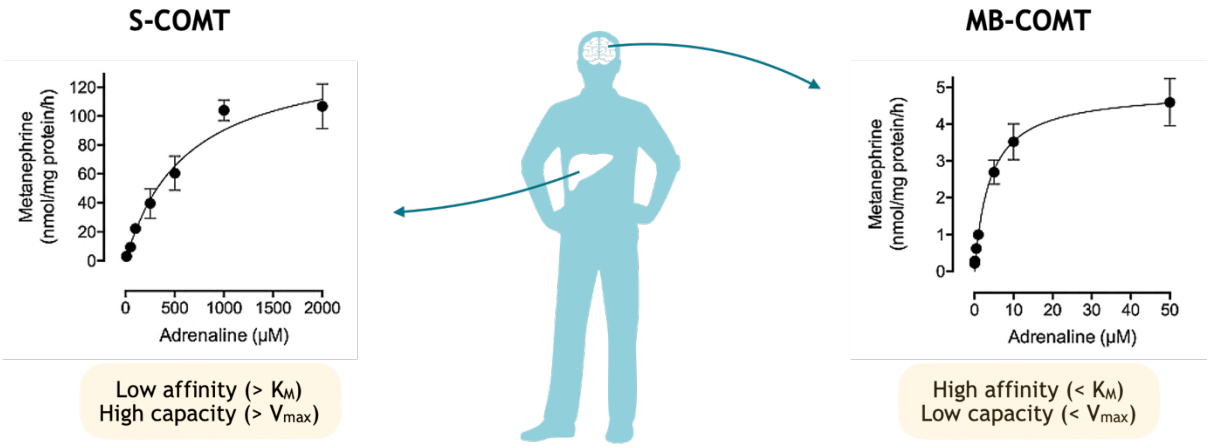

Figure 10: COMT isoform distribution and kinetics, adapted from Silva et. al [9].

1.4.3. Catechol-O-methyl transferase inhibitors

Catechol-O-methyl transferase (COMT) inhibitors are a widespread pharmacological therapy for PD. By inhibiting the peripheral degradation of L-DOPA, COMT increases the plasma half-life of this dopamine precursor. The first generation of COMT inhibitors arose in 1970 and they were based on simple catechol scaffolds, such as caffeic acid. Unfortunately, these inhibitors presented unsatisfactory pharmacokinetics, selectivity and toxicity [9].

The discovery of nitrocatechols led to the second generation of COMT-inhibitors, the first to be commercially available: tolcapone and entacapone, (Figure 11, with the nitrocatechol pharmacophore highlighted in yellow). Tolcapone, trade name Tasmar®, is a non-selective COMT inhibitor able to cross the BBB, acting both in peripheral and cerebral COMT. Despite its promising pharmacological properties, the administration of tolcapone is very restricted due to the high risk of hepatotoxicity. Tolcapone was withdrawn from the market for a short period of time as a result of such side effects. However, the absence of other equally effective and safer drugs led to its reintroduction. The clinical use of tolcapone is restricted to patients who do not respond to other peripheral inhibitors. Entacapone, trade name Comtan®, is a selective peripheral COMT inhibitor. Although it is less potent and presents shorter duration of action than tolcapone (less than 1 hour versus 2-3h, respectively [66]), it is not associated with hepatotoxicity. In 2003, tablets containing levodopa, carbidopa (DDC inhibitor) and entacapone, trade name Stalevo®, were approved for PD patients. When used as an early-stage levodopa therapy, this triple combination can delay the onset dyskinesia [68, 69].

Opicapone, tradename Ongentys®, is a potent, reversible peripheral COMT inhibitor, approved by the European Medicines Agency in 2016. Its administration is indicated as adjunctive therapy to levodopa and carbidopa in PD patients who have reached end-dose and symptoms are yet to be stabilized. Opicapone was shown to maintain significant COMT inhibition even after 24h. Thus, while tolcapone and entacapone may require frequent administration (more than 3 times a day), opicapone is only administered once daily. Furthermore, it presents a lower cytotoxic risk than second generation inhibitors. Opicapone is a pyridine-N-oxide derivative, structurally unrelated to catechols and its unique characteristics allow it to be presented as the first third generation COMT inhibitor [69-71].

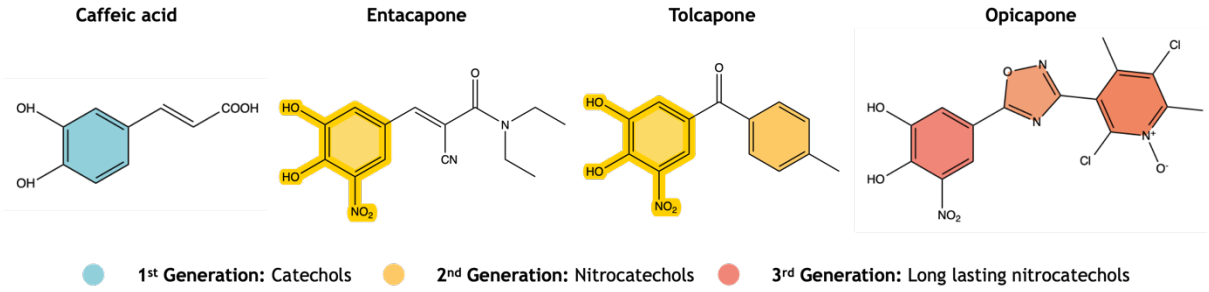

Figure 11: The structures of COMT inhibitors through generations.

1.5. Parkinson's Disease and Monoamine Oxidase

1.5.1. Monoamine Oxidase enzyme

Monoamine oxidases are flavin adenine dinucleotide (FAD)-containing enzymes located in the outer mitochondria layer. In the CNS, MAOs deaminate monoamine neurotransmitters such as serotonin, dopamine, norepinephrine and epinephrine, which is crucial for the correct functioning of synaptic neurotransmission. However, neurotoxic

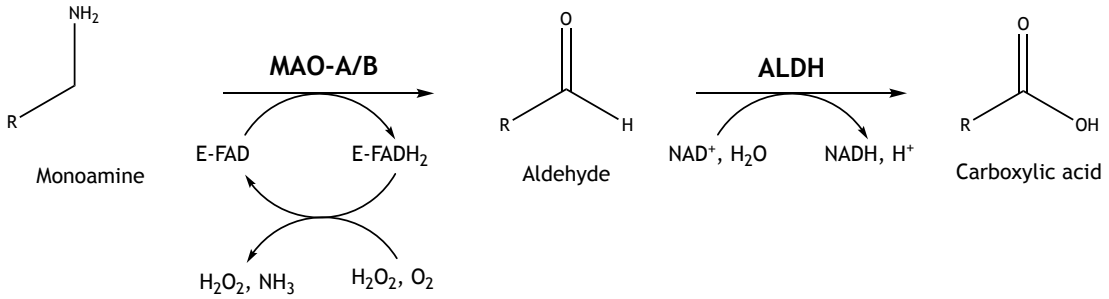

Figure 12: Oxidative deamination catalyzed by MAOs.

species such as hydrogen peroxide, ammonia and aldehydes (Figure 12) are formed as byproducts during MAO activity [72]. Therefore, unregulated MAO activity may trigger mitochondrial damage which is associated with the development and progression of NDs.

Similarly to COMT, MAO has two isoforms: MAO-A and MAO-B (Figure 13). These isoenzymes are encoded by distinct genes, sharing a homology of around 70% and presenting distinct tissue and cell distribution, substrate selectivity and inhibitor sensitivity [73]. MAO-A is predominantly found in the liver, skin and placenta, and its substrates include serotonin and norepinephrine. On the other hand, MAO-B is the main isoform present in brain tissues and its substrates include phenylethylamine and methylhistamine. Despite having different preferential substrates, dopamine is a substrate for both isoenzymes. Their active sites have different shapes, which dictates their distinct substrate and inhibitor selectivity [74, 75].

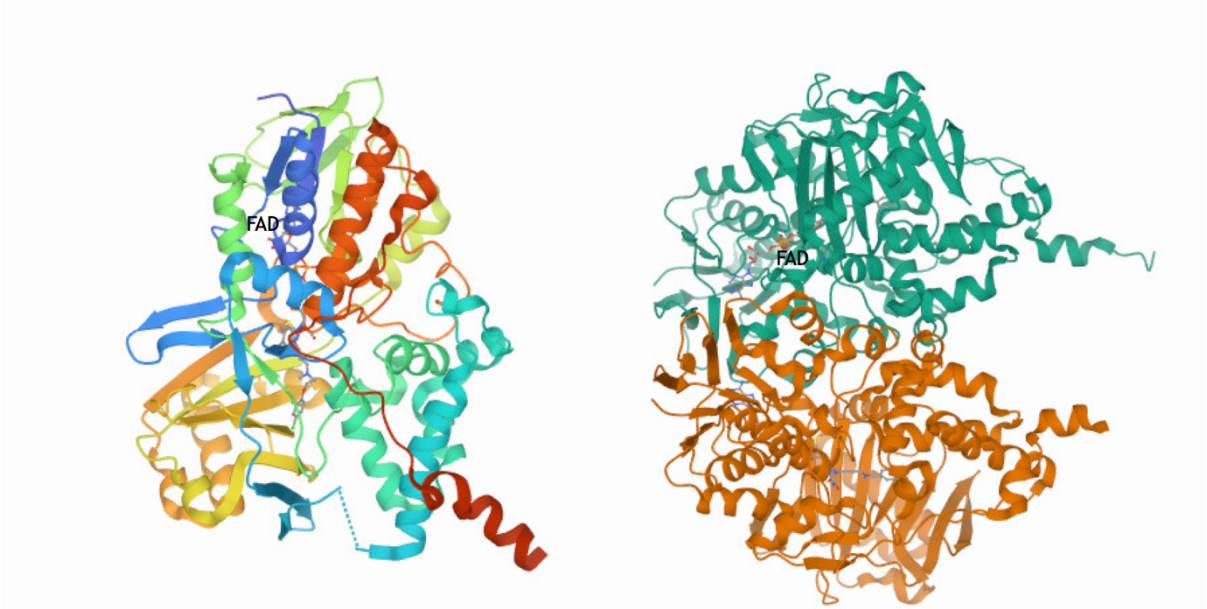

Figure 13: Crystaline structures of MAO-A in complex with clorgyline (PDB: 2BXS) (on the left) and MAO-B (PDB: 1GOS) (on the right). The FAD co-substrate is also depicted in both structures.

1.5.2. Monoamine oxidase inhibitors

It was shown that the role of MAOs in the brain is related to several neurological disorders such as AD, PD and depression. Thus, MAO inhibitors have a wide range of possible therapeutic uses. As a matter of fact, they were one of the first available antidepressants. In addition, MAO-B inhibitors (Figure 14) are commonly used to manage PD symptoms as an coadjutant to L-DOPA, with comparable efficacy to COMT inhibitors [6, 76].

The activity and density of MAOs increase with ageing, leading to increased generation of hydrogen peroxide from the oxidative deamination. Thus, in addition to the

ability to restore dopamine levels, MAO inhibitors can decrease oxidative stress in the brain by reducing the production of damaging ROS [77].

Selegiline, tradename Zelapar®, is a selective and irreversible MAO-B inhibitor. Selegiline has been available for over 30 years for the treatment of motor symptoms in PD and, if administered in early stages of the disease, it may delay the requirement for L-DOPA therapy [78]. In addition to the MAO inhibitory activity, selegiline displays antioxidant, anti-apoptotic and neurotrophic properties. Unfortunately, it presents poor bioavailability and can be metabolized into amphetamine, which is neurotoxic [79].

Rasagiline, tradename Azilect®, is a selective and irreversible MAO-B inhibitor. Studies showed that rasagiline improves motor function and can be administered for at least one year as monotherapy in the early-stage PD before L-DOPA is needed [76]. Comparing to selegiline, rasagiline cannot be metabolized to neutrotoxic metabolites [80] and is up to 15 times more potent [78].

Safinamide, trade name Xadago®, is a selective and reversible MAO-B inhibitor. Safinamide presents a selectivity for MAO-B superior to selegiline and rasagiline. Its underlying mechanism is associated with the blockage of sodium and voltage gated calcium channels. In addition, safinamide presents an anti-glutamatergic action which is thought to be related to a decrease in dyskinesia [78, 81, 82].

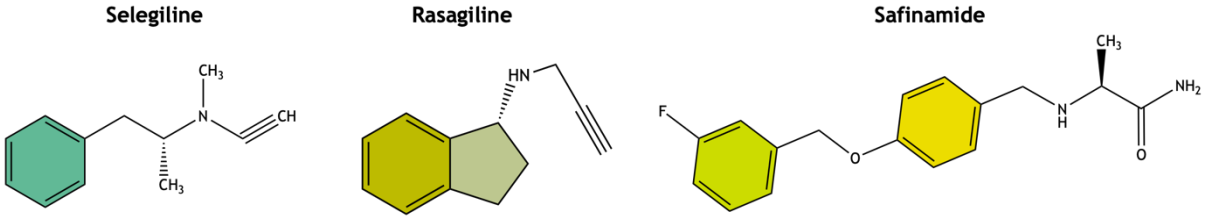

Figure 14: Structure of MAO-B inhibitors available for PD pharmacotherapy.

1.6. Metal Chelators

Lhermitte et al. described back in 1924 that the brains of people suffering from parkinsonism contained larger amounts of iron when compared to normal brains [83]. Since then, it has been demonstrated that there is iron deposition in the neurons of the *substantia nigra* of PD patients [63]. Other essential metal ions such as copper and zinc have also been studied [84].

As described in section 1.2.2., free iron may lead to excess ROS production through Fenton-like reactions. To prevent increased oxidative stress, several metal chelators, i.e., a molecule capable of forming stable coordination complexes with the metal ion in question, have been studied. A metal chelator is then expected to act as a scavenger by removing the metal ion and facilitating its elimination. An ideal metal chelator should gather the following characteristics: oral activity, low cost, suitable hydrophobicity in both ligand and formed complex and no redox activity [84].

Deferiprone (1,2-dimethyl-3-hydroxypyridin-4-one) (Figure 15) is an orally active bidentate iron chelator with low molecular weight, favorable hydrophobicity and neutral charge. These features enable good permeation across membranes, including those present in mitochondria and in the BBB. Pharmacological therapies with deferiprone were already established for patients with thalassemia major and Friedreich's ataxia [85].

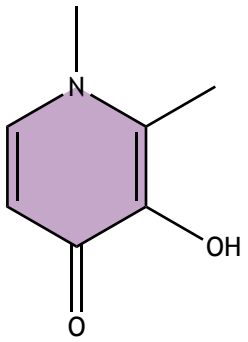

Figure 15: Chemical structure of deferiprone.

Deferiprone is capable of binding to iron in the active site of COMT and TH, inhibiting them [86]. Thus, the behavior of deferiprone as an iron chelator for the treatment of PD has also been studied. The first to present clinical evidence of the efficacy of deferiprone's iron chelation for human PD was Devos et. al, [87]. After oral administration of deferiprone for 12 months in patients with PD, iron deposits in the *substantia nigra* were dramatically reduced. In another clinical study, brain iron content changes and PD clinical status demonstrated that short-term administration of deferiprone is safe for PD patients [88]. Results showed decreased iron levels in specific brain regions, supporting the therapeutic potential of deferiprone as an iron chelator for PD.

1.7. Drug Design Strategy for Central Nervous System

1.7.1. The role of the Blood Brain Barrier

The BBB is a complex and dynamic vascular structure that acts as a physiological barrier between the CNS and the peripheral blood circulation. It controls the exchange of substances between circulating blood and the CNS [13]. The BBB must be intact to ensure that the correct microenvironment for neuronal function is maintained. For instance, oxidative stress can compromise the BBB's integrity and, consequently, increase its permeability. The disruption of the BBB's integrity has been observed in NDs such as PD and lead to further neuronal dysfunction and degeneration [89, 90].

The endothelial cells, ECs, that constitute the BBB are characterized by the presence of tight junctions and specific polarized transport systems. Tight junctions seal the ECs and represent the main physical paracellular barrier in the BBB, selectively restricting the flux of blood-borne molecules to the brain [91]. These blood vessels are the core anatomical element of the BBB. The ECs' monolayer is covered by a basement membrane in which pericytes and astrocytes are embedded. Together with other extracellular matrix components, these cells support the BBB structurally and functionally. Neurons and microglia play an important role in the barrier functions of the BBB and are capable of interacting with the other core elements [89]. These five types of cells (ECs, astrocytes, pericytes, neurons and microglia) form a neurovascular unit (Figure 16).

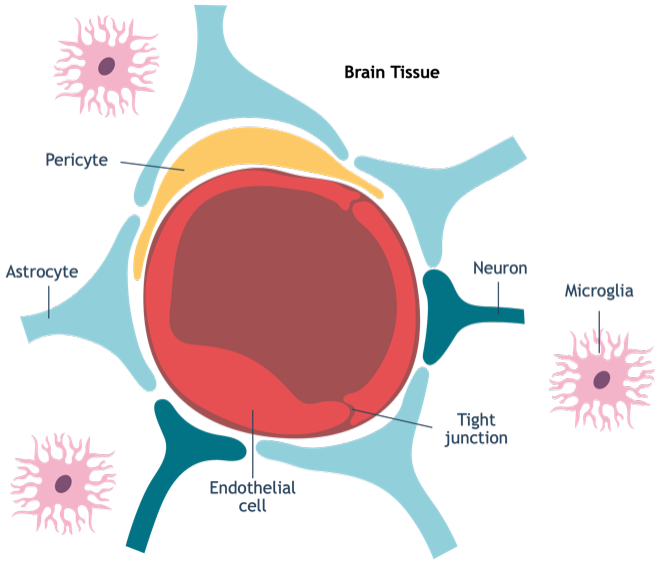

Figure 16: Representation of the neurovascular unit. Adapted from [7].

Due to the restrictions imposed by tight junctions, only small lipophilic gases like O_2 and CO_2, can diffuse freely across the BBB. Other large water-soluble molecules can only be transported through transporter proteins, energy dependent pumps or receptor-mediated

endocytosis (Figure 17) [7]. This is the case for glucose, amino acids and some metabolites. They cross the BBB with the aid of specific transport proteins, which are stereospecific and depend on chemical and/or electrical gradients. On the other hand, larger molecules like insulin, transferrin and other plasma proteins rely on receptor-mediated transcytosis or adsorptive transcytosis. The latter is triggered by electrostatic interactions between a positively charged substance and the negatively charged plasma membrane surface [92].

Efflux transporters prevent the passage of unwanted drugs and toxins across the BBB, playing a fundamental and protective role in the maintenance of the specific microenvironment in the brain. These energy-dependent membrane proteins are part of the adenosine triphosphate binding cassette superfamily and include P-glycoprotein (P-gp) and multidrug resistant protein. P-glycoprotein (P-gp) is one of the most important and abundant efflux pumps expressed in brain capillaries. Abnormal P-gp expression and activity has been observed in PD patients. P-glycoprotein (P-gp) has more than 200 known substrates, many of which are therapeutic agents. Therefore, this efflux transporter poses an obstacle in the development of new CNS drugs. Strategies like the use of P-gp inhibitors or chemical modification of drugs to avoid P-gp-mediated efflux are commonly employed [93, 94].

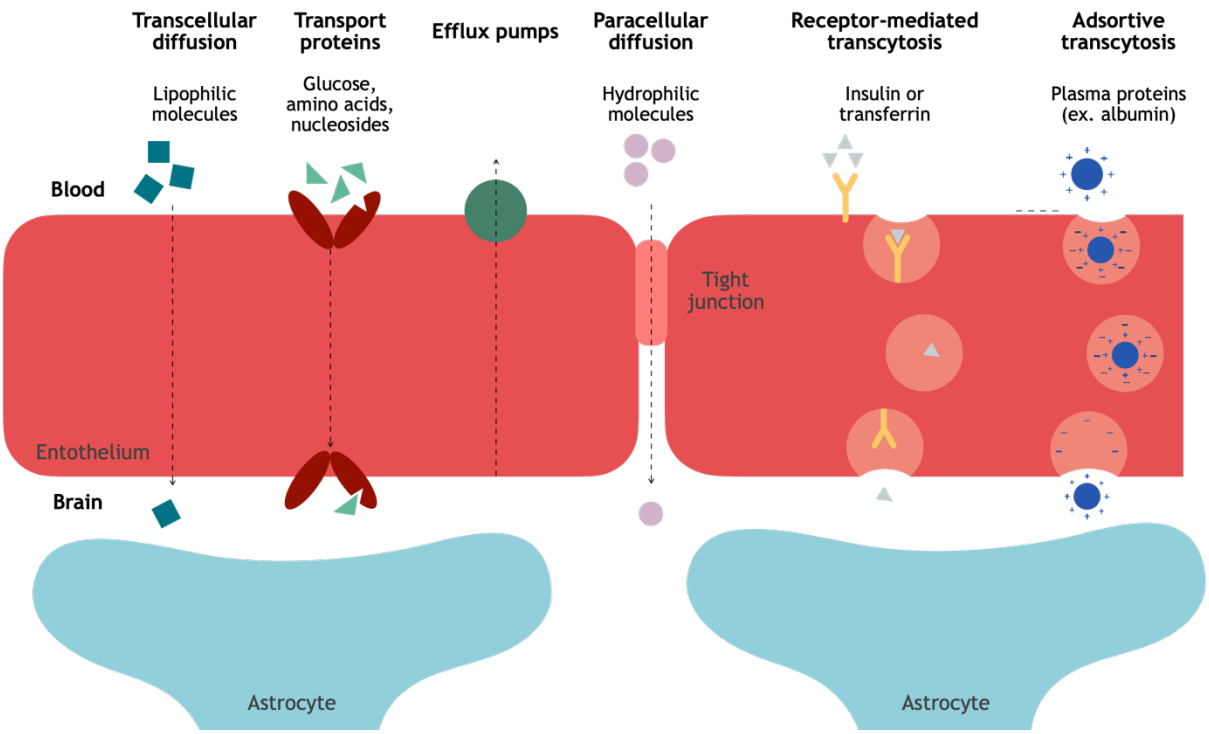

Figure 17: The main transport mechanisms through the BBB. Adapted from [3].

1.7.2. Drug Structural Requirements in the Central Nervous System

The complexity and impermeability of the BBB are one of the major hurdles faced in the development of therapeutics for CNS disorders. During drug development physicochemical properties such as molecular weight (MW), lipophilicity (calculated from Log P and Log D), topological polar surface area (tPSA), hydrogen bound donors and acceptors (HBD and HBA, respectively) and number of rotatable bound count (NROTB) are of particular importance. However, when developing compounds with BBB permeability these properties may have different optimal values when comparing to standard oral drugs [95].

Approximately 98% of small molecule and nearly 100% of large molecule drugs cannot cross the BBB. In the case of intravenous therapies, it was estimated that only around 0.1% is able to reach the brain [96]. Therefore, the development of molecules with low MW is a common strategy when developing CNS drugs. As a matter of fact, most of the currently available drugs for CNS diseases have a MW lower than 400 Da [97].

The lipophilicity of compounds is another critical physiochemical property. Due to the presence of tight junctions in the BBB, transcellular pathways are the main mechanisms through which compounds can enter the brain. Taking this into consideration, compounds must be able to move across the lipid bilayer of the cells through passive diffusion. Even though phospholipidic membranes are amphiphilic, most of the drugs developed have a more hydrophobic (or lipophilic) profile [98]. The assessment of the hydrophobicity of compounds is normally based on octanol/water partition coefficients through the logarithm of the octanol/water partition coefficient (LogP) and the logarithm of the octanol/water partition coefficient at physiological pH 7.4 (LogD). A study with several marketed CNS-active drugs showed that their brain permeability is correlated to logP values, presenting values between 2-3. When it comes to logD, optimum values are within 1-3 [99].

The BBB permeation through passive diffusion is also affected by the molecule's polarity, which is associated with the different electronegativity of the atoms in its structure. The tPSA corresponds to the surface associated with oxygen, nitrogen and polar hydrogen atoms. In other words, it gives us information about the ability of a molecule to form hydrogen bonds with its oxygen and nitrogen atoms [100]. Higher values of tPSA are related with impaired membrane penetration. For CNS-active drugs tPSA values should be lower than 90 Å. Furthermore, the formation of hydrogen bonds prevents a high brain/blood partitioning [101]. The hydrogen bond formation capacity is a property described by the number of HBDs and HBAs.

Closely related to tPSA and highly correlated with BBB penetration is the H-bonding capability of a molecule. On average, marketed CNS drugs contain 2.1 HBAs (expressed and the sum of N and O) and 1.5 HBDs (expressed as the sum of OH and NH), considerably less than the 3.7 HBA and 1.8 HBD for all oral drugs [102].

Finally, NROTB gives us information about the molecule's flexibility. In order to move across the BBB the compound must have a certain degree of flexibility. A number of rotatable bounds below 10 is considered ideal [103].

The mean results of a study analyzing the properties (MW, LogP, LogD, tPSA and HBD) of 119 CNS drugs and 108 CNS clinical candidates are summarized in Table 2 [104]. Literature values of HBA and NROTB are also depicted [99, 103].

Table 2 Median values of different properties of CNS drugs, [102-104].

Property	Median value
MW (Da)	305.3
Log P	2.8
Log D	1.7
tPSA (Å)	44.8
HBD	1
HBA	2.1
NROTB	< 10

1.8. Aim of the project

The main goal of the present work is the design and development of effective multi-target ligands, structurally based on deferiprone, for the treatment of PD. The innovative deferiprone-based compounds were synthetized using a Michael-type addition reaction between 3-hydroxypyran-4-one derivatives and a primary arylamine and structurally characterized by Nuclear Magnetic Resonance (NMR) techniques (^{1}H NMR, ^{13}C NMR and DEPT135). In addition, this project included the evaluation of the compounds' lipophilicity through High Performance Liquid Chromatography (HPLC) biomimetic approaches and the assessment of their iron and copper chelating capacity, antioxidant activity and MAO inhibition by spectrophotometric assays. The evaluation of BBB permeability of deferiprone-based compounds using the parallel artificial membrane permeability assay was also planned. However, this experiment was not performed due to time constraints.

CHAPTER II – Materials and Methods

2.1. Reagents and solvents

All reagents were purchased from Merck (Darmstadt, Germany), Fluorochem (Hadfield, UK), Alfa-Aesar (Kandel, Germany) and used without additional purification with the exception of 2-(3,4-dimethylphenyl)ethan-1-amine, which was synthetized and kindly provided by the Researcher Daniel Chavarria. Deionized water was used for all the experiments. All solvents were pro analysis grade and were acquired from Panreac and Merck. Thin layer chromatography (TLC) was carried out on precoated silica gel sheets 60 F_{254} acquired from Merck (Darmstadt, Germany). For analytical control, dichloromethane/methanol (DCM/MeOH) elution systems were used in several proportions (9.5:0.5, 9:1 and 8:2). The spots were detected using a UV lamp at 254 and 366 nm. A 10% (m/v) ferric chloride solution was used in order to intensify TLC spots. The crude products were purified by unmodified cellulose MN 2100 (Macherey Nagel, UK) and/or recrystallization. Following the workup, the organic phases were dried over anhydrous sodium sulphate (Na_2SO_4) (Honeywell Fluka™), filtered and concentrated.

2.2. Apparatus

For the compound synthesis, the different reagents were weighed in a KERN ABJ-NM/ABS-N scale and the solvents evaporated under reduced pressure in a Buchi Rotavapor. The syntheses were performed in Mya 4® reaction station (Radleys), which allows safe and precise heating, active cooling, software control and 24/7 unattended chemistry. For compound purification and hydrophobicity assays, Shimadzu Proeminence HPLC was used. A Biotek Synergy HT plate reader and an Epoch™ Microplate Spectrophotometer were used to read absorbances, using BRANDplates® pureGrade™ and Greiner bio-one UV-Star® plates. An ultrasound bath SONICA® Ultrasonic Cleaner and a WIZARD IR Infrared Vortex Mixer were used in the preparation of the solutions.

^{1}H and ^{13}C NMR spectra were acquired at the Centro de Materiais da Universidade do Porto (CEMUP) at room temperature and recorded on a Bruker Avance III operating at 400 and 100 MHz, respectively. The solvents methanol (MeOD-d_4) or chloroform ($CDCl_3$-d_1) were used with a deuteration degree above 99,0%. Chemical shifts are expressed in δ (ppm) values relative to tetramethylsilane (TMS) as internal reference and coupling constants (J) are given in Hz. Assignments were also made from DEPT135 (Distortionless Enhancement by Polarization Transfer) (underlined values).

2.3. Synthesis of deferiprone based compounds

General procedure A: To a mixture of 3-hydroxy-4*H*-pyran-4-one or 3-hydroxy-2-methyl-4*H*-pyran-4-one (1 equiv) with the appropriate amine (aniline, 3,4-dimethylaniline, 2-phenylethan-1-amine or 2-(3,4-dimethylphenyl)ethan-1-amine) (1.5 equiv) and methanol (2 mL), a solution of hydrochloric acid (HCl) 0.2 M (10 mL) was added. The reaction mixture was refluxed for 24 h or 48 h at 100 ºC under argon atmosphere. Upon completion, the resulting mixture was neutralized with NaOH 5 % and extracted with dichloromethane (2 x 20 mL). The combined organic phases were washed with water (3 x 20 mL), dried over anhydrous Na_2SO_4, filtered and concentrated. The crude product was purified with cellulose column chromatography, using dichloromethane/petroleum ether [9.5:0.5 ratio (v/v)] as elution system. The fractions containing the intended compound were combined and the solvent was evaporated. The resulting residue was then dissolved with a minimum amount of dichloromethane or methanol and recrystallized with excess ethyl acetate and petroleum ether. The solvent was decanted and the final solid residue was dried under vacuum.

The procedure was adapted from literature [105].

In an attempt to improve the reaction's yield, general protocol B was tested.

General procedure B: A mixture of 3-hydroxy-4*H*-pyran-4-one or 3-hydroxy-2-methyl-4*H*-pyran-4-one (1 equiv) and the appropriate amine (aniline, 3,4-dimethylaniline, 2-phenylethan-1-amine or 2-(3,4-dimethylphenyl)ethan-1-amine) (1 equiv) and camphor sulfonic acid (CSA) (0.1 equiv) in water (20 mL) was heated at 120 ºC for 24 h under argon atmosphere. Then, brine was added, and the mixture was extracted with dichloromethane (2 x 20 mL), the combined organic phases were washed with water (3 x 20 mL), dried over anhydrous Na_2SO_4, filtered and concentrated. The obtained residue was dissolved with a minimum amount of dichloromethane and recrystallized with excess ethyl acetate and petroleum ether. The solvent was decanted and the final solid residue was dried under vacuum.

The procedure was adapted from literature [106].

2.3.1. Synthesis of 1-(3,4-dimethylphenyl)-3-hydroxypyridin-4(1*H*)-one (compound 1)

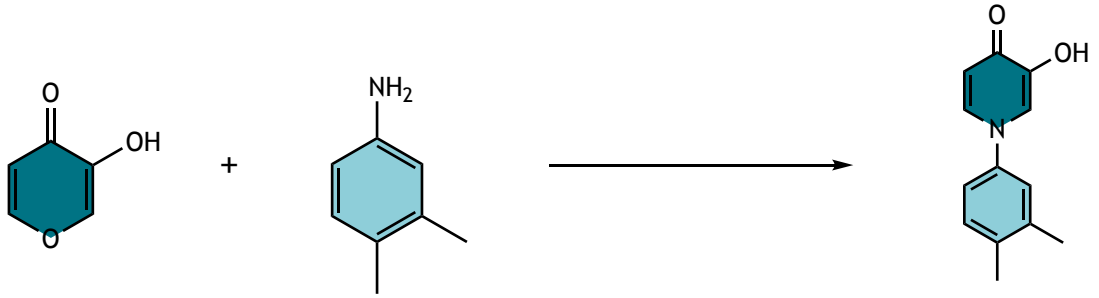

(1)

Compound **1** (Figure 18) was synthesized according to general procedures A and B. Procedure A was carried out twice: first, with an oil-bath reflux and then with Radleys Mya 4® reacting station.

a) Using an oil-bath reflux: to a solution of 3-hydroxy-4*H*-pyran-4-one (0.50 g, 4.46 mmol) and 3,4-dimethylaniline (0.82 g, 6.75 mmol) in methanol (2.0 mL), a solution of HCl 0.2 M (10.0 mL) was added. The reaction mixture was refluxed for 48 h at 100 ºC under an argon atmosphere. After performing the liquid-liquid extraction, a column chromatography in cellulose (dichloromethane/petroleum ether (9.5:0.5)) was carried out. However, the compound's purification was unsuccessful because of decomposition during the process.

In order to improve the reaction yield and minimize the formation of byproducts, the reactions that followed were performed in the Radleys Mya 4® reacting station.

b) Using Radleys Mya 4® reacting station:

a. to a mixture of 3-hydroxy-4*H*-pyran-4-one (1.00 g, 8.92 mmol), 3,4-dimethylaniline (1.62 g, 13.38 mmol) and methanol (3.9 mL), a solution of HCl 0.2 M (19.6 mL) was added. The reaction mixture was stirred (200 rpm) for 24 h at 100 ºC under an argon atmosphere. Upon completion, the mixture was neutralized and extracted using the aforementioned conditions. The solid obtained solid was recrystallized from ethyl acetate and petroleum ether. Unfortunately, the final compound decomposed during the process.
b. to a mixture of 3-hydroxy-4*H*-pyran-4-one (0.50 g, 4.46 mmol), 3,4-dimethylaniline (0.54 g, 4.46 mmol) and CSA (0.10 g, 0.45 mmol), water (10.0 mL) was added. The reaction mixture was stirred (150 rpm) for 24 h or 72 h at 120 ºC under an argon atmosphere. Once the reaction was complete, a liquid-liquid extraction was performed. The solid obtained was purified

through recrystallization with ethyl acetate and petroleum ether. The final compound presented a light brown color.

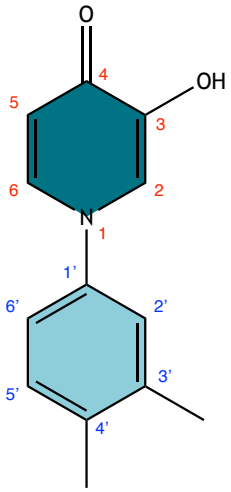

Figure 18: Chemical structure of compound 1.

Yield: 5.6 %

^{1}H NMR (400 MHz, MeOD-d_4): δ = 8.14 (1H, d, *J* = 6.2 Hz, H(6)), 8.07 (1H, s, H(2)), 7.38 (1H, d, *J* = 8.2 Hz, H(6')), 7.35 (1H, s, H(2')), 7.30 (1H, d, *J* = 8.2 Hz, H(5')), 6.99 (1H, d, *J* = 6.3 Hz, H(5)), 2.37 (3H, s, CH_3), 2.35 (3H, s, CH_3).

^{13}C NMR (101 MHz, MeOD-d_4): δ = 165.84 (C(4)), 146.89 (C(3)), 141.00 (C(1')), 139.04 (C(3')), 138.69 (C(4')), 137.42 (C(6)), 130.75 (C(2)), 126.90 (C(5')), 123.95 (C(6')), 120.34 (C(5)), 112.94 (C(2')), 18.43 (4'-CH_3), 18.01 (3'- CH_3).

2.3.2. Synthesis of 1-(3,4-dimethylphenyl)-3-hydroxy-2-methylpyridin-4(1*H*)-one (compound 2)

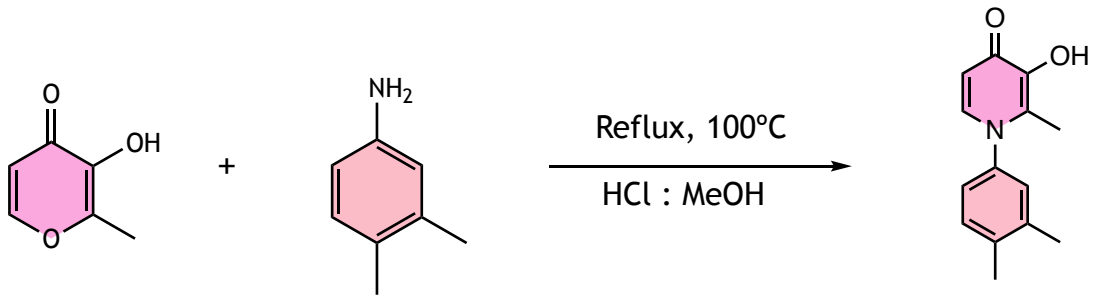

(2)

Compound **2** (Figure 19) was synthetized according to the general procedure A and using the Radleys Mya 4® reacting station. Briefly, to a mixture of 3-hydroxy-2-methyl-4*H*-pyran-4-one (0.50 g, 3.96 mmol), 3,4-dimethylaniline (0.67 g, 5.94 mmol) and methanol (2.0 mL), a solution of HCl 0.2 M (10.0 mL) was added. The reaction progression was monitored by TLC after 24 h and appeared incomplete. It was left in the reacting station for additional 24 h. The resulting solution was stirred (100 rpm) for 48 h at 100 ºC under an argon atmosphere. After performing a liquid-liquid extraction, the solid obtained was recrystallized from ethyl acetate and petroleum ether. The final compound presented a white color.

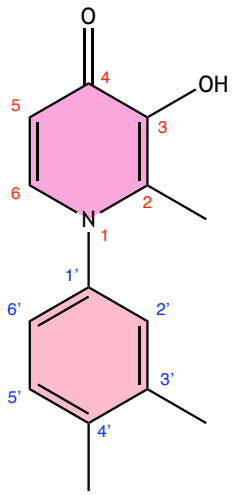

Figure 19: Chemical structure of compound 2.

Yield: 2.1 %

^{1}H NMR (400 MHz, MeOD-d_4): δ = 7.55 (1H, d, *J* = 7.2 Hz, H(6)), 7.33 (1H, d, J = 7.9 Hz, H(2')), 7.16 (1H, d, *J* = 2.4 Hz, H(5')), 7.09 (1H, dd, *J* = 8.0, 2.4 Hz, H(6')), 6.46 (1H, d, *J* = 7.2 Hz, H(5)), 2.35 (6H, d, *J* = 3.6 Hz, 2xCH_3), 2.11 (3H, s, CH_3).

^{13}C NMR (101 MHz, MeOD-d_4): δ = 171.41 (C(4)), 146.78 (C(2)), 140.95 (C(1')), 140.01 (C(3')), 139.84 (C(3)), 139.38 (C(6)), 133.15 (C(4')), 131.81 (C(5')), 128.53 (C(6')), 125.00 (C(5)), 112.42 (C(2')), 19.73 (4'- $\underline{C}H_3$), 19.48 (3'- $\underline{C}H_3$), 13.74 (2 - $\underline{C}H_3$).

2.3.3. Synthesis of 1-(3,4-dimethylphenethyl)-3-hydroxypyridin-4(1*H*)-one (compound 3)

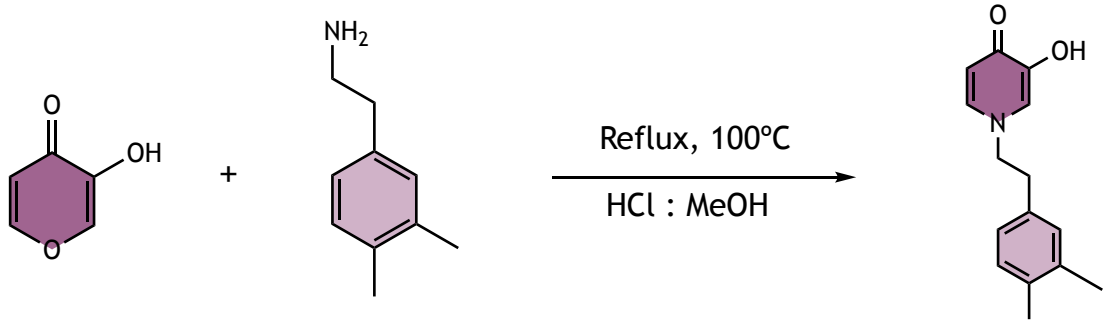

(3)

Compound **3** was synthetized according to the general procedure A and using the Radleys Mya 4® reacting station. To a mixture of 3-hydroxy-4*H*-pyran-4-one (0.37 g, 2.91 mmol), 2-(3,4-dimethylphenyl)ethan-1-amine (0.65 g, 4.36 mmol) and methanol (1.4 mL), a solution of HCl 0.2 M (7.2 mL) was added. The reaction mixture was stirred (150 rpm) for 24 h at 100 ºC under an argon atmosphere. After performing a liquid-liquid extraction, the solid obtained was recrystallized from ethyl acetate and petroleum ether. Unfortunately, compound **3** was not isolated under the conditions described.

2.3.4. Synthesis of 1-(3,4-dimethylphenethyl)-3-hydroxy-2-methylpyridin-4(1*H*)-one (compound 4)

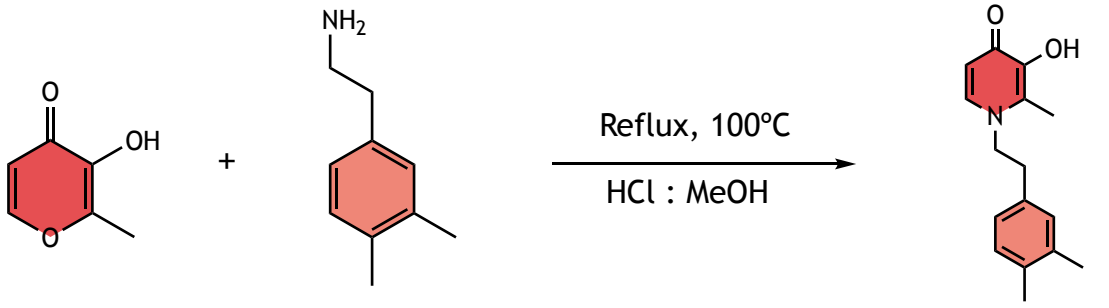

(4)

Compound **4** was synthetized according to the general procedure A and using the Radleys Mya 4® reacting station. To a mixture of 2-methyl-4*H*-pyran-4-one (0.49 g, 3.93 mmol), 2-(3,4-dimethylphenyl) ethan-1-amine (0.88 g, 5.90 mmol) and methanol (1.9 mL), a solution of HCl 0.2 M (9.7 mL) was added. The reaction mixture was stirred (150 rpm) for 24 h at 100 ºC under an argon atmosphere. After performing a liquid-liquid extraction, the solid obtained was recrystallized from dichloromethane and petroleum ether. Unfortunately, compound **4** was not isolated under the conditions described.

2.3.5. Synthesis of 3-hydroxy-1-phenethylpyridin-4(1*H*)-one (compound 5)

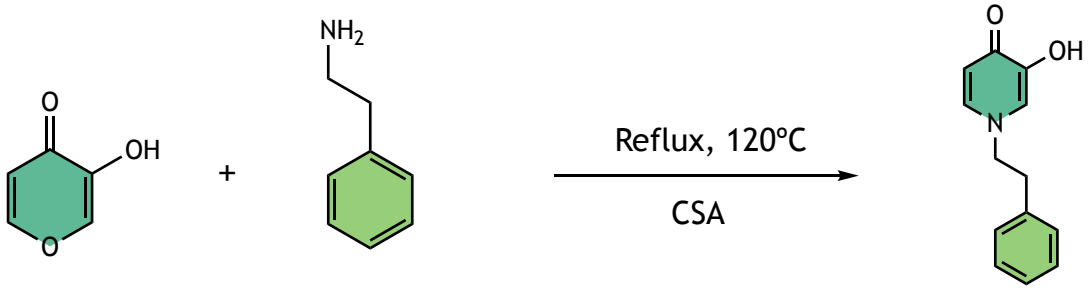

(5)

Compound **5** (Figure 20) was synthetized according to the general procedure B and using the Radleys Mya 4® reacting station. To a mixture of 3-hydroxy-4*H*-pyran-4-one (0.80 g, 7.14 mmol), 2-phenylethan-1-amine (0.87 g, 7.14 mmol) and CSA (0.17 g, 0.71 mmol) was added water (10.0 mL). The resulting solution was stirred (150 rpm) for 24 h at 120 °C under an argon atmosphere. After performing a liquid-liquid extraction, the solid obtained was recrystallized from dichloromethane and petroleum ether. The final compound presented a beige color.

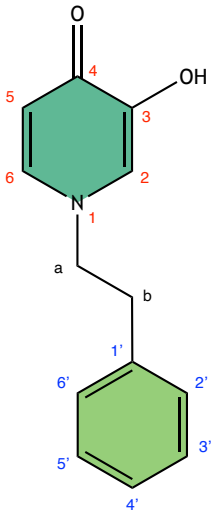

Figure 20: Chemical structure of compound 5.

Yield: 2.8 %

^{1}H NMR (400 MHz, MeOD-d_4): δ = 7.43 (1H, d, *J* = 2.3 Hz, H(2)), 7.36 (1H, dd, *J* = 7.0, 2.2 Hz, H(6)), 7.29 – 7.23 (2H, m, H(5') and H(3')), 7.23 – 7.20 (1H, m, H(4')), 7.14 – 7.10 (2H, m, H(2') and H(6')), 6.30 (1H, d, *J* = 7.0 Hz, H(5)), 4.20 (2H, t, *J* = 6.9 Hz, NCH_2), 3.08 (2H, t, *J* = 6.9 Hz, $C\underline{H_2}$Ar').

^{13}C NMR (101 MHz, MeOD-d_4): δ = 171.69 (C(4)), 149.05 (C(3)), 138.21 (C(6)), 137.91 (C(1')), 129.51 (C(5') and C(3')), 129.33 (C(6') and C(2')), 127.60 (C(4')), 124.18 (C(2)), 113.47 (C(5)), 59.56 (NCH_2), 37.66 ($\underline{C}H_2$Ar').

2.3.6. Synthesis of 3-hydroxy-2-methyl-1-phenethylpyridin-4(1*H*)-one (compound 6)

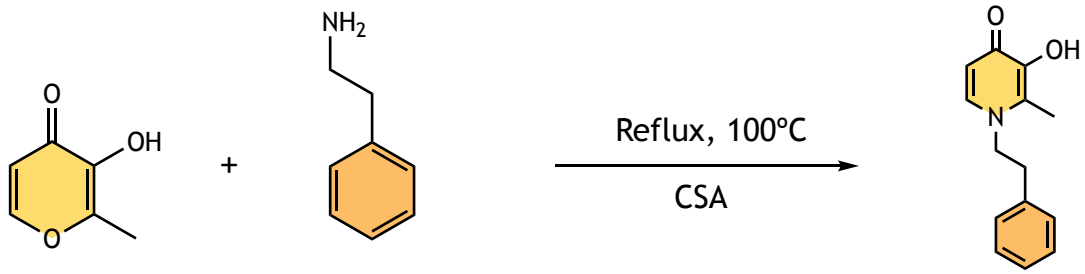

(6)

Compound **6** (Figure 21) was synthetized according to the general procedure B and using the Radleys Mya 4® reacting station. To a mixture of 2-methyl-4H-pyran-4-one (1.00 g, 7.93 mmol), 2-phenylethan-1-amine (900 µL, 7.93 mmol) and CSA (0.18 g, 0.79 mmol), water (20.0 mL) was added. The reaction progression was monitored after 24 h by TLC and appeared incomplete. An additional amount of 2-phenylethan-1-amine (450 µL, 3.57 mmol) was added to the reaction mixture and the mixture was stirred for another 24 h. After 48 h a new TLC control was performed, and the reaction progression remained incomplete. An additional amount of 2-phenylethan-1-amine (200 µL, 1.59 mmol) was added, and the mixture was stirred for additional 24 h. The reaction mixture was stirred (150 rpm) for a total of 72 h at 120 ºC under an argon atmosphere. After performing a liquid-liquid extraction, the solid obtained was recrystallized from ethyl acetate. The compound was further purified by HPLC using H_2O/acetonitrile (8:2) as elution system. The final compound presented an orange-like color.

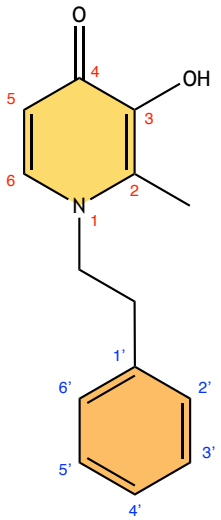

Figure 21: Chemical structure of compound 6.

Yield: 4.6 %

^{1}H NMR (400 MHz, MeOD-d_4): δ = 7.39 (1H, d, *J* = 7.3 Hz, H(6)), 7.31 – 7.26 (2H, m, H(5') and H(3')), 7.26 – 7.21 (1H, m, H(4')), 7.13 (2H, dd, *J* = 7.9, 1.6 Hz, H(2') and H(6')), 6.29 (1H, d, *J* = 7.2 Hz, H(5)), 4.29 (2H, t, *J* = 7.0 Hz, NCH_2), 3.07 (2H, t, *J* = 7.0 Hz, CH_2Ar'), 2.34 (3H, s, CH_3).

^{13}C NMR (101 MHz, MeOD-d_4): δ = 170.07 (C(4)), 146.64 (C(3)), 138.43 (C(6)), 137.83 (C(1')), 132.36 (C(2)), 129.59 (C(5') and C(3')), 129.29 (C(6') and C(2')), 127.61 (C(4')), 111.90 (C(5)), 55.84 (NCH_2), 37.34 (CH_2Ar'), 11.32 (2 - CH_3).

2.3.7. Synthesis of 3-hydroxy-1-phenylpyridin-4(1*H*)-one (compound 7)

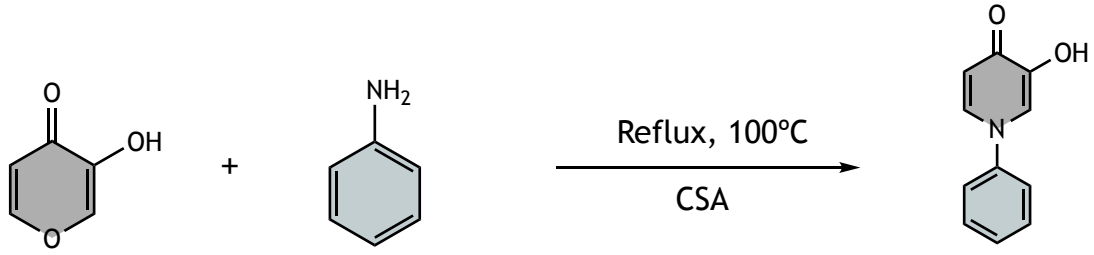

(7)

Compound **7** (Figure 22) was synthetized according to the general procedure B and using the Radleys Mya 4® reacting station. To a mixture of 3-hydroxy-4*H*-pyran-4-one (0.50 g, 4.46 mmol), aniline (0.40 g, 4.46 mmol) and CSA (0.10 g, 0.44 mmol), water (10.0 mL) was added. The reaction mixture was stirred (150 rpm) for 24 h at 120 ºC under an argon atmosphere. After performing a liquid-liquid extraction, the solid obtained was

recrystallized from ethyl acetate and petroleum ether. The final compound presented beige color.

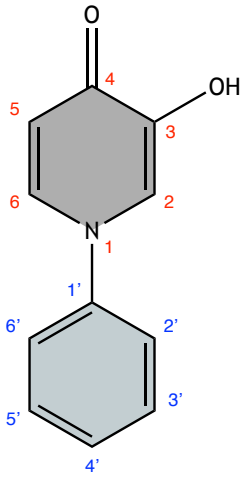

Figure 22: Chemical structure of compound 7.

Yield: 3.5 %

^{1}H NMR (400 MHz, MeOD-d_4): δ = 7.88 (1H, dd, *J* = 7.2, 2.4 Hz, H(6)), 7.78 (1H, d, *J* = 2.4 Hz, H(2)), 7.60 – 7.55 (2H, m, H(5') and H(3')), 7.54 (1H, d, *J* = 1.8 Hz, H(4')), 7.53 – 7.45 (2H, m, H(2') and H(6')), 6.57 (1H, d, *J* = 7.3 Hz, H(5)).

^{13}C NMR (101 MHz, MeOD-d_4): δ = 171.75 (C(4)), 148.25 (C(3)), 143.50 (C(1')), 136.76 (C(6)), 129.86 (C(5') and C(3')), 128.44 (C(4')), 122.86 (C(6') and C(2')), 122.58 (C(2)), 113.41 (C(5)).

2.3.8. Synthesis of 3-hydroxy-2-methyl-1-phenylpyridin-4(1*H*)-one (compound 8)

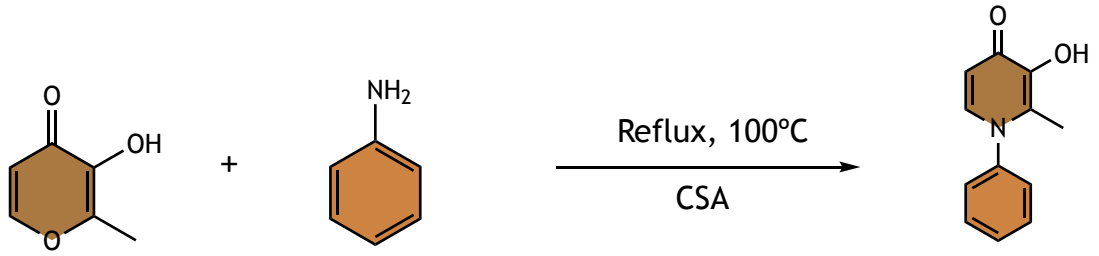

(8)

Compound **8** (Figure 23) was synthetized according to the general procedure B and using the Radleys Mya 4® reacting station. To a mixture of 2-methyl-4H-pyran-4-one (0.50 g, 3.96 mmol), aniline (0.40 g, 3.96 mmol) and CSA (0.09 g, 0.39 mmol), water (10.0 mL) was added. The resulting solution was stirred (150 rpm) for 24 h at 120 ºC under an argon

atmosphere. After performing a liquid-liquid extraction, the solid obtained was recrystallized from dichloromethane and petroleum ether.

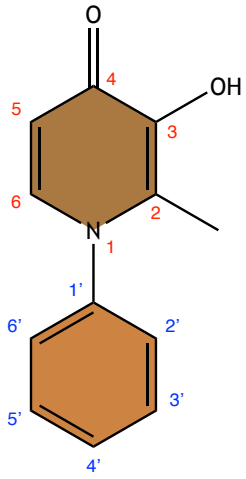

Figure 23: Chemical structure of compound 8.

Yield: 4.9 %

^{1}H NMR (400 MHz, $CDCl_3$-d_1): δ = 7.57 (1H, d, *J* = 7.3 Hz, H(6)), 7.53 – 7.50 (2H, m, H(5') and H(3')), 7.32 – 7.29 (1H, m, H(4')), 7.29 – 7.25 (2H, m, H(2') and H(6')), 6.47 (1H, d, *J* = 7.3 Hz, H(5)), 2.11 (3H, s, CH_3).

^{13}C NMR (101 MHz, $CDCl_3$): δ = 170.14 (C(4)), 145.66 (C(3)), 141.77 (C(1')), 137.42 (C(6)), 129.90 (C(5') and C(3')), 129.56 (C(4')), 128.47 (C(2)), 126.80 (C(6') and C(2')), 110.88 (C(5)), 13.62 (2 - CH_3).

2.4. Assessment of drug-like properties

The physicochemical properties of a molecule can dictate its potential as a drug candidate, influencing its interaction with cell membranes and consequent internalization. This takes particular importance when developing drugs aimed for the CNS. In order to reach the brain, drugs must be able to cross the BBB, whose endothelial cells are sealed by tight junctions, restricting paracellular diffusion. Thus, the assessment of physicochemical properties such as molecular weight (MW), lipophilicity (calculated from Log P and Log D), topological polar surface area (tPSA), hydrogen bound donors and acceptors (HBD and HBA, respectively) and number of rotatable bound count (NROTB) are fundamental to understand the drug-like properties of the deferiprone derivatives. It is also relevant to evaluate whether or not the derivatives are BBB permeable.

To predict the aforementioned properties of the deferiprone-based compounds, two free computational tools were employed. To predict the MW, Log P, tPSA, HBD, HBA and NROTB of compounds **1, 2, 5-8** Molinspiration Cheminformatics software (https://www.molinspiration.com/) was used. Blood Brain Barrier (BBB) penetration of the deferiprone derivatived was predicted using the BBB Prediction Server (https://www.cbligand.org/BBB/).

2.5. Evaluation of Chromatographic Hydrophobicity Index

The determination of the compounds' hydrophobicity (or lipophilicity) is crucial to understand of the different ADMET (absorption, distribution, metabolism, excretion and toxicity) properties in drug discovery. The Chromatographic Hydrophobicity Index (CHI) is one of the experimental methods available to determine the lipophilicity of a chemical compound. It is an index based on the retention times of compounds in a fast gradient Reverse-Phase High Performance Liquid Chromatography (RP-HPLC). From CHI measurements it is possible to estimate the logarithm of the 1-octanol/water partition coefficient (Log P) through equation (1), which is widely used as a measure of lipophilicity [107, 108].

$$\text{Log P} = 0.047\ \text{CHI} + 0.36\ \text{HBD} - 1.10 \quad \textbf{(1)}$$

The CHI values were determined at pH 7.4 and using an experimental protocol described in literature [8, 109, 110]. The CHI values are derived from experimental retention times (t_r) of the samples and a mixture of reference compounds. The results were obtained on the HPLC system with a Luna C18 (2) column (Phenomenex, CA, USA), 150x4.6 mm, 5 µm. Compounds **1**, **2**, **5-8** were diluted from a DMSO stock solution (10 mM) in a mixture of acetonitrile:water (1:1) to obtain a final concentration of 250 µM. The mobile phase A was ammonium acetate (pH 7.4) and the mobile phase B was acetonitrile. The following gradient program was applied: 1 mL/min flow, rt, injection volume 100 µL, gradient 0–6 min 0-100 % B, 6–14 min 100% B, 14–16 min 100-0 % B. The procedure was adapted from literature [8].

A calibration curve (Figure 24) was obtained using a mixture of the following reference compounds: Theophylline, Paracetamol, Caffeine, Benzimidazole, Colchicine, Carbamazepine, Indole, Propiophenone, Butyrophenone and Valerophenone. The results are expressed as mean values ± Standard Deviation (SD) of two experiments (Table 3).

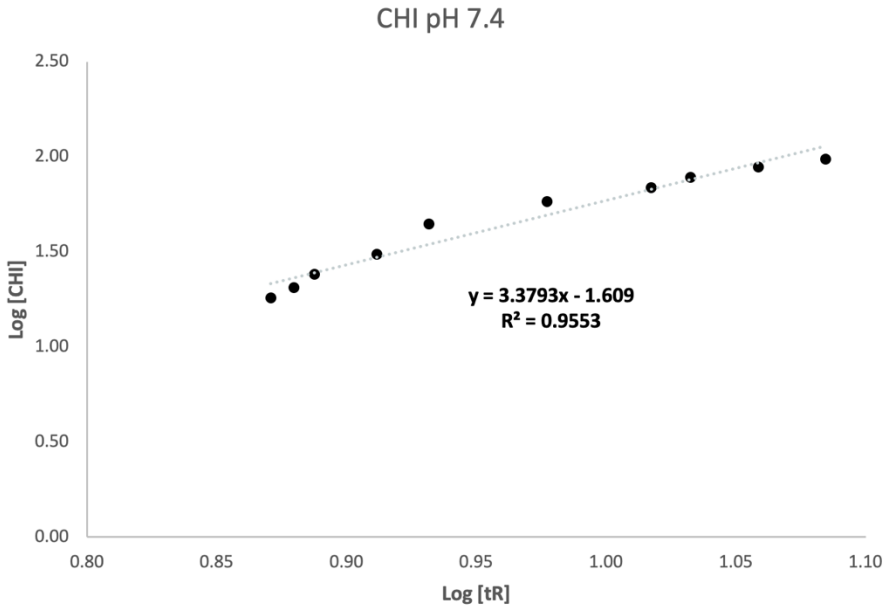

Figure 24: Calibration line obtained after plotting the logarithmic values of the retention times of the test mixture of compounds as a function of logarithmic values of their literature CHI values at pH 7.4. The CHI values at pH 7.4 were obtained from Valko et. al [8].

Table 3 Retention times (t_r) and literature CHI values at pH 7.4 of the reference compounds. The CHI values at pH 7.4 were obtained from Valko et. al [8].

	t_r (min) ± SD	CHI pH 7.4
Theophylline	7.43 ± 0.03	18.19
Paracetamol	7.58 ± 0.03	20.59
Caffeine	7.72 ± 0.03	24.12
Benzimidazole	8.16 ± 0.06	30.71
Colchicine	8.55 ± 0.02	44.32
Carbamazepine	9.49 ± 0.01	58.45
Indole	10.41 ± 0.01	69.15
Propiophenone	10.78 ± 0.01	78.41
Butyrophenone	11.45 ± 0.01	88.49
Valerophenone	12.15 ± 0.01	97.67
Heptanophenone	13.83 ± 0.01	111.80

2.5.1. Chromatographic Hydrophobicity Index on Immobilized Artificial Membrane

It is important to assess the interactions of potential new drugs with biological membranes, as transcellular permeation by passive diffusion represents the main mechanism through which drugs pass through them [10]. In the specific case of the BBB, the intercellular space is sealed by tight junctions, making paracellular transport more difficult.

The lipophilicity of a drug affects its ability to permeate biological membranes through passive diffusion. In this context, CHI values were also determined on an Immobilized Artificial Membrane (IAM). The column used in this assay contains a monolayer of phospholipids covalently bound to silica particles that mimics the biological environment that the compounds would encounter by covalent binding of a monolayer of phospholipids to silica particles [111]. Therefore, CHI (IAM) is an effective technique to estimate the compounds' interaction with membranes.

Similarly to the previously determined CHI values, the CHI (IAM) values were determined from experimental t_r of the samples and a mixture of reference compounds obtained on HPLC system with an IAM.PC.DD2 column (Regis Technologies, Inc., Morton Grove, IL, USA), 100x4.6 mm, 10 µm. Compounds **1**, **2**, **5-8** were diluted from a stock solution in DMSO (10 mM) in a mixture of acetonitrile:water (1:1) to obtain a final concentration of 250 µM. The mobile phase A was 1 % ammonium acetate solution (pH = 7.4) and mobile phase B was acetonitrile. The following gradient program was applied: 1 mL/min flow, rt, injection volume 100 µL, gradient 0−6 min 0-100 % B, 6−10 min 100 % B, 10−12 min 100-0 % B. The procedure was adapted from literature [10].

A calibration curve (Figure 25) was obtained using a mixture of the following compounds: Acetanilide, Acetophenone, Propiophenone, Butyrophenone, Valerophenone, Hexanophenone, Heptanophenone, Octanophenone. The results are expressed in Table 4.

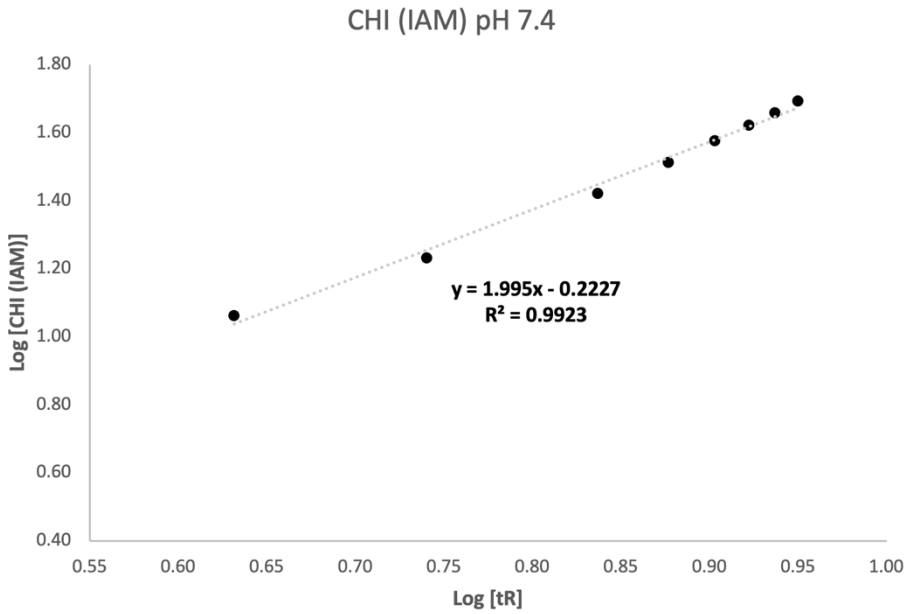

Figure 25: Calibration line obtained after plotting the logarithmic values of t_r of the test mixture of compounds as a function of logarithmic values of CHI (IAM) values at pH 7.4. The CHI (IAM) values at pH 7.4 were obtained from Valko et. al [10].

Table 4 Retention times and CHI (IAM) values at pH 7.4 of the reference compounds. The CHI(IAM) values at pH 7.4 were obtained Valko et. al [10].

	t_r (min)	CHI (IAM) pH 7.4
Acetanilide	4.28	11.57
Acetophenone	5.50	17.07
Propiophenone	6.87	26.39
Butyrophenone	7.53	32.55
Valerophenone	8.00	37.71
Hexanophenone	8.36	41.91
Heptanophenone	8.65	45.49
Octanophenone	8.91	49.40

From the obtained CHI(IAM) values it is possible to back-calculate the partition coefficient between the immobilized phospholipidic membrane and the mobile phase (Log K (IAM)), the affinity of the compounds for the stationary phospholipid membrane (Log k (IAM)) and the compounds' cellular partition (Log K_{pcell}) using equations (2), (3) and (4), respectively [112, 113]. The latter estimates the compound concentration between the intracellular and the external cellular media, considering the compound's passive permeability.

$$\text{Log K (IAM)} = 0.29e^{\text{Log k CHI(IAM)}} + 0.7 \quad \textbf{(2)}$$

$$\text{Log k (IAM)} = 0.046\ \text{CHI(IAM)} + 0.42 \quad \textbf{(3)}$$

$$\text{Log } K_{pcell} = 1.1\ \text{Log k(IAM)} - 1.9 \quad \textbf{(4)}$$

2.6. Evaluation of metal chelation properties

2.6.1. Iron

The iron chelation capacity of compounds **1**, **2**, **5-8** was assessed by the ferrozine method [114]. The iron chelator deferiprone and the COMT inhibitors tolcapone and entacapone were also included. This spectrophotometric assay is based on the formation of a purple colored complex between the ferrous ion and ferrozine, $[Fe(Ferrozine)_3]^{2+}$, with a maximum absorbance at 562 nm. Iron chelators compete with ferrozine, decreasing the absorbance and avoiding the formation of the colored complex. EDTA, a known metal chelator, was used as reference.

Aqueous ferrozine solution (5 mM), an ammonium acetate buffer (0.2 mM; pH 6.7) and an aqueous ammonium iron (II) sulfate solution (2 mM) were freshly prepared. The ammonium iron (II) sulfate solution was then diluted in ammonium acetate buffer (20 µM final concentration) and used as the source of ferrous ions. A solution of the test compound (100 µM) and ammonium iron (II) sulfate in ammonium acetate buffer (20 µM) were added in triplicate. The plate was incubated for 10 minutes at 37 ºC and the absorbance was read at 562 nm. Then, ferrozine solution was added (100 µM final concentration). The plate was incubated for additional 10 minutes at 37 ºC and the absorbance was read at 562 nm. Blank and control wells were run with DMSO and EDTA (100 µM), respectively. The absorbance of the first reading was subtracted from the final values to discard any absorbance from the test compounds. Data are the mean ± SEM of three independent experiments and are expressed as % of Fe(II) chelation (EDTA = 100%). EDTA, used as reference, was found to chelate all available iron as it completely inhibited the formation of the colored ferrozine−Fe(II) complex.

The procedure was adapted from literature [115].

2.6.2. Copper

The copper chelating studies of compounds **1**, **2**, **5-8** were carried out using a UV-Vis spectrophotometric assay. In each well, a solution of the test compounds alone (40 µM) or in the presence of copper(II) sulfate (20 µM) was added in triplicate. After 30 min of incubation protected from the light, the absorption spectra were recorded at room temperature in phosphate-buffer saline (PBS) (1X, pH 7.4) between 200-550 nm, with a reading step of 2 nm.

In addition, UV−Vis titration analysis was performed for the determination of the stoichiometry of the complex compound-Cu(II) following the molar ratio method [116]. Briefly, a solution of each compound (40 µM) was co-incubated with increasing concentrations of copper(II) sulfate (0-100 µM) in PBS, and the absorption spectra were recorded. Blank wells were run with PBS and ethanol.

The procedure was adapted from literature [117, 118].

2.7. Evaluation of Antioxidant Activity

The radical scavenging activity of the compounds was evaluated using the $ABTS^{\bullet+}$ radical scavenging assay. $ABTS^{\bullet+}$ is a blue chromophore that is reduced to ABTS when it

reacts with an antioxidant substance [119]. The reduction can be easily monitored by measuring the absorbance decay at 734 nm.

Ethanolic solutions (10 - 5000 μM) of the test compounds, tolcapone, entacapone, deferiprone and Trolox with increasing concentrations were prepared. Trolox was used as reference compound. $ABTS^{\bullet+}$ radical cation solution was obtained by addition of 150 mM aqueous potassium persulfate solution (163 μL) to 10 mL of 7 mM aqueous ABTS solution, followed by storage in the dark at room temperature for 16 h (2.45 mM final concentration). Then, the radical solution was diluted in ethanol until the desired absorbance of 0.72 ± 0.02 was obtained. In each well, the test compounds (20 μL) solutions and the $ABTS^{\bullet+}$ radical solution (180 μL) were added in triplicate. Blank and control experiments wells were run with ethanol (20 μL) and Trolox (20 μL), respectively. The spectrophotometric measurement was carried out each minute over a total of 15 minutes at 734 nm and at room temperature. By comparing the blank (100% radical) to test compounds solutions it was possible to assess the percent inhibition of radical. The dose-response curves allowed the determination of IC_{50} values.

The procedure was adapted from literature [115].

2.8. Evaluation of monoamine oxidase inhibitory activity

The inhibitory activity on human MAO-A (*h*MAO-A) and human MAO-B (*h*MAO-B) of compounds was studied through a spectrophotometric assay using kynuramine as substrate for both MAO isoforms. The oxidative deamination of kynuramine yields an aldehyde, which undergoes a non-enzymatic condensation into 4-hydroxyquinoline, 4-HQ. The formation of 4-HQ can be monitored spectrophotometrically at 316 nm (Figure 26).

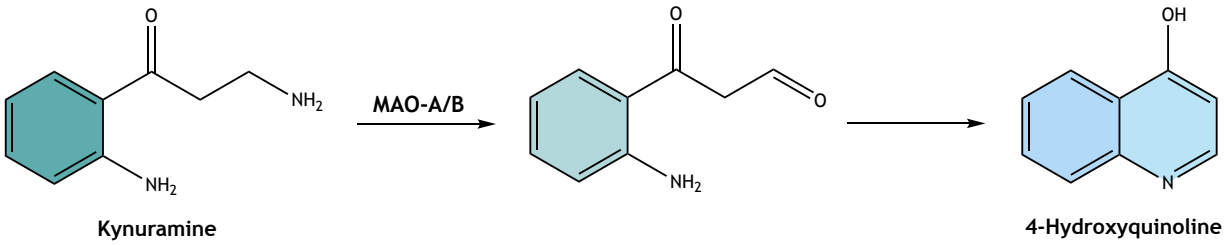

Figure 26: Deamination of kynuramine catalyzed by MAO-A or MAO-B, followed by non-enzymatic condensation to 4-HQ.

The amounts of *h*MAO-A and *h*MAO-B were adjusted to obtain the same maximum velocity (V_{max} = 50 pmol/min) for both isoforms (hMAO-A: 4 μg/mL and hMAO-B: 12 μg/mL). A preliminary screening was performed with compounds **1**, **2**, **5-8** to assess if they present relevant *h*MAO inhibitor activity (> 50 % inhibition) at a final concentration of 10 μM. The

test compounds were diluted from stock solutions in DMSO (5 mM) to obtain a final concentration of 2 mM. An aqueous stock solution of kynuramine (10 mM) was diluted in phosphate buffer (50 mM, pH 7.4) to obtain a final concentration of 4 μM. Clorgyline (2 mM) and rasagiline (2 mM) were used as reference MAO-A and MAO-B inhibitors, respectively.

In each well the phosphate buffer (160 μL), substrate (20 μL) and the test compounds/reference inhibitors (1 μL; final concentration: 10 μM) were added in triplicate. Control wells were run with DMSO (1 μL). The plate was pre-incubated at 37 ºC for 10 minutes. Then, *h*MAO-A or *h*MAO-B were added (20 μL) in order to start the reaction. Initial velocities were determined by measuring the formation of 4-HQ at 316 nm every minute for 30 minutes. The initial velocities were obtained from the linear phase of product formation. The percentage of inhibition were determined using equation (5) where $[v_0]_{CTRL}$ is the initial velocity obtained in control experiments and $[v_0]_{compound}$ is the initial velocity obtained with the test compounds or reference inhibitors. The procedure was adapted from literature [120-123].

$$\% \text{ inhibition} = \frac{[v_0]_{CTRL} - [v_0]_{compound}}{[v_0]_{CTRL}} \times 100 \quad (5)$$

CHAPTER III – Results and Discussion

3.1. Chemistry

Deferiprone-based compounds **1**, **2**, **5-8** were successfully obtained in a single step synthesis using 3-hydroxy-4*H*-pyran-4-one or 3-hydroxy-2-methyl-4*H*-pyran-4-one and primary arylamines as starting materials. The chemical structures of all synthesized compounds were confirmed through NMR spectroscopy (^{1}H NMR, ^{13}C NMR and DEPT135) (see 6.1. Appendix 1: ^{1}H, ^{13}C and DEPT NMR spectra of the synthesized compounds). The synthesis of N-substituted 3-hydroxypyridine-4-ones from primary arylamines and 3-hydroxypyran-4-one derivatives is a Micheal-type addition, and the reaction mechanism is well established [106, 124]. Accordingly, the reaction involves two nucleophilic attacks by the amino group at the α,β-unsaturated functions of the pyran-4-one and the loss of a water molecule (Figure 27). Under the basic conditions employed in the amination step, 3-hydroxyl group on the pyran-4-one undergoes a side reaction, which results in the formation of byproducts and, consequently, the decrease of the yields [124, 125]. In order to circumvent the generation of secondary reaction, the use of HCl and CSA as an acidic catalyst is usually employed [125, 126]. It should be noted that, under in these conditions, the aryl amines are not completely protonated and still act as nucleophiles.

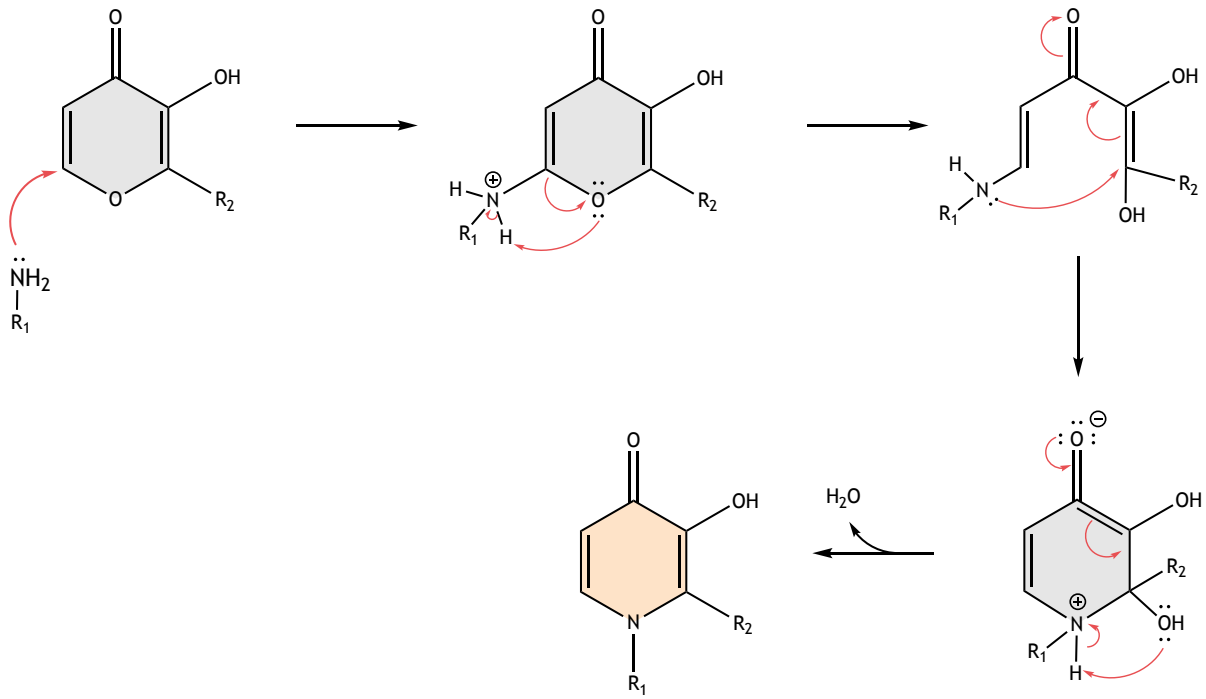

Figure 27: Mechanism of Michael-type addition reaction between a 3-hydroxypyran-4-one derivatives and primary arylamines.

From the two tested protocols (A and B), general procedure B proved to be more successful. In fact, only compound **2** was obtained using general procedure A. Although oil bath reflux and Radleys Mya 4® reaction station following general procedure A were initially tested, compound **1** was only successfully synthesized through general procedure B. Unfortunately, compounds **3** and **4** were the only compounds whose synthesis was not successfully accomplished. Their synthesis was performed using the experimental conditions described in general procedure A. NMR spectra confirmed that the reaction yielded a byproduct and, due to time constraints, general procedure B was not tested to synthesize compounds **3** and **4**.

Although procedure B proved to be more effective, the overall yields remained very low (2.1-5.6 %). The protection of 3-hydroxyl group of pyran-4-one by ether formation using the Harris method [127, 128] can be an alternative approach to avoid the formation of byproducts and to improve the reaction yields. Moreover, microwave irradiation can be a powerful ally for the synthesis of these compounds by reducing the reaction times and improving the reaction yields [105, 129, 130].

3.2. Assessment of drug-like properties

As aforementioned in section 1.7.2., the evaluation of the physicochemical properties of compounds during drug development is of upmost importance. These studies provide a valuable information concerning the ADMET properties of the drug candidates. In the particular case of potential CNS drugs, these properties help dictate whether the compound in question is able to cross the BBB or not. Therefore, the MW, NROTB, HBD, HBA and tPSA (topological Polar Surface Area) of compounds **1, 2, 5-8** together with metal chelator deferiprone were predicted using the Molinspiration Cheminformatics software (https://www.molinspiration.com/) (Table 5).

The MW is known to affect a molecule's ability to cross the BBB. CNS drugs tend to have lower values of MW compared with other therapeutics; for marketed CNS drugs, the mean value of MW is 310 Da, whereas the average MW for all marketed oral drugs is 377 Da [131]. Rules for predicting BBB tend to place the MW cutoff for BBB penetration in the 400 Da range [97]. In fact, the MW of deferiprone derivatives **1**, **2**, **5**-**8** range between 187.20 - 229.28 Da, falling within the optimal values for CNS-active drugs (< 400 Da).

The NROTB concerns the compounds' flexibility, which is needed to a certain extent to cross the BBB. While compounds **1**, **2**, **7** and **8** display 1 NROTB, compounds **5** and **6**, present 3 NORTB, due to the presence a 2-carbon linker between the pyrone core and aromatic ring. The values lower than 10 are considered a valuable attribute for successful CNS drug candidates.

Moreover, the HBD and HBA values indicate the H-bonding capacity of compounds and are associated with membrane penetration. All compounds display 1 HBD and 3 HBA, which is in line with optimal values (HBD = 1; HBA = 2.1).

The tPSA gives us information about the compounds' ability to form hydrogen bonds with their oxygen and nitrogen atoms. High tPSA values are associated with impaired membrane penetration. Since all compounds share the same number of oxygen and nitrogen atoms, tPSA values were similar (42.33 Å) and fell within the limit of CNS-active drugs (< 90 Å).

Finally, BBB penetration of compounds **1, 2, 5-8** and metal chelator deferiprone was predicted using the blood-brain barrier (BBB) Prediction Server (https://www.cbligand.org/BBB/) (Table 5) [132]. BBB penetration is one of the major hurdles that new neurotherapeutics face, due to the BBB's complex structure. Being able to cross the BBB is a major advantage for CNS drugs, allowing a more direct action and increased bioavailability in the brain. With the exception of compounds **2** and **8**, deferiprone derivatives are predicted to successfully cross the BBB.

Table 5 Predicted drug-like properties of compounds 1, 2, 5-8 and metal chelator deferiprone.

Compound	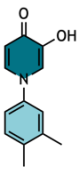	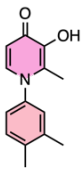	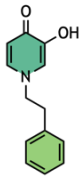	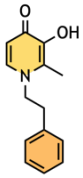	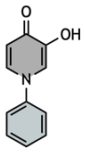	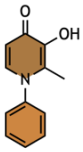	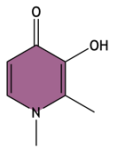
	1	**2**	**5**	**6**	**7**	**8**	**Deferiprone**
MW (Da)	215.25	229.28	215.25	229.28	187.20	201.22	139.15
NROTB	1	1	3	3	1	1	0
HBD	1	1	1	1	1	1	1
HBA	3	3	3	3	3	3	3
tPSA (Å)	42.33	42.33	42.33	42.33	42.33	42.33	42.23
BBB permeation	+	-	+	+	+	-	+

MW, NROTB, HBD, HBA and tPSA were calculated using Molinspiration Cheminformatics software. BBB permeation was predicted using the blood-brain barrier (BBB) Prediction Server: (+) permeable and (-) not permeable.

In summary, the synthesized compounds exhibited promising physicochemical properties, showing predicted MW, NROTB, HBD, HBA and tPSA values within optimal ranges. Among all compounds, deferiprone derivatives **1**, **5-7** are predicted to cross the BBB and to act as CNS-active drugs.

3.3. Chromatographic Hydrophobicity Index

As described in section 1.7.2., there are a number of physicochemical properties that determine the characteristics of a drug candidate. The determination of compound's lipophilicity is crucial in the early stages of drug discovery. Lipophilicity affects the ability of small molecules to interact with physiological membranes and, consequently, the cell permeability and toxicity. Thus, the experimental determination of the lipophilicity of the synthetized compounds is essential to estimate their behavior in the organism. Accordingly, we initially determined the CHI values of the compounds, a parameter directly correlated with the compound's lipophilicity, using HPLC biomimetic approaches [8, 110]. The results obtained are depicted in Table 6. CHI values normally range between 0 and 100, but for compounds with very hydrophilic or lipophilic characters it can go below zero or above 100, respectively.

Due to the amphiphilic nature of biological membranes, it is important that compounds are neither too hydrophobic nor too hydrophilic. From the data acquired, it was concluded that CHI values increased with the presence of two methyl groups in the benzene ring (compound **1**, LogD = 1.27; compound **2**, LogD = 1.59), which are associated with a higher lipophilicity. Moreover, compounds bearing a 2-methyl group at the pyran-4-one moiety (compounds **2**, **6** and **8**) displayed higher lipophilic character than the 2-H-containing derivatives (compounds **1**, **5** and **7**). Finally, compounds **5** (LogD = 0.71) and **6** (LogD = 1.13) are more lipophilic than compounds **7** (LogD = 0.36) and **8** (LogD = 0.90), but less hydrophobic than **1** and **2**. This suggests that the introduction of a linker between the pyrone core and aromatic ring also affects the hydrophobic character of the compounds.

To further evaluate the interaction of compounds with biological membranes, the CHI (IAM) values were determined using a column containing phospholipids covalently bound to silica particles. The results are presented in Table 6. Among all derivatives, compound **1** exhibited the highest Log K(IAM) value (Log K(IAM) = 5.47) indicating higher affinity for the phospholipid membranes. Compounds derived from 2-methyl-4*H*-pyran-4-one (compounds **2**, **6** and **8**) shared similar Log K(IAM) values to compounds derived from 3-hydroxy-4*H*-pyran-

4-one (compounds **1**, **5** and **7**). As evidenced by the calculated cell partition coefficient (Log K_{pcell}) (Table 6) that predicts the passive permeability of compounds in cells, compound **1** presented the highest value (Log K_{pcell} = 1.18), suggesting a higher cellular internalization. On the other hand, compounds **7** and **8** presented negative K_{pcell} values. Thus, they are predicted to be less internalized by cells.

Finally, concerning both CHI and CHI(IAM) values, the compounds **1, 2, 5-8** displayed adequate lipophilicity and membrane affinity. Among all derivatives, compound **1** stands out, showing not only the highest lipophilic character (Log D = 1.27), but also the highest phospholipid affinity and cellular internalization (Log K(IAM) = 5.47 and Log K_{pcell} = 1.18). These results are in line with the BBB (+) penetration prediction described in section 3.2.

Table 6 Experimental CHI and CHI IAM values, number of hydrogen donors (HBD) and calculated Log P, Log K(IAM), Log k(IAM) and Log K_{pcell} of compounds 1, 2, 5-8.

Compound	CHI	HBD[a]	Log D[b]	CHI (IAM)	Log K (IAM)[c]	Log k (IAM)[d]	Log K_{pcell}[e]
1	42.73	1	1.27	51.76	5.47	2.80	1.18
2	49.48		1.59	31.87	2.61	1.89	0.17
5	30.81		0.71	31.05	2.54	1.85	0.13
6	39.77		1.13	30.25	2.47	1.81	0.09
7	23.36		0.36	26.33	2.18	1.63	-0.11
8	34.99		0.90	27.10	2.24	1.67	-0.07

[a] Values calculated using Molinspiration Cheminformatics software; [b] Log D represents the partition coefficient of a compound between octanol and water at pH 7.4 and were back-calculated from the compounds CHI values using the equation (1); [c] Log *K* (IAM) represents the compound partition coefficient between the immobilized phospholipidic membrane and the mobile phase and were back-calculated from the compounds CHI (IAM) values using the equation (2); [d] Log *k*(IAM) gives the affinity of the compound to the stationary phospholipid membrane and were obtained according to the equation (3); [e] Log K_{pcell} estimates the compound concentration between the intracellular and the external cellular media considering their passive permeability and were obtained according to the equation (4).

3.4. Evaluation of metal chelating properties

3.4.1. Iron

Redox active metals like iron react with H_2O_2 in Fenton or Harber-Weiss reactions, producing $^{\bullet}OH$ radicals with harmful effects for human health [47]. As such, the iron (II) chelating properties of the synthesized compounds, tolcapone, entacapone and deferiprone were evaluated by the ferrozine assay. In this spectrophotometric method, the formation of colored $[Fe(Ferrozine)_3]^{2+}$ complex can be prevented by iron chelators that compete with ferrozine and, consequently, decrease the absorbance at 562 nm. The data presented in

Figure 28 expresses the mean percentage of iron chelation (% Fe(II) chelation) ± standard error deviation of six experiments. EDTA was used as reference compound.

Overall, deferiprone and derivatives thereof exhibited remarkable iron chelating properties, with values ranging from 79.91-95.64 % (Figure 28). The results obtained were similar to the potent chelators tolcapone (94.24 %) and entacapone (84.00 %) [84]. The deferiprone derivatives that presented higher iron chelation capacity are those derived from 2-methyl-4*H*-pyran-4-one (compounds **2**, **6** and **8**), being compound **8** the best iron chelator (95.64 %) of the series. These results suggest that the introduction of the methyl group at the C2 position of the 3-hyddroxypyridinone ring enhances the iron chelating activity of compounds. The other structural modifications shared similar effect on chelation properties.

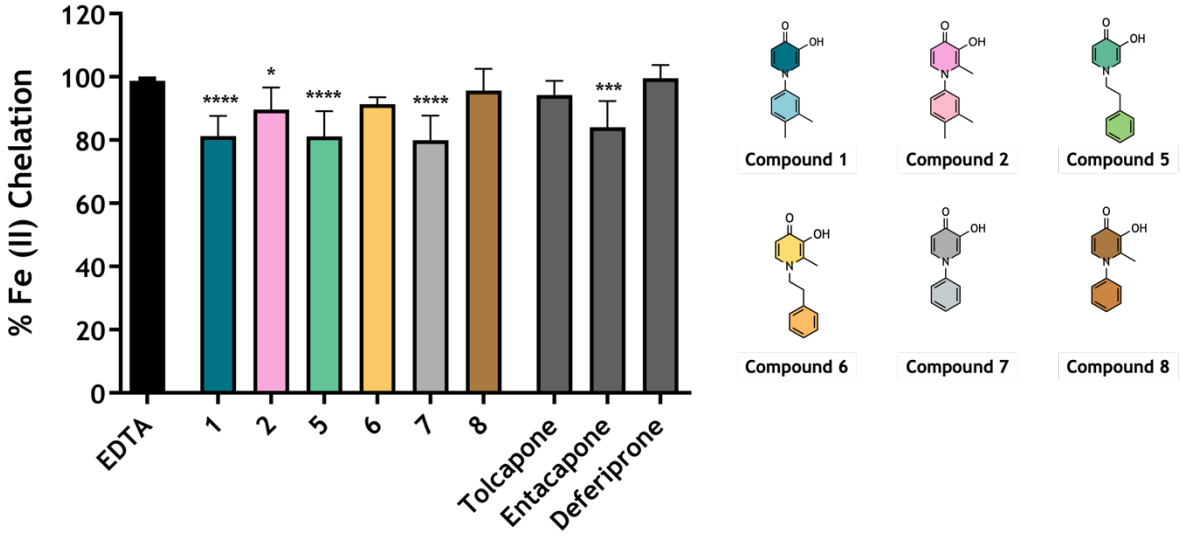

*Figure 28: Iron chelating properties of test compounds expressed as mean % Fe (II) chelation ± SEM (n= 6). Statistical comparisons were made using one-way ANOVA followed by the Dunnett multiple comparison post hoc test (*p < 0.05, *** p < 0.0005, ****p < 0.0001 vs EDTA).*

3.4.2. Copper

The copper chelating abilities of compounds **1**, **2**, **5-8** was investigated using UV-vis spectrometry. As shown in Figure 29, a full scan of a 40 μM solution of compounds in phosphate buffer (pH 7.4) was recorded and compared with the same solutions co-incubated with 20 μM of copper(II) sulfate. All compounds showed a sharp peak at 202 nm in their UV spectra that remains unaltered in the presence of copper sulfate. On the other hand, the spectra showed a decrease in the absorbance in the presence of copper between 280-290 nm, which indicates that a complex between the ligand and copper(II) was formed.

Hereafter, titration analysis of compounds **1**, **2**, **5-8** was carried out using the molar ratio method [116] with fixed concentrations of the test compounds and increasing concentrations of copper(II) sulfate (0-100 µM) (Figure 30). The results showed that compounds **2**, **5**, **7** and **8** present a 2:1 Cu^{2+}/ligand stoichiometry, compound **1** a 1.5:1 stoichiometry and compound **6** a 1:1 stoichiometry. As a result, the obtained data suggests that the synthetized compounds exhibit significant copper(II) chelating properties, specially compounds **6** and **1**. Structural modifications do not seem to affect the copper(II) chelating properties of compounds.

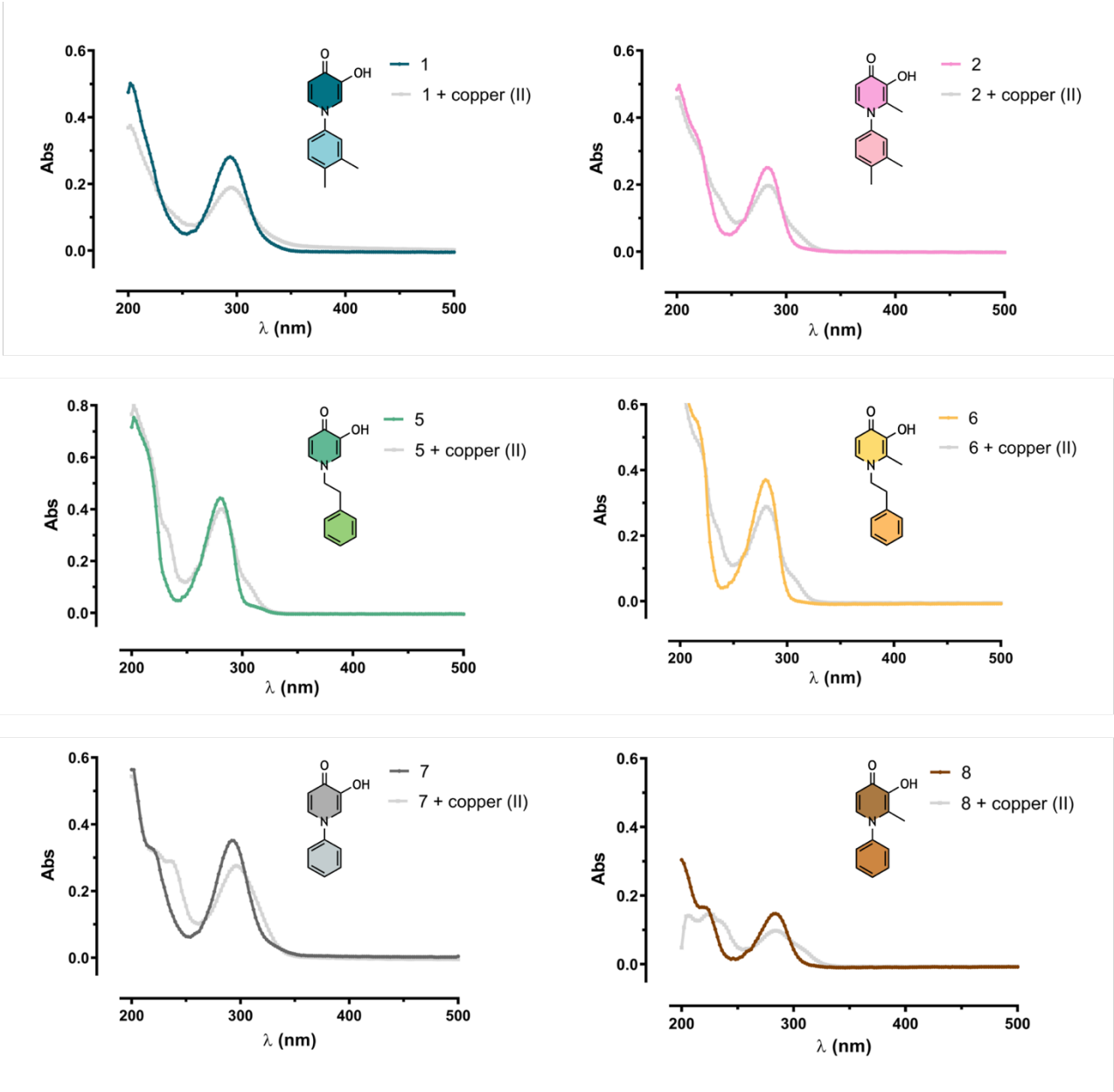

Figure 29: UV spectra of compounds 1, 2, 5-8 at 40 µM alone or co-incubated with copper (II) sulfate 20 µM (grey). All solutions were prepared in phosphate-buffered saline (pH 7.4).

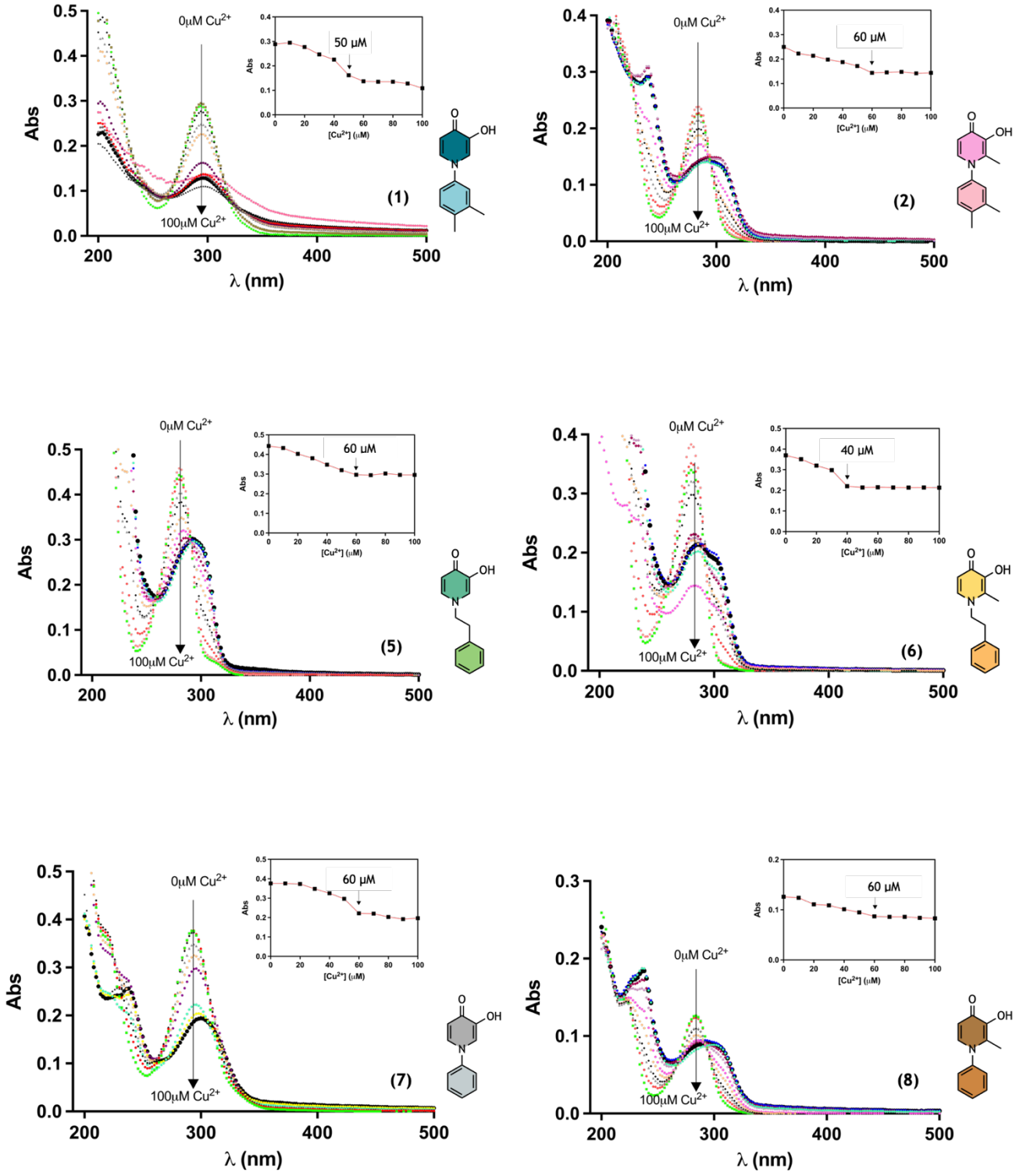

Figure 30: UV-vis titration of compounds 1,2, 5-8 with Cu^{2+} in phosphate-buffered saline at room temperature with Cu^{2+} (0-100 μM). Inset: change in absorbance with increased Cu^{2+} derived from the titration; a breakpoint was observed at 50 μM un compound 1, 60 μM in compounds 2, 5, 7 and 8 and 40 μM in compound 6. The concentration of compounds was 40 μM.

3.5. Evaluation of Antioxidant Activity

The total antioxidant capacity of the new compounds was evaluated using 2,2'-azino-bis(3-ethylbenzothiazoline-6-sulphonic acid) radical ($ABTS^{\bullet+}$) radical scavenging assay. The IC_{50} values were calculated as the minimum concentration of an antioxidant required to scavenge 50 % of the radical. The antioxidant activity of Trolox, a water-soluble vitamin E analogue, as well as tolcapone, entacapone, deferiprone was also assessed. From the data acquired (Figure 31), it was concluded that, with the exception of 3-hydroxy-4*H*-pyran-4-one derivatives (compounds **1**, **5** and **7**), all compounds were able to efficiently scavenge $ABTS^{\bullet+}$ radical. These results suggests that the presence of a methyl group at the C2 position of 3-hydroxypyridinone ring enhances the antioxidant activity of compounds. Overall, the antioxidant activity of compound **6** was higher than Trolox and deferiprone. Unlike compounds **2** and **8**, compound **6** contains a 2-carbon linker between the 3-hydroxypyridinone core and aromatic ring that may decrease the steric hindrance. Thus, compound **6** can access the radical center more easily and thus act as a better antioxidant. It was also observed that all compounds showed lower radical scavenging activity in $ABTS^{\bullet+}$ assay than the COMT inhibitors tolcapone and entacapone.

In summary, deferiprone derivatives containing a methyl group on the 3-hydroxypyridinone ring were endowed with radical scavenging properties. The presence of an alkyl linker between the pyrone core and the aromatic ring enhances the radical scavenging activity of compounds.

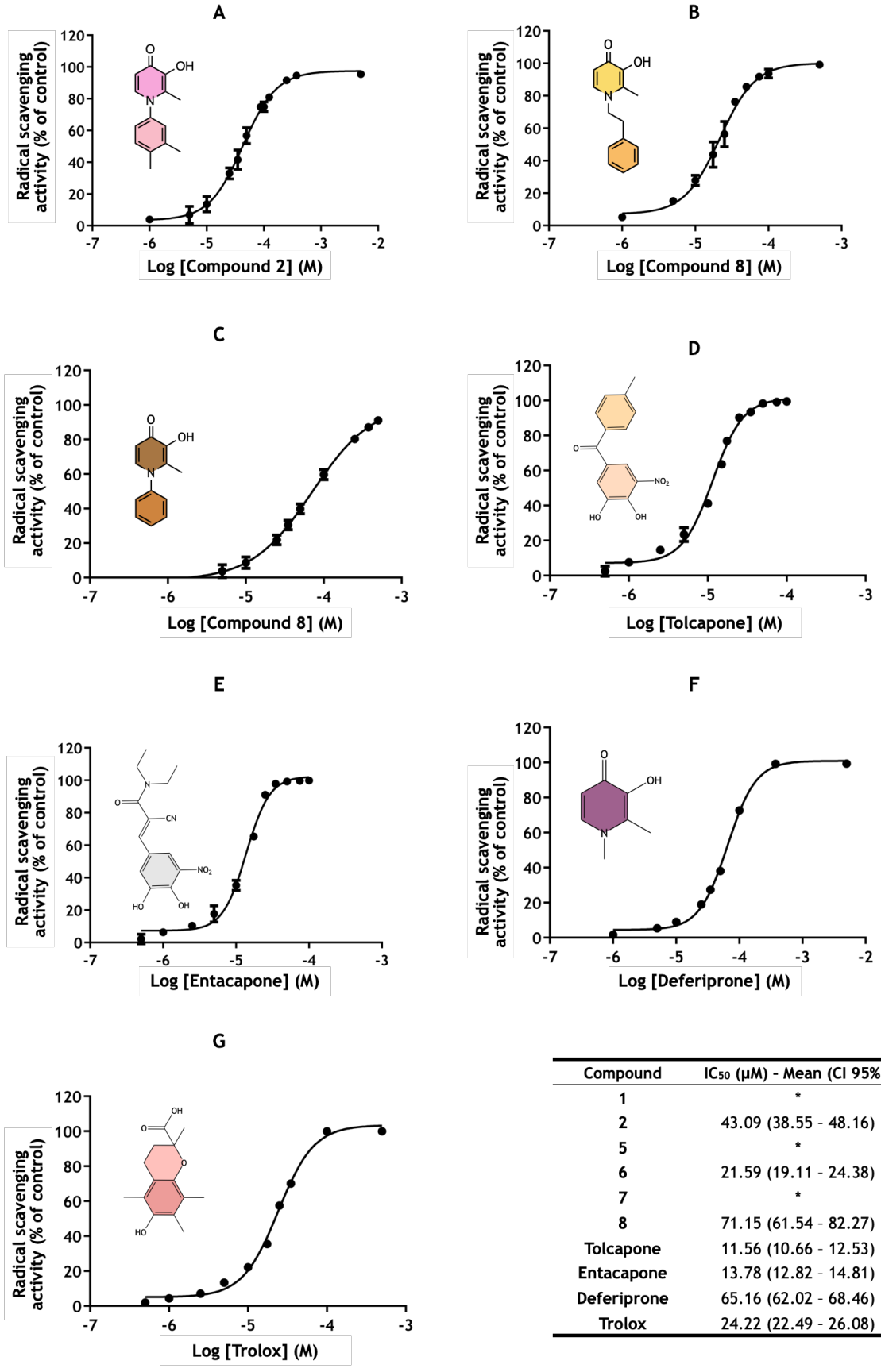

Compound	IC_{50} (μM) - Mean (CI 95%)[a]
1	*
2	43.09 (38.55 - 48.16)
5	*
6	21.59 (19.11 - 24.38)
7	*
8	71.15 (61.54 - 82.27)
Tolcapone	11.56 (10.66 - 12.53)
Entacapone	13.78 (12.82 - 14.81)
Deferiprone	65.16 (62.02 - 68.46)
Trolox	24.22 (22.49 - 26.08)

*Figure 31: Dose-response curves for test compounds compound 2 (A), compound 6 (B), compound 8 (C), tolcapone (D), entacapone (E), deferiprone (F) and Trolox (G) and Total antioxidant activity of test compounds, tolcapone, entacapone, deferiprone and Trolox. [a] CI: confidence interval at 95 %; * inactive at 1 mM (highest concentration tested).*

3.6. Evaluation of monoamine oxidase inhibitory activity

The inhibitory activity on *h*MAO-A and *h*MAO-B of compounds **1**, **2**, **5-8** was studied using a spectrophotometric assay based on the formation of 4-HQ. A preliminary screening with test compounds was carried out to assess if they present relevant *h*MAO inhibitory activity at a concentration of 10 μM. The results are presented in Table 7. Although the test compounds present higher inhibitory activity for the isoform B, the percentages of inhibition obtained at 10 μM against both *h*MAO-A and *h*MAO-B were always below 50 %. Therefore, compounds **1**, **2**, **5-8** did not display relevant *h*MAO inhibition properties.

Table 7: Percentages of hMAO-A and hMAO-B inhibition of compounds 1, 2, 5-8 and reference inhibitors (clorgyline for hMAO-A and rasagiline for hMAO-B) at 10 μM.

Compound	% inhibition	
	*h*MAO-A	*h*MAO-B
1	6.6	46.2
2	5.7	14.9
5	1.9	14.6
6	5.1	13.2
7	11.4	26.3
8	4.1	30.7
Clorgyline	100	85.4
Rasagiline	83.4	100

CHAPTER IV – Conclusion and Future Prospects

4. Conclusion and future prospects

In this work, six compounds based on the deferiprone scaffold were successfully synthesized. On the other hand, compounds **3** and **4** were not successfully obtained. The chemical structures of all the synthesized compounds were confirmed using NMR techniques (^{1}H NMR, ^{13}C NMR and DEPT135). Since compounds **3** and **4** were not fulfilled, it would be interesting to re-do the synthesis following general procedure B or, alternatively, using the Harris method. Following the synthesis, the evaluation of the bioactivity and the physicochemical properties of compounds **3** and **4** can also be performed.

Overall, compounds **1**, **2**, **5-8** displayed remarkable drug-like properties with predicted MW, NROTB, HBD, HBA and tPSA values within the optimal range. Except for compounds **2** and **8**, all compounds were predicted to penetrate the BBB. Given the promising theoretical calculations, a thorough analyses of physicochemical properties and the biological activities of compounds were carried out using HPLC biomimetic approaches and different spectrophotometric methods.

First, the lipophilicity of the synthesized compounds was evaluated by the determination of CHI and CHI(IAM) values through RP-HPLC. From the obtained CHI data, it was concluded that compounds derived from 2-methyl-4*H*-pyran-4-one (compounds **2**, **6** and **8**) displayed a more lipophilic character when compared with compounds derived from 3-hydroxy-4*H*-pyran-4-one (compounds **1**, **5** and **7**). The studied structural modifications did not markedly affect the phospholipid membrane affinity, as shown by CHI(IAM) values.

The iron and copper chelating ability of compounds **1**, **2**, **5**-**8** were investigated using spectrophotometric assays. The results obtained showed that that all the deferiprone-based compounds were able to chelate more than 79.91% of iron, being compounds derived from 2-methyl-4*H*-pyran-4-one (compounds **2**, **6** and **8**) better iron chelators than compounds derived from 3-hydroxy-4H-pyran-4-one (compounds **1**, **5** and **7**). Moreover, compounds **1**, **2**, **5**-**8** also demonstrated significant copper(II) chelating properties. Compounds **1** and **6** were the best Copper(II) chelators, showing Cu^{2+}/ligand complex stoichiometries of 1.5:1 and 1:1, respectively. The studied structural modifications did not seem to play a significant role in the copper chelating properties of compounds.

The total antioxidant activity of the synthesized compounds was assessed using the $ABTS^{\bullet+}$ radical scavenging assay. Apart for 3-hydroxy-4*H*-pyran-4-one derivatives (compounds **1**, **5** and **7**), all compounds were able to efficiently scavenge $ABTS^{\bullet+}$ radical. In general, the presence of a methyl group bound to the 3-hydroxypyridinone ring (compounds

2, **6** and **8**) and an alkyl linker between the 3-hydroxypyridinone core and the benzenic ring enhance the radical scavenging activity of compounds.

The inhibitory activity on *h*MAO-A and *h*MAO-B of compounds **1**, **2**, **5-8** was studied using a spectrophotometric assay based on the formation of 4-HQ. Although the synthesized compounds displayed higher inhibitory activity or *h*MAO-B, the preliminary screening concluded that they did not present relevant inhibitory activity at 10 μM (i.e. percentage of inhibition below 50 %). Therefore, no further tests were made.

Altogether, the results obtained under this thesis instigate the chemical framework of deferiprone as a valid scaffold for development of promising candidate for PD. Compound **6** stands out with excellent metal chelating and antioxidant properties. Concerning its lipophilicity, CHI and CHI(IAM) values suggest an adequate lipophilicity and cell internalization. In addition, it is predicted to be able to cross the BBB. Altogether, compound **6** displays remarkable drug-like properties.

One of the main goals of future research will be the evaluation of the BBB permeability of the synthesized compounds through a parallel artificial membrane permeability assay. Moreover, the evaluation of cytotoxicity and neuroprotection in PD specific models will be the focus in the future work. Finally, time-dependent stability studies of the synthesized compounds should also be considered. Possible changes in the stability of a drug or drug candidate result in changes in the physicochemical properties and, consequently, in the therapeutic effects and expected clinical responses.

CHAPTER V – References

5. References

1. Juárez Olguín, H., D. Calderón Guzmán, E. Hernández García, *et al.*, *The Role of Dopamine and Its Dysfunction as a Consequence of Oxidative Stress*. Oxid. Med. Cell. Longev., 2016: p. 9730467. doi: 10.1155/2016/9730467.
2. Ju, D.W., *Neuroscience: Canadian 1st Edition Open Textbook*, ed. I.B. Georgia Bains, Maksym Shcherbina, and Summer Lee 2018.
3. Islam, M. and Z. Mohamed, *Computational and Pharmacological Target of Neurovascular Unit for Drug Design and Delivery*. BioMed Research International, 2015. doi: 10.1155/2015/731292.
4. Bazazeh, D., R. Shubair, and W. Malik, *Biomarker Discovery and Validation for Parkinson's Disease: A Machine Learning Approach*. 2016. doi: 10.1109/BIOSMART.2016.7835465
5. Váradi, C., *Clinical Features of Parkinson's Disease: The Evolution of Critical Symptoms*. Biology, 2020. **9**(5): p. 103. doi:10.3390/biology9050103
6. Youdim, M.B.H., D. Edmondson, and K.F. Tipton, *The therapeutic potential of monoamine oxidase inhibitors*. Nature Reviews Neuroscience, 2006. **7**(4): p. 295-309. doi: 10.1038/nrn1883.
7. Wolff, A., M. Antfolk, B. Brodin, *et al.*, *In Vitro Blood-Brain Barrier Models: An Overview of Established Models and New Microfluidic Approaches*. J. Pharm. Sci., 2015. **104**(9): p. 2727-2746. doi: 10.1002/jps.24329.
8. Valkó, K., C. Bevan, and D. Reynolds, *Chromatographic Hydrophobicity Index by Fast-Gradient RP-HPLC: A High-Throughput Alternative to log P/log D*. Anal. Chem., 1997. **69**(11): p. 2022-9. doi: 10.1021/ac961242d. 21639241
9. Silva, T.B., F. Borges, M.P. Serrão, *et al.*, *Liver says no: the ongoing search for safe catechol O-methyltransferase inhibitors to replace tolcapone*. Drug Discov Today, 2020. doi: 10.1016/j.drudis.2020.07.015. 32687872
10. Valko, K., C.M. Du, C.D. Bevan, *et al.*, *Rapid-gradient HPLC method for measuring drug interactions with immobilized artificial membrane: comparison with other lipophilicity measures*. J. Pharm. Sci., 2000. **89**(8): p. 1085-96. doi: 10.1002/1520-6017(200008)89:8<1085::aid-jps13>3.0.co;2-n. 10906732
11. Kalia, L.V. and A.E. Lang, *Parkinson's disease*. Lancet, 2015. **386**(9996): p. 896-912. doi: 10.1016/s0140-6736(14)61393-3. 25904081
12. Rogers, K., *The Brain and the Nervous System (The Human Body)* 2010: Britannica Educational Publishing.
13. Lindsay M. Biga, S.D., Amy Harwell, Robin Hopkins, Joel Kaufmann, Mike LeMaster, Philip Matern, Katie Morrison-Graham, Devon Quick & Jon Runyeon, *Anatomy & Physiology*. 2020: OpenStax.
14. Brown, R.C., A.H. Lockwood, and B.R. Sonawane, *Neurodegenerative diseases: an overview of environmental risk factors*. Environ. Health Perspect., 2005. **113**(9): p. 1250-1256. doi: 10.1289/ehp.7567. 16140637
15. Hussain, R., H. Zubair, S. Pursell, *et al.*, *Neurodegenerative Diseases: Regenerative Mechanisms and Novel Therapeutic Approaches*. Brain Sci, 2018. **8**(9). doi: 10.3390/brainsci8090177. 30223579
16. Maiti, P., J. Manna, and G.L. Dunbar, *Current understanding of the molecular mechanisms in Parkinson's disease: Targets for potential treatments*. Translational Neurodegeneration, 2017. **6**(1): p. 28. doi: 10.1186/s40035-017-0099-z.
17. Keener, A.M. and Y.M. Bordelon, *Parkinsonism*. Semin. Neurol., 2016. **36**(4): p. 330-4. doi: 10.1055/s-0036-1585097. 27643900
18. Segura-Aguilar, J., I. Paris, P. Muñoz, *et al.*, *Protective and toxic roles of dopamine in Parkinson's disease*. J. Neurochem., 2014. **129**(6): p. 898-915. doi: 10.1111/jnc.12686.

19. Klein, M.O., D.S. Battagello, A.R. Cardoso, *et al.*, *Dopamine: Functions, Signaling, and Association with Neurological Diseases*. Cell. Mol. Neurobiol., 2019. **39**(1): p. 31-59. doi: 10.1007/s10571-018-0632-3. 30446950

20. Rubí, B. and P. Maechler, *Minireview: New Roles for Peripheral Dopamine on Metabolic Control and Tumor Growth: Let's Seek the Balance*. Endocrinology, 2010. **151**: p. 5570-81. doi: 10.1210/en.2010-0745.

21. Riederer, P., M. Gerlach, T. Müller, *et al.*, *Relating mode of action to clinical practice: dopaminergic agents in Parkinson's disease*. Parkinsonism Relat. Disord., 2007. **13**(8): p. 466-79. doi: 10.1016/j.parkreldis.2007.06.015. 17919963

22. Dauer, W. and S. Przedborski, *Parkinson's Disease: Mechanisms and Models*. Neuron, 2003. **39**(6): p. 889-909. doi: 10.1016/S0896-6273(03)00568-3.

23. Erkkinen, M.G., M.O. Kim, and M.D. Geschwind, *Clinical Neurology and Epidemiology of the Major Neurodegenerative Diseases*. Cold Spring Harb. Perspect. Biol., 2018. **10**(4). doi: 10.1101/cshperspect.a033118. 28716886

24. Bose, A. and M.F. Beal, *Mitochondrial dysfunction in Parkinson's disease*. J. Neurochem., 2016. **139**(S1): p. 216-231. doi: 10.1111/jnc.13731.

25. Raza, C., R. Anjum, and N.U.A. Shakeel, *Parkinson's disease: Mechanisms, translational models and management strategies*. Life Sci., 2019. **226**: p. 77-90. doi: 10.1016/j.lfs.2019.03.057. 30980848

26. Jankovic, J., *Parkinson's disease: clinical features and diagnosis*. Journal of Neurology, Neurosurgery & Psychiatry, 2008. **79**(4): p. 368-376. doi: 10.1136/jnnp.2007.131045.

27. Chaudhuri, K.R., L. Yates, and P. Martinez-Martin, *The non-motor symptom complex of Parkinson's disease: a comprehensive assessment is essential*. Curr. Neurol. Neurosci. Rep., 2005. **5**(4): p. 275-83. doi: 10.1007/s11910-005-0072-6. 15987611

28. Sellbach, A. and P. Silburn, *Management of Parkinson's disease*. Australian Prescriber, 2012. **35**: p. 183-188. doi: 10.18773/austprescr.2012.084.

29. Heusinkveld, L.E., M.L. Hacker, M. Turchan, *et al.*, *Impact of Tremor on Patients With Early Stage Parkinson's Disease*. Front. Neurol., 2018. **9**(628). doi: 10.3389/fneur.2018.00628.

30. Findley, L.J., *The economic impact of Parkinson's disease*. Parkinsonism Relat. Disord., 2007. **13 Suppl**: p. S8-s12. doi: 10.1016/j.parkreldis.2007.06.003. 17702630

31. Organization, W.H., *Neurological disorders : public health challenges*. 2006.

32. N. Maserejian, L.V.-I., A. Dilley, *Estimation of the 2020 Global Population of Parkinson's Disease (PD) [abstract]*. Mov. Disord., 2020.

33. Dorsey, E.R., A. Elbaz, E. Nichols, *et al.*, *Global, regional, and national burden of Parkinson's disease, 1990–2016: a systematic analysis for the Global Burden of Disease Study 2016*. The Lancet Neurology, 2018. **17**(11): p. 939-953. doi: 10.1016/S1474-4422(18)30295-3.

34. Dorsey, E.R., T. Sherer, M.S. Okun, *et al.*, *The Emerging Evidence of the Parkinson Pandemic*. J. Parkinsons Dis., 2018. **8**(s1): p. S3-s8. doi: 10.3233/jpd-181474. 30584159

35. Organization, W.H., *Atlas : country resources for neurological disorders 2004*. 2004.

36. Martinez-Martin, P., D. Macaulay, Y.J. Jalundhwala, *et al.*, *The long-term direct and indirect economic burden among Parkinson's disease caregivers in the United States*. Mov. Disord., 2019. **34**(2): p. 236-245. doi: 10.1002/mds.27579.

37. Verboket, R.D., N. Mühlenfeld, M. Woschek, *et al.*, *Inpatient treatment costs, cost-driving factors and potential reimbursement problems due to fall-related fractures in patients with Parkinson's disease*. Der Chirurg; Zeitschrift fur alle Gebiete der operativen Medizen, 2020. **91**(5): p. 421-427. doi: 10.1007/s00104-019-01074-w. 31807819

38. Hayes, M.T., *Parkinson's Disease and Parkinsonism*. Am. J. Med., 2019. **132**(7): p. 802-807. doi: 10.1016/j.amjmed.2019.03.001. 30890425

39. Beitz, J.M., *Parkinson's disease: a review*. Front Biosci (Schol Ed), 2014. **6**: p. 65-74. doi: 10.2741/s415. 24389262

40. Soto, C. and S. Pritzkow, *Protein misfolding, aggregation, and conformational strains in neurodegenerative diseases*. Nat. Neurosci., 2018. **21**(10): p. 1332-1340. doi: 10.1038/s41593-018-0235-9.

41. Antony, P.M.A., N.J. Diederich, R. Krüger, *et al.*, *The hallmarks of Parkinson's disease*. The FEBS Journal, 2013. **280**(23): p. 5981-5993. doi: 10.1111/febs.12335.

42. Rocha, E.M., B. De Miranda, and L.H. Sanders, *Alpha-synuclein: Pathology, mitochondrial dysfunction and neuroinflammation in Parkinson's disease*. Neurobiol. Dis., 2018. **109**: p. 249-257. doi: 10.1016/j.nbd.2017.04.004.

43. Sampaio-Marques, B. and P. Ludovico, *Sirtuins and Proteolytic Systems: Implications for Pathogenesis of Synucleinopathies*. Biomolecules, 2015. **5**(2): p. 735-757. doi:10.3390/biom5020735

44. Pickrell, A.M. and R.J. Youle, *The roles of PINK1, parkin, and mitochondrial fidelity in Parkinson's disease*. Neuron, 2015. **85**(2): p. 257-273. doi: 10.1016/j.neuron.2014.12.007. 25611507

45. Schapira, A.H.V., *Calcium dysregulation in Parkinson's disease*. Brain, 2013. **136**(7): p. 2015-2016. doi: 10.1093/brain/awt180.

46. Hare, D. and K. Double, *Iron and dopamine: A toxic couple*. Brain, 2016. **139**: p. aww022. doi: 10.1093/brain/aww022.

47. Benfeito, S., C. Oliveira, C. Fernandes, *et al.*, *Fine-tuning the neuroprotective and blood-brain barrier permeability profile of multi-target agents designed to prevent progressive mitochondrial dysfunction*. Eur. J. Med. Chem., 2019. **167**: p. 525-545. doi: 10.1016/j.ejmech.2019.01.055. 30784884

48. Jomova, K., D. Vondrakova, M. Lawson, *et al.*, *Metals, oxidative stress and neurodegenerative disorders*. Mol. Cell. Biochem., 2010. **345**(1-2): p. 91-104. doi: 10.1007/s11010-010-0563-x. 20730621

49. Tysnes, O.-B. and A. Storstein, *Epidemiology of Parkinson's disease*. J. Neural Transm., 2017. **124**(8): p. 901-905. doi: 10.1007/s00702-017-1686-y.

50. López-Otín, C., M.A. Blasco, L. Partridge, *et al.*, *The hallmarks of aging*. Cell, 2013. **153**(6): p. 1194-1217. doi: 10.1016/j.cell.2013.05.039. 23746838

51. Hou, Y., X. Dan, M. Babbar, *et al.*, *Ageing as a risk factor for neurodegenerative disease*. Nature Reviews Neurology, 2019. **15**(10): p. 565-581. doi: 10.1038/s41582-019-0244-7.

52. Maria Angeles, M., C. Maria Jose, S. Rosa Maria, *et al.*, *Half a Century of l-DOPA*. Curr. Top. Med. Chem., 2009. **9**(10): p. 880-893. doi: 10.2174/156802609789378263.

53. Contin, M. and P. Martinelli, *Pharmacokinetics of levodopa*. J. Neurol., 2010. **257**(2): p. 253-261. doi: 10.1007/s00415-010-5728-8.

54. Masato, A., N. Plotegher, D. Boassa, *et al.*, *Impaired dopamine metabolism in Parkinson's disease pathogenesis*. Mol. Neurodegener., 2019. **14**(1): p. 35. doi: 10.1186/s13024-019-0332-6.

55. Meiser, J., D. Weindl, and K. Hiller, *Complexity of dopamine metabolism*. Cell Communication and Signaling, 2013. **11**(1): p. 34. doi: 10.1186/1478-811X-11-34.

56. Kremer, T., K.I. Taylor, J. Siebourg-Polster, *et al.*, *Longitudinal Analysis of Multiple Neurotransmitter Metabolites in Cerebrospinal Fluid in Early Parkinson's Disease*. Mov. Disord. **n/a**(n/a). doi: 10.1002/mds.28608.

57. LeWitt, P.A., *Dopamine Metabolite Biomarkers and Testing for Disease Modification in Parkinson Disease*. JAMA Neurology, 2020. **77**(8): p. 1038-1039. doi: 10.1001/jamaneurol.2020.1928.

58. Stefani, A., M. Pierantozzi, E. Olivola, *et al.*, *Homovanillic acid in CSF of mild stage Parkinson's disease patients correlates with motor impairment*. Neurochem. Int., 2017. **105**: p. 58-63. doi: 10.1016/j.neuint.2017.01.007.

59. Abbott, A., *Levodopa: the story so far*. Nature, 2010. **466**(7310): p. S6-S7. doi: 10.1038/466S6a.

60. Stoker, T.B. and J.C. Greenland, *Parkinson's Disease: Pathogenesis and Clinical Aspects*. 2018, Codon Publications: Brisbane (AU).doi: 10.15586/codonpublications.parkinsonsdisease.2018

61. Sarkar, S., J. Raymick, and S. Imam, *Neuroprotective and Therapeutic Strategies against Parkinson's Disease: Recent Perspectives*. Int. J. Mol. Sci., 2016. **17**(6). doi: 10.3390/ijms17060904. 27338353

62. Brooks, D.J., *Dopamine agonists: their role in the treatment of Parkinson's disease*. Journal of Neurology, Neurosurgery & Psychiatry, 2000. **68**(6): p. 685. doi: 10.1136/jnnp.68.6.685.

63. Elkouzi, A., V. Vedam-Mai, R.S. Eisinger, *et al.*, *Emerging therapies in Parkinson disease - repurposed drugs and new approaches*. Nat. Rev. Neurol., 2019. **15**(4): p. 204-223. doi: 10.1038/s41582-019-0155-7. 30867588

64. Doi, D., H. Magotani, T. Kikuchi, *et al.*, *Pre-clinical study of induced pluripotent stem cell-derived dopaminergic progenitor cells for Parkinson's disease*. Nature Communications, 2020. **11**(1): p. 3369. doi: 10.1038/s41467-020-17165-w.

65. Stoker, T.B., K.M. Torsney, and R.A. Barker, *Emerging Treatment Approaches for Parkinson's Disease*. Front. Neurosci., 2018. **12**(693). doi: 10.3389/fnins.2018.00693.

66. Bonifácio, M.J., P.N. Palma, L. Almeida, *et al.*, *Catechol-O-methyltransferase and its inhibitors in Parkinson's disease*. CNS Drug Rev, 2007. **13**(3): p. 352-79. doi: 10.1111/j.1527-3458.2007.00020.x. 17894650

67. Bastos, P., T. Gomes, and L. Ribeiro, *Catechol-O-Methyltransferase (COMT): An Update on Its Role in Cancer, Neurological and Cardiovascular Diseases*, in *Reviews of Physiology, Biochemistry and Pharmacology, Vol. 173*, B. Nilius, et al., Editors. 2017, Springer International Publishing: Cham. p. 1-39.doi: 10.1007/112_2017_2

68. Solla, P., A. Cannas, F. Marrosu, *et al.*, *Therapeutic interventions and adjustments in the management of Parkinson disease: Role of combined carbidopa/levodopa/entacapone (Stalevo)*. Neuropsychiatr. Dis. Treat., 2010. **6**: p. 483-90. doi: 10.2147/ndt.s5190.

69. Palma, P.N., L. Kiss, and P. Soares-da-Silva, *Catechol-O-Methyl-Transferase Inhibitors: Present Problems and Relevance of the New Ones*. 2013. p. 83-109.doi: 10.13140/2.1.1292.3848

70. St. Onge, E., M. Vanderhoof, and S. Miller, *Ongentys (Opicapone): A New COMT Inhibitor for the Treatment of Parkinson's Disease*. Ann. Pharmacother., 2020. **0**(0): p. 1060028020974560. doi: 10.1177/1060028020974560. 33233916

71. Annus, Á. and L. Vécsei, *Spotlight on opicapone as an adjunct to levodopa in Parkinson's disease: design, development and potential place in therapy*. Drug Des. Devel. Ther., 2017. **11**: p. 143-151. doi: 10.2147/DDDT.S104227. 28123288

72. Bortolato, M., K. Chen, and J.C. Shih, *Monoamine oxidase inactivation: from pathophysiology to therapeutics*. Adv Drug Deliv Rev, 2008. **60**(13-14): p. 1527-33. doi: 10.1016/j.addr.2008.06.002. 18652859

73. Hubálek, F., J. Pohl, and D.E. Edmondson, *Structural Comparison of Human Monoamine Oxidases A and B: MASS SPECTROMETRY MONITORING OF CYSTEINE REACTIVITIES **. J. Biol. Chem., 2003. **278**(31): p. 28612-28618. doi: 10.1074/jbc.M303712200.

74. Kumar, B., V.P. Gupta, and V. Kumar, *A Perspective on Monoamine Oxidase Enzyme as Drug Target: Challenges and Opportunities*. Curr. Drug Targets, 2017. **18**(1): p. 87-97. doi: 10.2174/1389450117666151209123402. 26648064

75. Tripathi, R.K.P. and S.R. Ayyannan, *Monoamine oxidase-B inhibitors as potential neurotherapeutic agents: An overview and update*. Med. Res. Rev., 2019. **39**(5): p. 1603-1706. doi: 10.1002/med.21561. 30604512

76. Dezsi, L. and L. Vecsei, *Monoamine Oxidase B Inhibitors in Parkinson's Disease*. CNS Neurol. Disord. Drug Targets, 2017. **16**(4): p. 425-439. doi: 10.2174/1871527316666170124165222. 28124620

77. Engelbrecht, I., J.P. Petzer, and A. Petzer, *Nitrocatechol Derivatives of Chalcone as Inhibitors of Monoamine Oxidase and Catechol-O-Methyltransferase*. Cent. Nerv. Syst. Agents Med. Chem., 2018. **18**(2): p. 115-127. doi: 10.2174/1871524918666180426125714. 29697034

78. Schapira, A.H., *Monoamine oxidase B inhibitors for the treatment of Parkinson's disease: a review of symptomatic and potential disease-modifying effects*. CNS Drugs, 2011. **25**(12): p. 1061-71. doi: 10.2165/11596310-000000000-00000. 22133327

79. Tripathi, A.C., S. Upadhyay, S. Paliwal, *et al.*, *Privileged scaffolds as MAO inhibitors: Retrospect and prospects*. Eur. J. Med. Chem., 2018. **145**: p. 445-497. doi: 10.1016/j.ejmech.2018.01.003. 29335210

80. Edmondson, D.E. and C. Binda, *Monoamine Oxidases*. Subcell. Biochem., 2018. **87**: p. 117-139. doi: 10.1007/978-981-10-7757-9_5. 29464559

81. Teixeira, F.G., M.F. Gago, P. Marques, *et al.*, *Safinamide: a new hope for Parkinson's disease?* Drug Discovery Today, 2018. **23**(3): p. 736-744. doi: 10.1016/j.drudis.2018.01.033.

82. Fabbri, M., M.M. Rosa, D. Abreu, *et al.*, *Clinical pharmacology review of safinamide for the treatment of Parkinson's disease*. Neurodegener. Dis. Manag., 2015. **5**(6): p. 481-496. doi: 10.2217/nmt.15.46. 26587996

83. Lhermitte, J., W.M. Kraus, and D. McAlpine, *Original Papers: ON THE OCCURRENCE OF ABNORMAL DEPOSITS OF IRON IN THE BRAIN IN PARKINSONISM WITH SPECIAL REFERENCE TO ITS LOCALISATION*. J. Neurol. Psychopathol., 1924. **5**(19): p. 195-208. doi: 10.1136/jnnp.s1-5.19.195. 21611545

84. Tosato, M. and V. Di Marco, *Metal Chelation Therapy and Parkinson's Disease: A Critical Review on the Thermodynamics of Complex Formation between Relevant Metal Ions and Promising or Established Drugs*. Biomolecules, 2019. **9**(7): p. 269. doi:10.3390/biom9070269

85. Abbruzzese, G., G. Cossu, M. Balocco, *et al.*, *A pilot trial of deferiprone for neurodegeneration with brain iron accumulation*. Haematologica, 2011. **96**(11): p. 1708-11. doi: 10.3324/haematol.2011.043018. 21791473

86. Oliveri, V. and G. Vecchio, *Prochelator strategies for site-selective activation of metal chelators*. J. Inorg. Biochem., 2016. **162**: p. 31-43. doi: 10.1016/j.jinorgbio.2016.05.012.

87. Devos, D., C. Moreau, J.C. Devedjian, *et al.*, *Targeting chelatable iron as a therapeutic modality in Parkinson's disease*. Antioxidants & redox signaling, 2014. **21**(2): p. 195-210. doi: 10.1089/ars.2013.5593. 24251381

88. Martin-Bastida, A., R.J. Ward, R. Newbould, *et al.*, *Brain iron chelation by deferiprone in a phase 2 randomised double-blinded placebo controlled clinical trial in Parkinson's disease*. Sci. Rep., 2017. **7**(1): p. 1398. doi: 10.1038/s41598-017-01402-2.

89. Obermeier, B., R. Daneman, and R.M. Ransohoff, *Development, maintenance and disruption of the blood-brain barrier*. Nat. Med., 2013. **19**(12): p. 1584-1596. doi: 10.1038/nm.3407.

90. Sweeney, M.D., A.P. Sagare, and B.V. Zlokovic, *Blood-brain barrier breakdown in Alzheimer disease and other neurodegenerative disorders*. Nature Reviews Neurology, 2018. **14**(3): p. 133-150. doi: 10.1038/nrneurol.2017.188.

91. Bauer, H.-C., I.A. Krizbai, H. Bauer, *et al.*, *"You Shall Not Pass"—tight junctions of the blood brain barrier*. Front. Neurosci., 2014. **8**(392). doi: 10.3389/fnins.2014.00392.

92. Fu, B.M., *Transport Across the Blood-Brain Barrier*, in *Molecular, Cellular, and Tissue Engineering of the Vascular System*, B.M. Fu and N.T. Wright, Editors. 2018, Springer International Publishing: Cham. p. 235-259.doi: 10.1007/978-3-319-96445-4_13

93. Demeule, M., A. Régina, J. Jodoin, *et al.*, *Drug transport to the brain: key roles for the efflux pump P-glycoprotein in the blood-brain barrier*. Vascul. Pharmacol., 2002. **38**(6): p. 339-348. doi: 10.1016/S1537-1891(02)00201-X.

94. Chen, Y. and L. Liu, *Modern methods for delivery of drugs across the blood-brain barrier*. Advanced Drug Delivery Reviews, 2012. **64**(7): p. 640-665. doi: 10.1016/j.addr.2011.11.010.

95. Geldenhuys, W.J., A.S. Mohammad, C.E. Adkins, *et al.*, *Molecular determinants of blood-brain barrier permeation*. Ther. Deliv., 2015. **6**(8): p. 961-71. doi: 10.4155/tde.15.32. 26305616

96. Pandit, R., L. Chen, and J. Götz, *The blood-brain barrier: Physiology and strategies for drug delivery*. Advanced Drug Delivery Reviews, 2020. **165-166**: p. 1-14. doi: 10.1016/j.addr.2019.11.009.

97. Dong, X., *Current Strategies for Brain Drug Delivery*. Theranostics, 2018. **8**(6): p. 1481-1493. doi: 10.7150/thno.21254. 29556336

98. Tajes, M., E. Ramos-Fernández, X. Weng-Jiang, *et al.*, *The blood-brain barrier: Structure, function and therapeutic approaches*. Mol. Membr. Biol., 2014. **31**: p. 1-16. doi: 10.3109/09687688.2014.937468.

99. Waring, M.J., *Lipophilicity in drug discovery*. Expert Opinion on Drug Discovery, 2010. **5**(3): p. 235-248. doi: 10.1517/17460441003605098.

100. Caron, G. and G. Ermondi, *Molecular descriptors for polarity: the need for going beyond polar surface area*. Future Med. Chem., 2016. **8**(17): p. 2013-2016. doi: 10.4155/fmc-2016-0165. 27739329

101. Ciura, K., M. Belka, P. Kawczak, *et al.*, *Combined computational-experimental approach to predict blood-brain barrier (BBB) permeation based on "green" salting-out thin layer chromatography supported by simple molecular descriptors*. J. Pharm. Biomed. Anal., 2017. **143**: p. 214-221. doi: 10.1016/j.jpba.2017.05.041.

102. Di, L. and E.H. Kerns, *Blood-Brain Barrier in Drug Discovery: Optimizing Brain Exposure of CNS Drugs and Minimizing Brain Side Effects for Peripheral Drugs*. 2015: Wiley.

103. Kouskoura, M.G., A.I. Piteni, and C.K. Markopoulou, *A new descriptor via bio-mimetic chromatography and modeling for the blood brain barrier (Part II)*. J. Pharm. Biomed. Anal., 2019. **164**: p. 808-817. doi: 10.1016/j.jpba.2018.05.021.

104. Gupta, M., H.J. Lee, C.J. Barden, *et al.*, *The Blood-Brain Barrier (BBB) Score*. J. Med. Chem., 2019. **62**(21): p. 9824-9836. doi: 10.1021/acs.jmedchem.9b01220.

105. Silva, A.M.G., A. Leite, M. Andrade, *et al.*, *Microwave-assisted synthesis of 3-hydroxy-4-pyridinone/naphthalene conjugates. Structural characterization and selection of a fluorescent ion sensor*. Tetrahedron, 2010. **66**(44): p. 8544-8550. doi: 10.1016/j.tet.2010.08.065.

106. Petrović, V., A. Gojmerac Ivšić, Z. Car, *et al.*, *Synthesis of 3-Hydroxy-1-(p-methoxyphenyl)-2-methylpyridine-4-one and Spectrophotometric Extraction Studies on its Complexation of Vanadium(V)*. Croatica Chemica Acta, 2014. **87**: p. 103-109. doi: 10.5562/cca2366.

107. Subirats, X., M. Rosés, and E. Bosch, *High-throughput logPo/w determination from UHPLC measurements: Revisiting the chromatographic hydrophobicity index*. J. Pharm. Biomed. Anal., 2016. **127**: p. 26-31. doi: 10.1016/j.jpba.2015.12.015.

108. Valko, K., C. My Du, C. Bevan, *et al.*, *Rapid method for the estimation of octanol/water partition coefficient (log P(oct)) from gradient RP-HPLC retention and a hydrogen bond acidity term (zetaalpha(2)(H))*. Curr. Med. Chem., 2001. **8**(9): p. 1137-46. doi: 10.2174/0929867013372643. 11472245

109. Klara Valko, M.K., James Evans, Dorothy Ko, *In vitro biomimetic HPLC and in vivo characterisation of GM6, an endogenous regulator peptide drug candidate for amyotrophic lateral sclerosis*. ADMET and DMPK, 2018. **6**: p. 176-189. doi: 10.5599/admet.547

110. Camurri, G. and A. Zaramella, *High-throughput liquid chromatography/mass spectrometry method for the determination of the chromatographic hydrophobicity index.* Anal. Chem., 2001. **73**(15): p. 3716-22. doi: 10.1021/ac001388j. 11510839

111. Taillardat-Bertschinger, A., F. Barbato, M.T. Quercia*, et al.*, *Structural Properties Governing Retention Mechanisms on Immobilized Artificial Membrane (IAM) HPLC Columns.* Helv. Chim. Acta, 2002. **85**: p. 519-532. doi: 10.1002/1522-2675(200202)85:2<519::AID-HLCA519>3.0.CO;2-Q.

112. Hollósy, F., K. Valkó, A. Hersey*, et al.*, *Estimation of Volume of Distribution in Humans from High Throughput HPLC-Based Measurements of Human Serum Albumin Binding and Immobilized Artificial Membrane Partitioning.* J. Med. Chem., 2006. **49**(24): p. 6958-6971. doi: 10.1021/jm050957i.

113. Gordon, L.J., M. Allen, P. Artursson*, et al.*, *Direct Measurement of Intracellular Compound Concentration by RapidFire Mass Spectrometry Offers Insights into Cell Permeability.* J. Biomol. Screen., 2016. **21**(2): p. 156-164. doi: 10.1177/1087057115604141. 26336900

114. Stookey, L.L., *Ferrozine-A New Spectrophotometric Reagent for Iron.* Anal. Chem., 1970. **42**: p. 779-781.

115. Teixeira, J., F. Cagide, S. Benfeito*, et al.*, *Development of a Mitochondriotropic Antioxidant Based on Caffeic Acid: Proof of Concept on Cellular and Mitochondrial Oxidative Stress Models.* J. Med. Chem., 2017. **60**(16): p. 7084-7098. doi: 10.1021/acs.jmedchem.7b00741. 28745898

116. Marcus, Y., *On the Use of the Molar Ratio Method for Determining Association Stoichiometry.* Isr. J. Chem., 1967. **5**(4): p. 143-149. doi: 10.1002/ijch.196700028.

117. Xie, S., J. Chen, X. Li*, et al.*, *Synthesis and evaluation of selegiline derivatives as monoamine oxidase inhibitor, antioxidant and metal chelator against Alzheimer's disease.* Bioorg. Med. Chem., 2015. **23**(13): p. 3722-9. doi: 10.1016/j.bmc.2015.04.009. 25934229

118. Silva, T., T. Mohamed, A. Shakeri*, et al.*, *Repurposing nitrocatechols: 5-Nitro-a-cyanocarboxamide derivatives of caffeic acid and caffeic acid phenethyl ester effectively inhibit aggregation of tau-derived hexapeptide AcPHF6.* Eur. J. Med. Chem., 2019. **167**: p. 146-152. doi: 10.1016/j.ejmech.2019.02.006. 30771602

119. Moharram, H. and M. Youssef, *Methods for Determining the Antioxidant Activity: A Review.* Alex. J. Fd. Sci. & Technol., 2014. **11**: p. 31-42.

120. Tipton, K.F., G. Davey, and M. Motherway, *Monoamine oxidase assays.* Curr. Protoc. Toxicol., 2006. **Chapter 4**: p. Unit4.21. doi: 10.1002/0471141755.tx0421s30. 23045135

121. Ramsay, R.R. and K.F. Tipton, *Assessment of Enzyme Inhibition: A Review with Examples from the Development of Monoamine Oxidase and Cholinesterase Inhibitory Drugs.* Molecules, 2017. **22**(7). doi: 10.3390/molecules22071192. 28714881

122. Hagenow, S., A. Stasiak, R.R. Ramsay*, et al.*, *Ciproxifan, a histamine H3 receptor antagonist, reversibly inhibits monoamine oxidase A and B.* Sci. Rep., 2017. **7**(1): p. 40541. doi: 10.1038/srep40541.

123. Reis, J., F. Cagide, D. Chavarria*, et al.*, *Discovery of New Chemical Entities for Old Targets: Insights on the Lead Optimization of Chromone-Based Monoamine Oxidase B (MAO-B) Inhibitors.* J. Med. Chem., 2016. **59**(12): p. 5879-5893. doi: 10.1021/acs.jmedchem.6b00527.

124. Saghaie, L., M. Sadeghi, and A. Nikazma, *Synthesis, analysis and determination of partition coefficients of N-arylhydroxypyridinone derivatives as iron chelators.* Res. Pharm. Sci., 2007. **1**.

125. Saghaie, L. and R.C. Hider, *Synthesis and physico-chemical properties of a series of bidentate 3-hydroxypyridin-4-ones iron chelating agents.* Res. Pharm. Sci., 2008. **3**.

126. Zhang, Z., S.J. Rettig, and C. Orvig, *Physical and structural studies of N-carboxymethyl- and N-(p-methoxyphenyl)-3-hydroxy-2-methyl-4-pyridinone.* Can. J. Chem., 1992. **70**(3): p. 763-770. doi: 10.1139/v92-101.

127. Kumar, B., M.A. Aga, A. Rouf, *et al.*, *Tetrahydropyranyl ether (THPE) formation in hydroxyl group protection and conversion to other useful functionalities.* RSC Advances, 2014. **4**(40): p. 21121-21130. doi: 10.1039/C4RA02093F.

128. Saghaie, L., H. Sadeghi-Aliabadi, and M. Kafiri, *Synthesis and biological evaluation of bidentate 3-hydroxypyridin-4-ones iron chelating agents.* Res. Pharm. Sci., 2011. **6**(2): p. 117-122. PMID: 22224095

129. Hall, S.R., R. Roy, D.T. McLaughlin, *et al.*, *The Synthesis and Molecular Structure of 1-(3,4-Dihydroxyphenethyl)-3-hydroxy-2-methylpyridin-4(1H)-one Hydrochloride Methanol Solvate.* Crystals, 2013. **3**(2): p. 333-338. doi:10.3390/cryst3020333

130. Ghisalberti, C.A., E. Falletta, C. Lammi, *et al.*, *Nonabsorbable Iron(III) binding polymers: Synthesis and evaluation of the chelating properties.* Polymer Testing, 2020. **90**: p. 106693. doi: 10.1016/j.polymertesting.2020.106693.

131. Leeson, P.D. and A.M. Davis, *Time-related differences in the physical property profiles of oral drugs.* J. Med. Chem., 2004. **47**(25): p. 6338-48. doi: 10.1021/jm049717d. 15566303

132. Liu, H., L. Wang, M. Lv, *et al.*, *AlzPlatform: An Alzheimer's Disease Domain-Specific Chemogenomics Knowledgebase for Polypharmacology and Target Identification Research.* J. Chem. Inf. Model., 2014. **54**(4): p. 1050-1060. doi: 10.1021/ci500004h.

CHAPTER VI – Appendix

6.1. Appendix 1: ^{1}H, ^{13}C and DEPT NMR spectra of the synthesized compounds

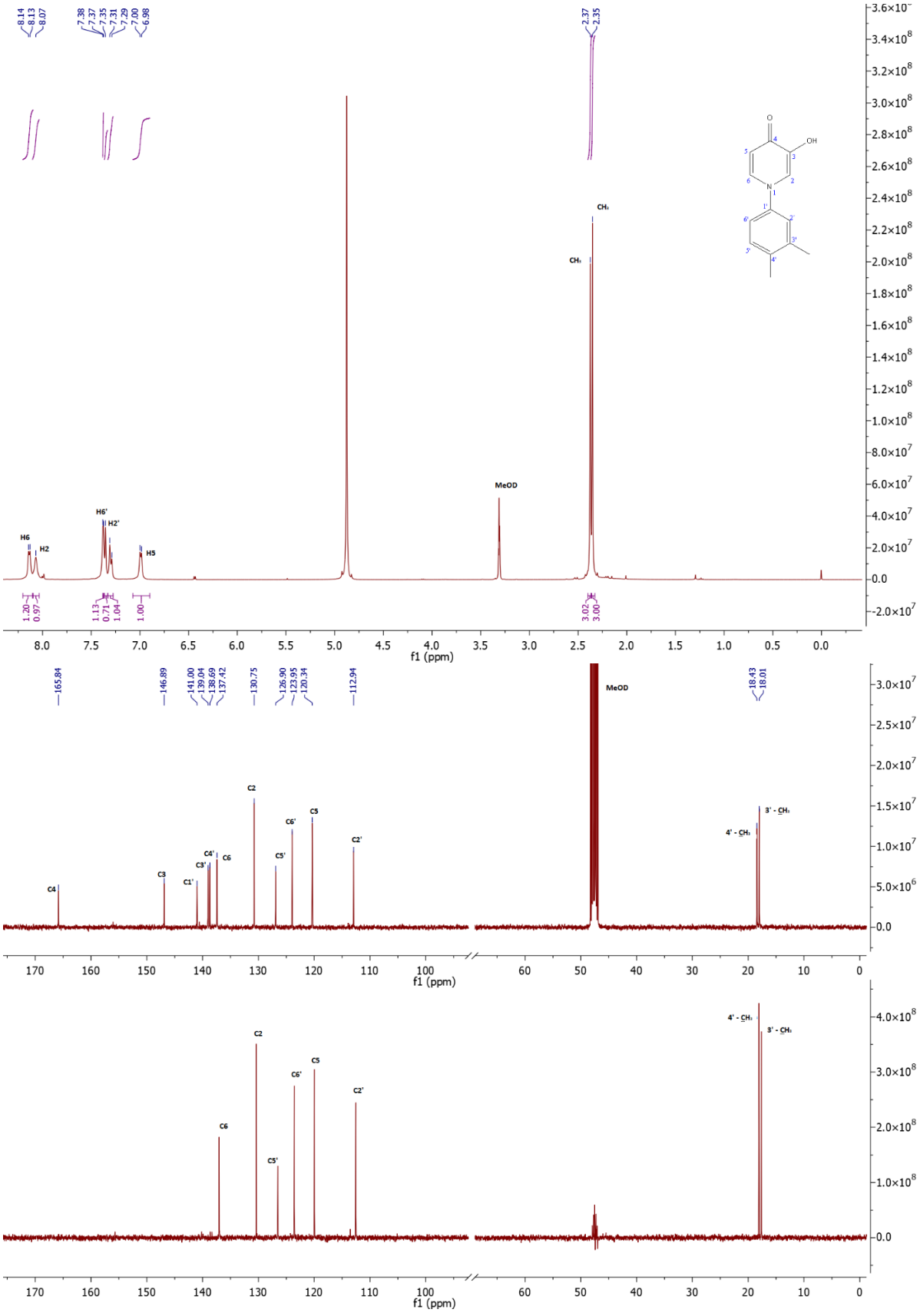

Figure 32: ^{1}H, ^{13}C and DEPT NMR spectra of compound 1 in MeOD-d_4.

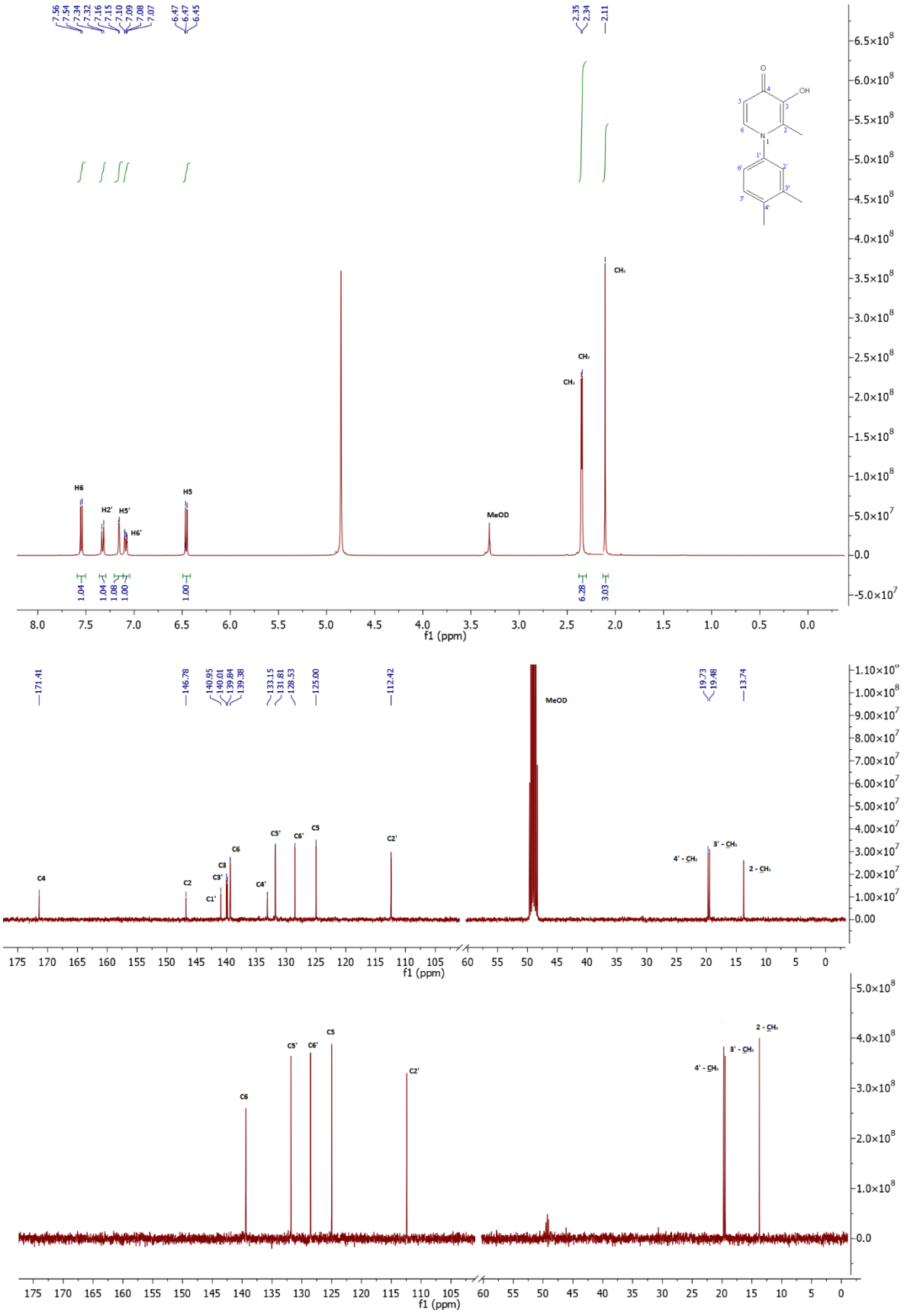

Figure 33: ^{1}H, ^{13}C and DEPT NMR spectra of compound 2 in MeOD-d_4.

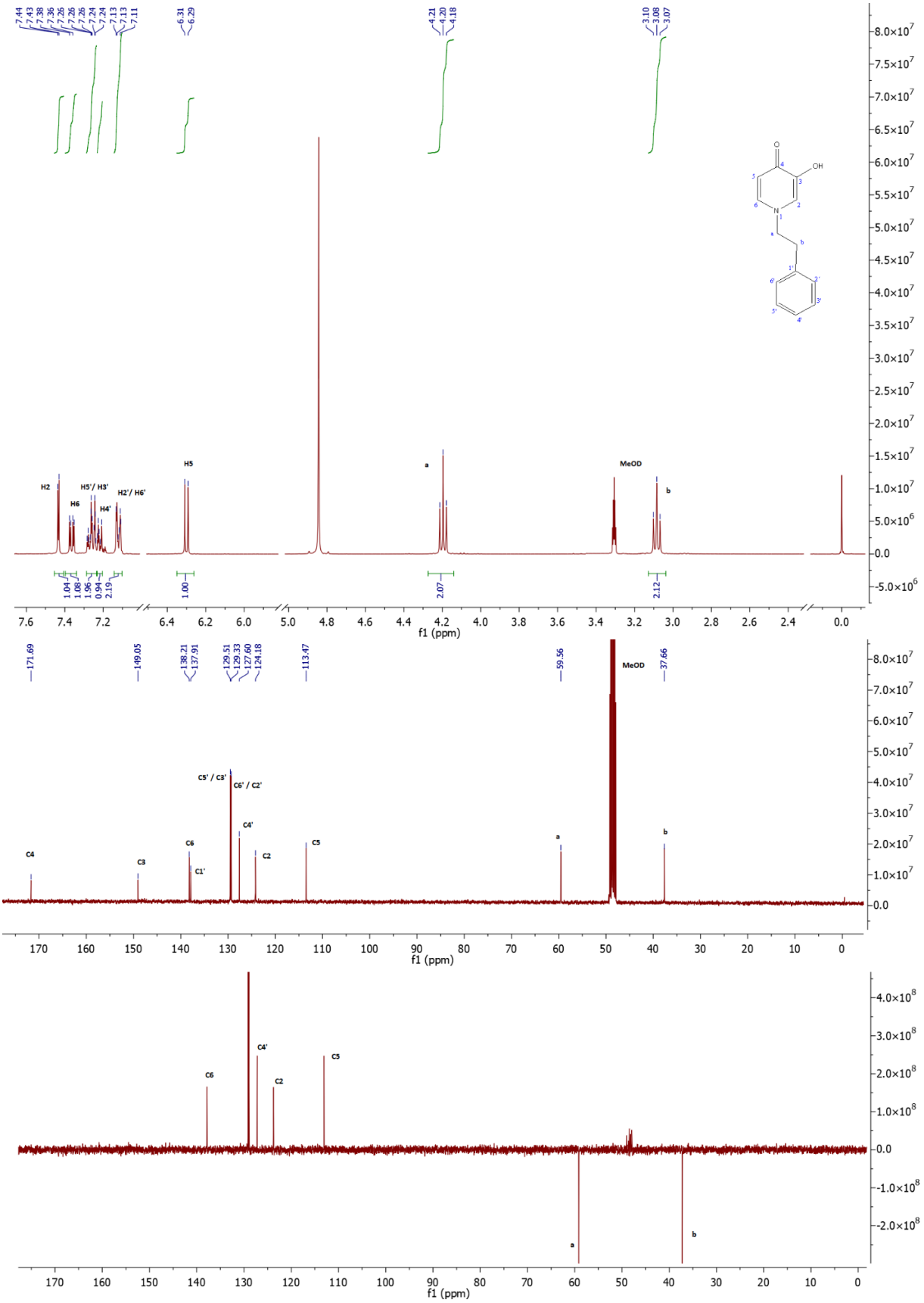

Figure 34: ^{1}H, ^{13}C and DEPT NMR spectra of compound 5 in MeOD-d_4.

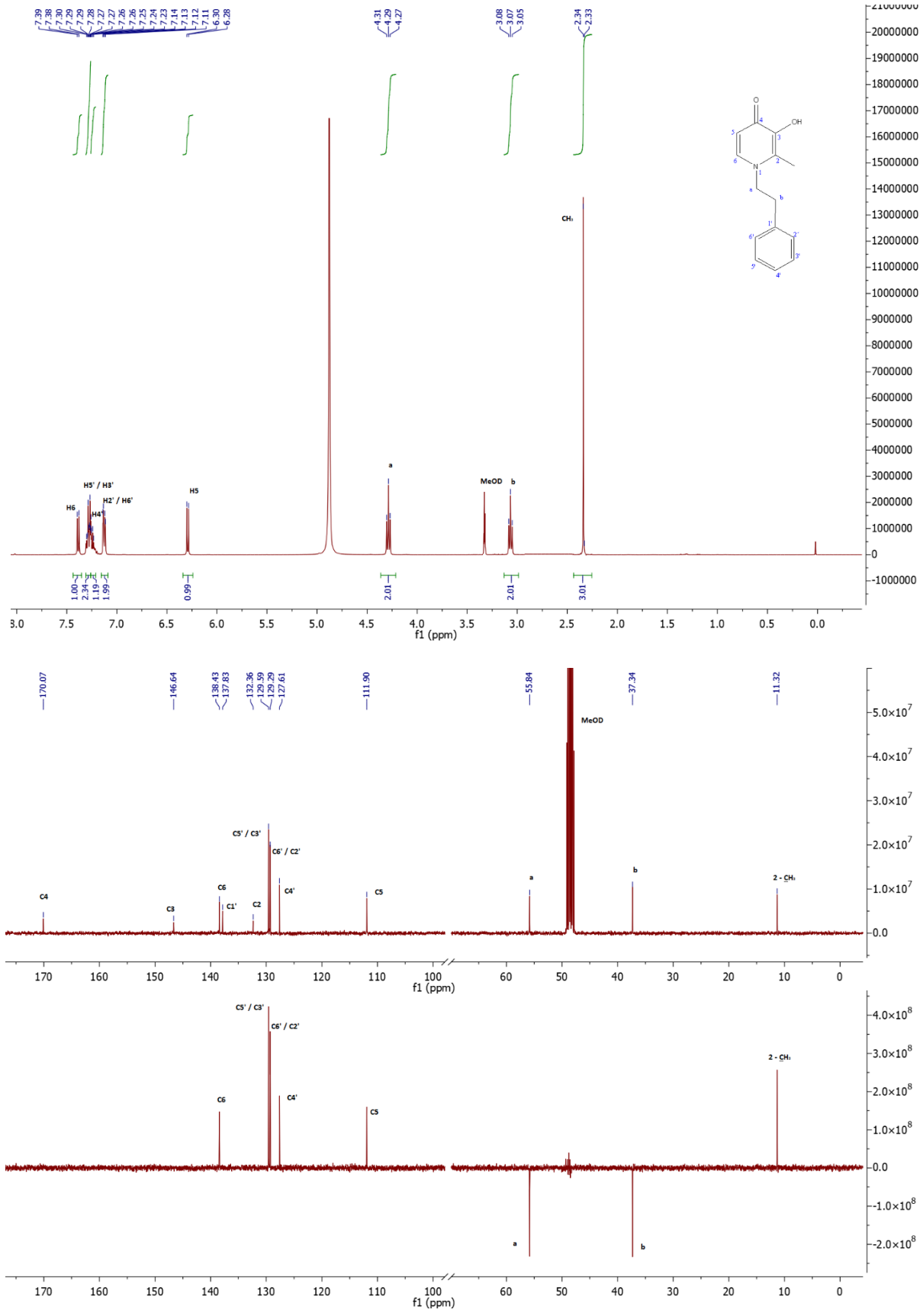

Figure 35: ^{1}H, ^{13}C and DEPT NMR spectra of compound 6 in MeOD-d_4.

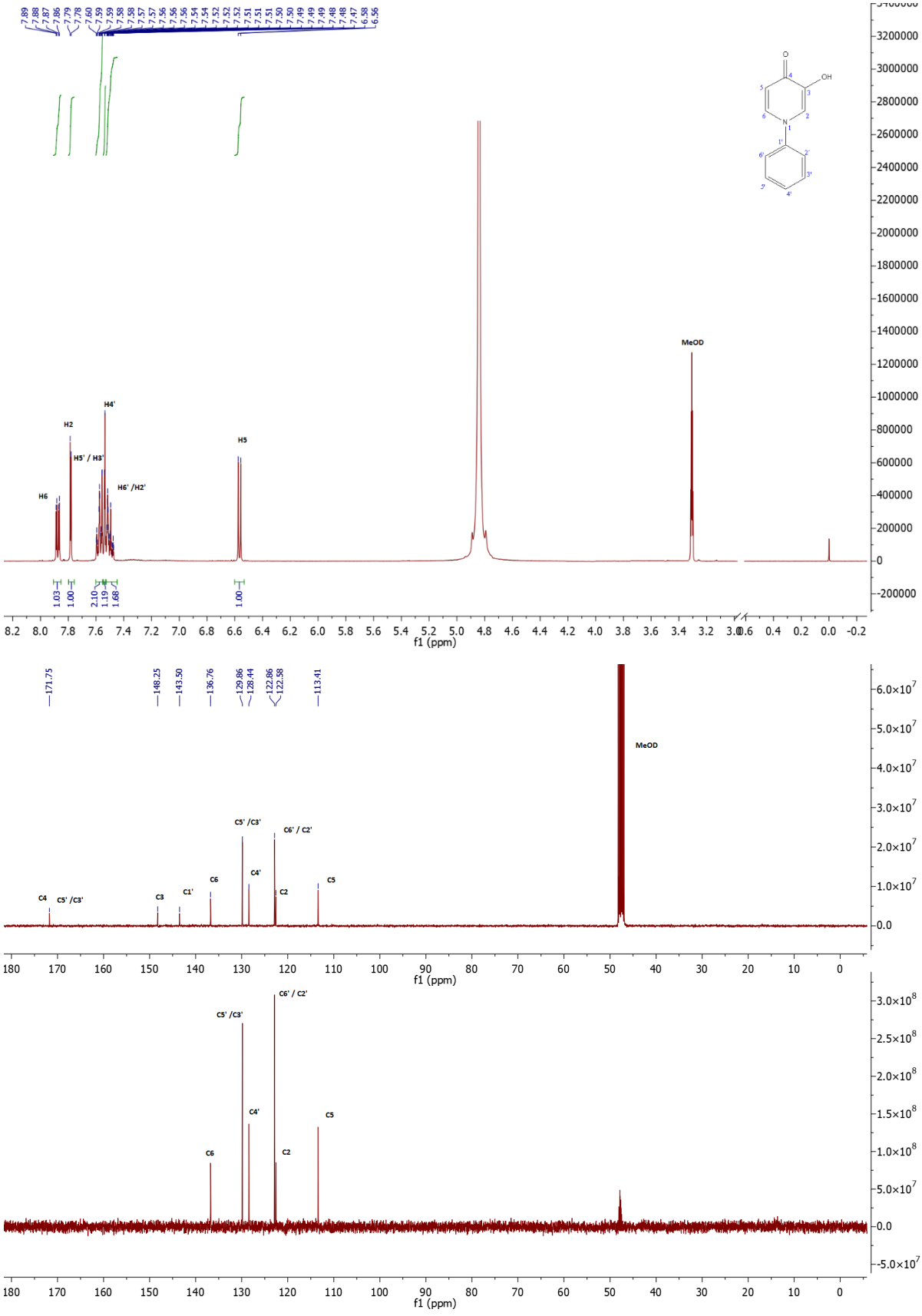

Figure 36: ^{1}H, ^{13}C and DEPT NMR spectra of compound 7 in MeOD-d_4.

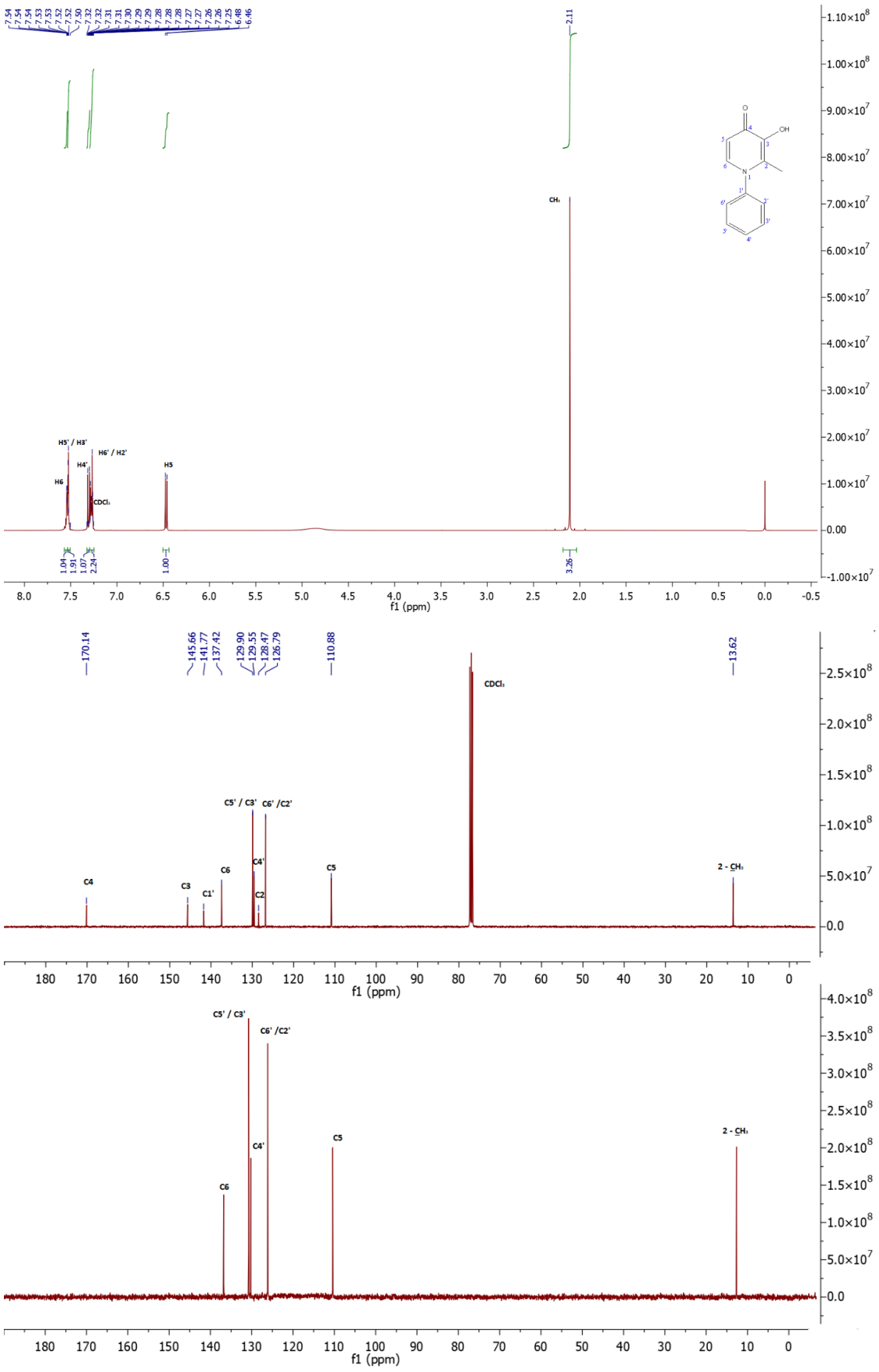

Figure 37: ^{1}H, ^{13}C and DEPT NMR spectra of compound 8 in $CDCl_3$-d_1.